Eur. Phys. J. C (2018) 78:18
https://doi.org/10.1140/epjc/s10052-017-5486-1

THE EUROPEAN PHYSICAL JOURNAL C

Regular Article - Experimental Physics

Search for dark matter produced in association with bottom or top quarks in $\sqrt{s} = 13$ TeV pp collisions with the ATLAS detector

ATLAS Collaboration[*]

CERN, 1211 Geneva 23, Switzerland

Received: 31 October 2017 / Accepted: 18 December 2017 / Published online: 11 January 2018

Abstract A search for weakly interacting massive dark-matter particles produced in association with bottom or top quarks is presented. Final states containing third-generation quarks and missing transverse momentum are considered. The analysis uses 36.1 fb^{-1} of proton–proton collision data recorded by the ATLAS experiment at $\sqrt{s} = 13$ TeV in 2015 and 2016. No significant excess of events above the estimated backgrounds is observed. The results are interpreted in the framework of simplified models of spin-0 dark-matter mediators. For colour-neutral spin-0 mediators produced in association with top quarks and decaying into a pair of dark-matter particles, mediator masses below 50 GeV are excluded assuming a dark-matter candidate mass of 1 GeV and unitary couplings. For scalar and pseudoscalar mediators produced in association with bottom quarks, the search sets limits on the production cross-section of 300 times the predicted rate for mediators with masses between 10 and 50 GeV and assuming a dark-matter mass of 1 GeV and unitary coupling. Constraints on colour-charged scalar simplified models are also presented. Assuming a dark-matter particle mass of 35 GeV, mediator particles with mass below 1.1 TeV are excluded for couplings yielding a dark-matter relic density consistent with measurements.

1 Introduction

Astrophysical observations have provided compelling evidence for the existence of a non-baryonic dark component of the universe: dark matter (DM) [1,2]. The currently most accurate, although somewhat indirect, determination of DM abundance comes from global fits of cosmological parameters to a variety of observations [3,4], while the nature of DM remains largely unknown. One of the candidates for a DM particle is a weakly interacting massive particle (WIMP) [5]. At the large hadron collider (LHC), one can search for WIMP DM (χ) pair production in pp collisions. WIMP DM would not be detected and its production leads to signatures with missing transverse momentum. Searches for the production of DM in association with Standard Model (SM) particles have been performed at the LHC [6–12].

Recently proposed simplified benchmark models for DM production assume the existence of a mediator particle which couples both to the SM and to the dark sector [13–15]. The searches presented in this paper focus on the case of a fermionic DM particle produced through the exchange of a spin-0 mediator, which can be either a colour-neutral scalar or pseudoscalar particle (denoted by ϕ or a, respectively) or a colour-charged scalar mediator (ϕ_b). The couplings of the mediator to the SM fermions are severely restricted by precision flavour measurements. An ansatz that automatically relaxes these constraints is Minimal Flavour Violation [16]. This assumption implies that the interaction between any new neutral spin-0 state and SM matter is proportional to the fermion masses via Yukawa-type couplings.[1] It follows that colour-neutral mediators would be sizeably produced through loop-induced gluon fusion or in association with heavy-flavour quarks. The characteristic signature used to search for the former process is a high transverse momentum jet recoiling against missing transverse momentum [7,11].

This paper focuses on dark matter produced in association with heavy flavour (top and bottom) quarks. These final states were addressed by the CMS Collaboration in Ref. [17]. For signatures with two top quarks ($t\bar{t} + \phi/a$), final states where both W bosons decay into hadrons or both W bosons decay into leptons are considered in this paper. They are referred to as fully hadronic and dileptonic $t\bar{t}$ decays, respectively. Searches in final-state events characterised by fully hadronic or dileptonic top-quark pairs have been carried out targeting supersymmetric partners of the top quarks [18,19]. Due to the

[*] e-mail: atlas.publications@cern.ch

[1] Following Ref. [14], couplings to W and Z bosons, as well as explicit dimension-4 ϕ–h or a–h couplings, are set to zero in this simplified model. In addition, the coupling of the mediator to the dark sector are not taken to be proportional to the mass of the DM candidates.

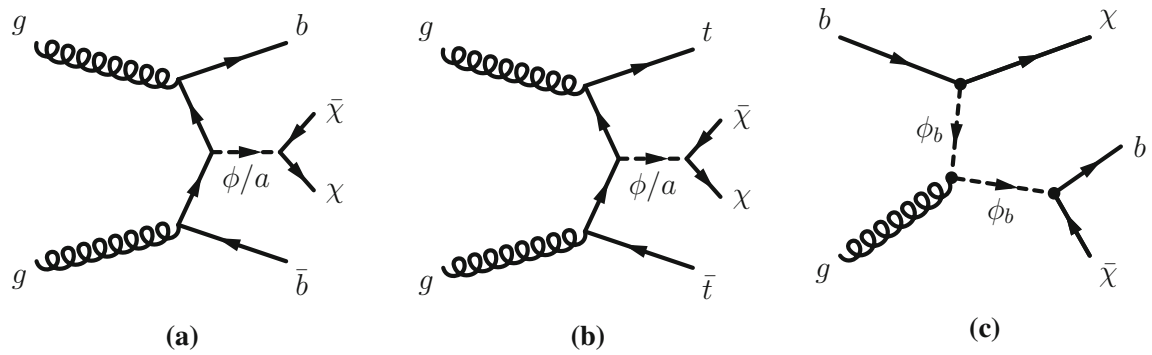

Fig. 1 Representative diagrams at the lowest order for spin-0 mediator associated production with top and bottom quarks: **a** colour-neutral spin-0 mediator associated production with bottom quarks $b\bar{b}+\phi/a$; **b** colour-neutral spin-0 mediator associated production with top quarks $t\bar{t}+\phi/a$; **c** colour-charged scalar mediator model decaying into a bottom quark and a DM particle b-FDM

different kinematics of the events under study, those searches are not optimal for the DM models considered in this paper. The search in the channel where one W boson decays into hadrons and one W boson decays into leptons (semileptonic $t\bar{t}$ decays) is presented together with the searches for top squarks in the same channel [20]. Signatures with bottom quarks in the final state are denoted $b\bar{b}+\phi/a$ in the following. Representative diagrams for tree-level production of these models are shown in Fig. 1a, b. Processes with similar kinematic properties might also occur in two-Higgs-doublet models [21]. Following the notation of Ref. [14], the model has four parameters: the mass of the mediator m_ϕ or m_a, the DM mass m_χ, the DM–mediator coupling g_χ, and the flavour-universal SM–mediator coupling g_q. The mediator width is assumed to be the minimal width, which is the one calculated from the masses and couplings assumed by the model [13]. The mediator can decay into SM particles or into DM particles. This search is sensitive to decays of the mediator into a pair of DM particles. Off-shell DM production is also taken into account. The effective production cross-section of DM particles at pp colliders is a function of the production cross-section of the mediator, depending on g_q, and on the branching ratio for the mediator to decay into a pair of DM particles, which is a function of g_q and g_χ [13]. The cross-section for DM production is therefore proportional to the squared product of the couplings $(g_q \cdot g_\chi)^2$, and an additional assumption of $g_q = g_\chi = g$ is made to reduce the number of parameters. Since the cross-section of annihilation and scattering from nucleons has the same functional dependence on the couplings, the same assumption is made when the results are compared to non-collider experiments.

The second category of models considered in this search is the case of colour-charged scalar mediators [22]. The model assumes bottom-flavoured dark matter (b-FDM) and was proposed to explain the excess of gamma rays from the galactic centre observed by the Fermi Gamma-ray Space Telescope, if this excess is to be interpreted as a signal for DM annihilation [23], while alternative conjectures without DM are also discussed [24]. A representative diagram for the production of this signal is shown in Fig. 1c. In this model, a new scalar field, ϕ_b, mediates the interaction between DM and quarks. Dark matter is assumed to be the lightest Dirac fermion that belongs to a flavour-triplet coupling to right-handed, down-type quarks. The cosmological DM is the third component of the triplet and couples preferentially to bottom quarks. It explains the galactic-centre excess if a DM mass around 35 GeV is assumed. The other Dirac fermions in the flavour-triplet are heavy and couple weakly, and are therefore neglected. The b-FDM model has three parameters: the mediator and the DM masses ($m(\phi_b)$ and $m(\chi)$, respectively), and the coupling strength between the mediator and the DM particle, λ_b [22]. For each pair of mass values considered, λ_b is set to the value, generally larger than one, predicting a DM relic density compatible with the astrophysical observations as detailed in Ref. [22]. Strong-interaction pair production of ϕ_b, which does not depend on the coupling, is equivalent to the pair production of the lightest supersymmetric partner of the bottom quark (bottom squark, $\tilde{b}_1$) assuming that it decays exclusively into a bottom quark and the lightest neutralino ($\tilde{\chi}_1^0$). Exclusion limits on $m(\tilde{b}_1)$, which depend on $m(\tilde{\chi}_1^0)$, are set in dedicated searches by the ATLAS and CMS collaborations [25,26]. The target of this search is the single production mode represented in Fig. 1(c), which can dominate the production rate of the ϕ_b mediator due to the relatively large values assumed for λ_b. The parameter space considered corresponds to ϕ_b masses of a few hundred GeV. A search by the ATLAS Collaboration with the $\sqrt{s} = 8$ TeV LHC Run-1 dataset has already excluded $m(\phi_b) < 600$ GeV for $m(\chi) = 35$ GeV [27].

Four experimental signatures are considered in this paper. The first two signatures consist of event topologies with large missing transverse momentum and either one or two bot-

tom quarks, while the other two consist of events with large missing transverse momentum and two top quarks, decaying either dileptonically or fully hadronically. The search presented in this paper is based on a set of independent analyses optimised for these four experimental signatures and searches for dark-matter production via colour-charged and colour-neutral mediators.

2 Detector description and event reconstruction

The ATLAS experiment [28] is a multi-purpose particle detector with a forward-backward symmetric cylindrical geometry and nearly 4π coverage in solid angle.[2] It consists of an inner tracking detector (ID) surrounded by a superconducting solenoid, electromagnetic and hadronic calorimeters, and an external muon spectrometer incorporating large superconducting toroidal magnets. The inner tracking detector consists of pixel and silicon microstrip detectors covering the pseudorapidity region $|\eta| < 2.5$, surrounded by a transition radiation tracker which provides electron identification in the region $|\eta| < 2.0$. Between Run 1 and Run 2, a new inner pixel layer, the insertable B-layer [29,30], was inserted at a mean sensor radius of 3.3 cm. The inner detector is surrounded by a thin superconducting solenoid providing an axial 2 T magnetic field and by a fine-granularity lead/liquid-argon (LAr) electromagnetic calorimeter covering $|\eta| < 3.2$. A steel/scintillator-tile calorimeter provides hadronic coverage in the central pseudorapidity range ($|\eta| < 1.7$). The endcap and forward regions ($1.5 < |\eta| < 4.9$) of the hadronic calorimeter are made of LAr active layers with either copper or tungsten as the absorber material. A muon spectrometer with an air-core toroid magnet system surrounds the calorimeters. Three stations of high-precision tracking chambers provide coverage in the range $|\eta| < 2.7$, while dedicated chambers allow triggering in the region $|\eta| < 2.4$. The ATLAS trigger system consists of a hardware-based level-1 trigger followed by a software-based high-level trigger [31].

The events used in this analysis are required to pass either an online trigger requiring a minimum of two electrons, two muons or an electron and a muon, or an online missing transverse momentum trigger selection. The trigger thresholds are such that a plateau of the efficiency is reached for events passing the analysis requirements presented in Sect. 4. The events are also required to have a reconstructed vertex [32] with at least two associated tracks with transverse momentum (p_{T}) larger than 400 MeV which are consistent with originating from the beam collision region. The vertex with the highest scalar sum of the squared transverse momenta of the associated tracks is considered to be the primary vertex of the event.

This analysis requires the reconstruction of jets, muons, electrons, photons and missing transverse momentum. Jets are reconstructed from three-dimensional energy clusters in the calorimeter [33] using the anti-k_t jet clustering algorithm [34] with a radius parameter $R = 0.4$ implemented in the FastJet package [35]. Jets are calibrated as described in Ref. [36], and the expected average energy contribution from clusters resulting from additional pp interactions in the same or nearby bunch crossings (pile-up interactions) is subtracted according to the jet area [37]. Only jet candidates (baseline jets) with $p_{\mathrm{T}} > 20$ GeV and $|\eta| < 2.8$ are considered in the analysis. Quality criteria identify jets arising from non-collision sources or detector noise and any event containing such a jet is removed [38,39]. Additional selection requirements are imposed on jets with $p_{\mathrm{T}} < 60$ GeV and $|\eta| < 2.4$ in order to reject jets produced in pile-up interactions [40]. Jets are also reclustered into larger-radius jets ($R = 0.8$ or 1.2) by applying the anti-k_t clustering algorithm to the $R = 0.4$ jets. These jets are exploited to identify W-boson decays into a pair of quarks and also to identify top-quark candidates.

Jets containing b-hadrons (b-jets) and which are within the inner detector acceptance ($|\eta| < 2.5$) are identified (b-tagged) with a multivariate algorithm that exploits the impact parameters of the charged-particle tracks, the presence of secondary vertices and the reconstructed flight paths of b- and c-hadrons inside the jet [41,42]. Depending on the signal region requirements detailed in Sect. 4, a "medium" or "tight" working-point is used for the b-jet identification, corresponding to an average efficiency for b-quark jets in simulated $t\bar{t}$ events of 77 and 60%, respectively. An additional "loose" working-point with 85% efficiency for b-quark jets in simulated $t\bar{t}$ events is used to resolve ambiguities in the reconstruction of physics objects, as described at the end of this section.

Muon candidates are reconstructed in the region $|\eta| < 2.7$ from muon spectrometer tracks matching ID tracks (where applicable). The pseudorapidity requirements are restricted to $|\eta| < 2.4$ for events passing the muon online trigger criteria, due to the coverage of the muon triggering system. Events containing one or more muon candidates that have a transverse (longitudinal) impact parameter with respect to the primary vertex larger than 0.2 mm (1 mm) are rejected to suppress muons from cosmic rays. Baseline candidate muons, used for the definition of vetoes in all signal regions but those searching for fully hadronic top decays, must have

[2] ATLAS uses a right-handed coordinate system with its origin at the nominal interaction point (IP) in the centre of the detector and the z-axis along the beam pipe. The x-axis points from the IP to the centre of the LHC ring, and the y-axis points upward. Cylindrical coordinates (r, ϕ) are used in the transverse plane, ϕ being the azimuthal angle around the beam pipe. The pseudorapidity is defined in terms of the polar angle θ as $\eta = -\ln\tan(\theta/2)$. Rapidity is defined as $y = 0.5 \ln\left[(E + p_z)/(E - p_z)\right]$ where E denotes the energy and p_z is the component of the momentum along the beam direction.

$p_{\mathrm{T}} > 10$ GeV and pass the "medium" identification requirements defined in Ref. [43]. The baseline candidate muons used in fully hadronic $t\bar{t}$ final states are instead required to pass the "loose" identification requirements [43] and to have $p_{\mathrm{T}} > 6$ GeV, in order to strengthen the veto definition. Baseline electron candidates are reconstructed from isolated electromagnetic calorimeter energy deposits matched to ID tracks and are required to have $|\eta| < 2.47$ and $p_{\mathrm{T}} > 10$ GeV, and must pass a "loose" likelihood-based identification requirement [44,45].

Stricter requirements are imposed on the baseline lepton (electron or muon) definitions for the selection criteria requiring leptons in the final state. Signal muon candidates, used for all selection requirements with leptons in the final state, must have $p_{\mathrm{T}} > 20$ GeV and satisfy "medium" identification criteria [43]. Furthermore, they are required to be isolated using a "loose" criterion designed to be 99% efficient for muons from Z-boson decays [43]. Signal electron candidates are required to pass "tight" requirements on the likelihood-based identification [44] and must have $p_{\mathrm{T}} > 20$ GeV. In order to improve signal acceptance, the requirement on the likelihood-based identification is relaxed to "medium" for the signal region optimised for the two-lepton final state. Like the muons, signal electrons are required to be isolated from other activity using a "loose" isolation criterion [46]. Signal electrons (muons) are matched to the primary vertex (PV) of the event (see Sect. 4) by requiring their transverse impact parameter d_0^{PV}, with respect to the primary vertex, to have a significance $|d_0^{\mathrm{PV}}/\sigma(d_0^{\mathrm{PV}})| < 5$ (3). In addition, for both the electrons and muons the longitudinal impact parameter z_0^{PV} and the polar angle θ are required to satisfy $|z_0^{\mathrm{PV}} \sin\theta| < 0.5$ mm. In the following, the combination of signal electrons and muons optimised for the two-lepton final state is referred to as the medium-lepton requirement. Similarily, the combination of the signal electrons and muons passing the "tight" identification criteria is referred to as the tight-lepton requirement. The number of leptons passing the medium and tight requirements is denoted by $\mathcal{N}_\ell^{\mathrm{M}}$ and $\mathcal{N}_\ell^{\mathrm{T}}$, respectively.

Photons are reconstructed from clusters of energy deposits in the electromagnetic calorimeter measured in projective towers [47,48]. Photon candidates are required to have $p_{\mathrm{T}} > 10$ GeV and $|\eta| < 2.37$, whilst being outside the transition region $1.37 < |\eta| < 1.52$ between the barrel and end-cap calorimeters, and to satisfy "tight" identification criteria [48]. The photons used in this analysis are further required to have $p_{\mathrm{T}} > 130$ GeV and to be isolated [47].

To resolve reconstruction ambiguities, an overlap removal algorithm is applied to loose candidate leptons and jets. Jet candidates with $p_{\mathrm{T}} > 20$ GeV and $|\eta| < 2.8$ are removed if they are not b-tagged when employing the loose working-point and are within $\Delta R = \sqrt{(\Delta y)^2 + (\Delta\phi)^2} = 0.2$ of an electron candidate. The same is done for jets which lie close to a muon candidate and have less than three associated tracks or a ratio of muon p_{T} to jet p_{T} greater than 0.5. Finally, any lepton candidate within $\Delta R = 0.4$ of the direction of a surviving jet candidate is removed, in order to reject leptons from the decay of a b- or c-hadron. Electrons which share an ID track with a muon candidate are also removed.

The missing transverse momentum vector, $\vec{p}_{\mathrm{T}}^{\,\mathrm{miss}}$, whose magnitude is denoted by $E_{\mathrm{T}}^{\mathrm{miss}}$, is defined as the negative vector sum of the transverse momenta of all identified physics objects (electrons, photons, muons, jets) and an additional soft term. The soft term is constructed from all tracks that originate from the primary vertex but are not associated with any physics object. In this way, the $E_{\mathrm{T}}^{\mathrm{miss}}$ is adjusted for the calibration of the jets and the other identified physics objects above, while maintaining pile-up independence in the soft term [49,50].

3 Data and simulated event samples

The dataset used in this analysis consists of pp collision data recorded at a centre-of-mass energy of $\sqrt{s} = 13$ TeV with stable beam conditions. The integrated luminosity of the combined 2015 + 2016 dataset after requiring that all detector subsystems were operational during data recording is 36.1 fb^{-1}. The uncertainty in the total integrated luminosity is 3.2%, derived following a methodology similar to that detailed in Ref. [51].

Monte Carlo (MC) simulated event samples are used to aid in the estimation of the background from SM processes and to model the dark-matter signal. All simulated events were processed through an ATLAS detector simulation [52] based on GEANT4 [53] or through a fast simulation using a parameterisation of the calorimeter response and GEANT4 for the other parts of the detector [54]. The simulated events are reconstructed with the same reconstruction algorithms used for data. Correction factors are applied to the simulated events to compensate for differences between data and MC simulation in the b-tagging efficiencies and mis-tag rates, lepton and photon identification, reconstruction and trigger efficiencies. The MC samples are reweighted so that the pile-up distribution matches the one observed in the data.

The matrix element (ME) generator, parton shower (PS), cross-section normalisation, parton distribution function (PDF) set and the set of tuned parameters (known as tune) describing the underlying event for these samples are given in Table 1, and more details of the generator configurations can be found in Refs. [55–58]. The generation of $t\bar{t}$ pairs and single-top-quark processes in the Wt- and s-channels was performed using the POWHEG- BOX v2 generator with the CT10 PDF set for the matrix element calculations. Electroweak t-channel single-top-quark events were generated

Table 1 Simulated signal and background event samples: the corresponding generator, parton shower, cross-section normalisation, PDF set and underlying-event tune are shown

Physics process	Generator	Parton shower	Cross-section normalisation	PDF set	Tune
Dark-matter signals	MadGraph 2.3.3 [67]	Pythia 8.212 [68]	NLO [69,70]	NNPDF23LO [71]	A14 [72]
$W(\to \ell\nu)$ + jets	Sherpa 2.2.1 [73]	Sherpa 2.2.1	NNLO [74]	NNPDF30NNLO [71]	Sherpa default
$Z/\gamma^*(\to \ell\ell)$ + jets	Sherpa 2.2.1	Sherpa 2.2.1	NNLO [74]	NNPDF30NNLO	Sherpa default
$t\bar{t}$	powheg-box v2 [75]	Pythia 6.428 [76]	NNLO+NNLL [77–82]	NLO CT10 [71]	Perugia 2012 [83]
Single-top (t-channel)	powheg-box v1	Pythia 6.428	NNLO+NNLL [59]	NLO CT104f	Perugia2012
Single-top (s- and Wt-channel)	powheg-box v2	Pythia 6.428	NNLO+NNLL [60,61]	NLO CT10	Perugia2012
$t\bar{t} + W/Z/\gamma^*/h$	MadGraph5_aMC@NLO 2.2.3 (NLO)	Pythia 8.186	NLO [67]	NNPDF30NLO	A14
Diboson	Sherpa 2.2.1 [73]	Sherpa 2.2.1	NLO	NNPDF30NNLO	Sherpa default
$h + W/Z$	MadGraph5_aMC@NLO 2.2.3 (NLO)	Pythia 8.186	NLO [84]	NNPDF30NLO	A14
$t\bar{t} + WW/t\bar{t}$	MadGraph5_aMC@NLO 2.2.3 (LO)	Pythia 8.186	NLO [67]	NNPDF23LO	A14
$t + Z/WZ/t\bar{t}$	MadGraph5_aMC@NLO 2.2.3 (LO)	Pythia 8.186	LO	NNPDF23LO	A14
Triboson	Sherpa 2.2.1	Sherpa 2.2.1	NLO	NNPDF30NNLO	Sherpa default

using the Powheg- Box v1 generator. For all processes, a top-quark mass of 172.5 GeV is assumed. The PS and the underlying event were simulated using Pythia 6.428 with the CT10 PDF set. Samples of single-top-quark and $t\bar{t}$ production are normalised to their NNLO cross-section including the resummation of soft gluon emission at next-to-next-to-leading-log (NNLL) accuracy using Top++2.0 [59–61].

Events containing W or Z bosons with associated jets, including jets from the hadronisation of b- and c-quarks, were simulated using the Sherpa v2.2.1 generator. Matrix elements were calculated for up to two additional partons at next-to-leading order (NLO) and four partons at leading order (LO) using the Comix [62] and Open Loops [63] matrix element generators and merged with the Sherpa PS [64] using the ME+PS@NLO prescription [65]. The NNPDF30NNLO [66] PDF set was used in conjunction with the dedicated PS tune developed by the Sherpa authors.

Diboson and triboson processes were also simulated using the Sherpa generator using the NNPDF30NNLO PDF set in conjunction with a dedicated PS tune developed by the Sherpa authors. Matrix elements for these samples were calculated for up to one (diboson processes) or zero (triboson processes) additional partons at NLO and up to three (diboson processes) or two (triboson processes) additional partons at LO. Additional contributions to the SM backgrounds in the signal regions arise from the production of $t\bar{t}$ pairs in association with $W/Z/h$ bosons and possibly additional jets. These processes were modelled by event samples generated at NLO using the MadGraph5_aMC NLO [67] v2.2.3 generator and showered with the Pythia v8.186 PS.

In all MC samples, except those produced by Sherpa, the EvtGen v1.2.0 program [85] was used to model the properties of the bottom and charm hadron decays. All Pythia v6.428 samples used the PERUGIA2012 [83] tune for the underlying event, while Pythia v8.186 and Herwig++ showering were run with the A14 and UEEE5 [86] underlying-event tunes, respectively. To simulate the effects of additional pp collisions in the same and nearby bunch crossings, additional interactions were generated using the soft QCD processes of Pythia 8.186 with the A2 tune [87] and the MSTW2008LO PDF [88], and overlaid onto each simulated hard-scatter event.

Alternative samples are employed to derive systematic uncertainties associated with the specific configuration of the MC generators used for the nominal SM background samples, as detailed in Sect. 6. They include variations of the renormalisation and factorisation scales, the CKKW-L matching [89] scale, as well as different PDF sets and hadronisation models.

The event generation for the dark-matter signal samples followed the prescriptions in Ref. [13]. Events were generated from leading-order (LO) matrix elements using the MadGraph generator v2.3.3 interfaced to Pythia v8.212 with the A14 tune for the modelling of the top-quark decay chain (when applicable), parton showering, hadronisation and the description of the underlying event. The renormalisation and factorisation scale choice adopted is the default

MadGraph dynamical scale as documented in Ref. [90]. For the $b\bar{b}+\phi/a$ and $t\bar{t}+\phi/a$ models the events were generated with up to one additional parton, while for the b-FDM models the events were generated with up to two additional partons. The $t\bar{t}+\phi/a$ and b-FDM samples were generated in the 5-flavour scheme, while the $b\bar{b}+\phi/a$ samples were generated in the 4-flavour scheme. Following Ref. [13], the minimum p_{T} requirement for b-jets in the final state in MadGraph was set to 30 GeV for the $b\bar{b}+\phi/a$ model, in order to increase the number of events in the relevant phase space for the analysis. This requirement does not affect the MC signal sample passing the event selection. The PDF set NNPDF23LO was used, adopting $\alpha_{\mathrm{S}} = 0.130$ and either the 5-flavour or the 4-flavour scheme consistently with the choice made for generating the events. The jet–parton matching was realised following the CKKW-L prescription. For the $t\bar{t}+\phi/a$ model the matching scale was set to one quarter of the mass of the particle mediating the interaction between the SM and DM sectors. For the $b\bar{b}+\phi/a$ and b-FDM models the matching scale was set to 30 GeV. The coupling g between the colour-neutral mediator for the $t\bar{t}+\phi/a$ and $b\bar{b}+\phi/a$ models and both the SM and the dark sector was assumed to be one, which implies pure Yukawa-type couplings between the mediator and the SM quarks. This choice impacts the mediator width and cross-section calculation for these models, but it was shown to have no significant impact on the kinematic properties [13].

For the $t\bar{t}+\phi/a$ and $b\bar{b}+\phi/a$ models the production cross-section was computed at NLO accuracy in the strong coupling constant α_{S} using the MadGraph5_aMC@NLO generator with the NNPDF30NLO PDF set using $\alpha_{\mathrm{S}} = 0.118$. For this procedure a dynamical scale equal to $P_{\mathrm{T}}/2$ was adopted, with P_{T} being the scalar sum of the transverse momenta of all final-state particles. The flavour scheme adopted is consistent with that used for event generation. For the mass range in which this analysis is sensitive, the NLO value of the cross-sections for the $t\bar{t}+\phi/a$ model is about 25% larger than the corresponding LO value [69,70]. For the $b\bar{b}+\phi/a$ samples the NLO value of the cross-section is between 56% and 75% of the corresponding LO value. This is driven by the MadGraph minimum b-jet p_{T} requirement due to the strong dependence of the NLO cross-section on this parameter. For the b-FDM signal models, the cross-section was computed at LO accuracy using the MadGraph5_aMC@NLO generator and the same flavour scheme used for the event generation.

4 Event selection

Five signal regions (SR) are defined and optimised to detect dark-matter production via spin-0 mediators. Two signal regions, SRb1 and SRb2, are optimised for models in which dark matter is produced in conjunction with one or two b-quarks, respectively. Specifically, SRb1 is designed to optimally select candidate signal events of the colour-charged scalar mediator models (bFDM) introduced in Sect. 1. SRb2 focuses instead on scalar and pseudoscalar colour-neutral mediators and was specifically optimised for low mediator masses (below 200 GeV). These SRs require events with no leptons and low jet multiplicity. SRt1, SRt2 and SRt3 are optimised to detect events in which DM is produced in association with a $t\bar{t}$ pair, which either decays fully hadronically (SRt1 and SRt2) or dileptonically (SRt3). The SRt1 and SRt2 SRs are optimised for low (< 100 GeV) and high (between 100 and 350 GeV) mediator mass assumptions, respectively, and are assigned fully hadronic events with high jet multiplicity. The regions SRt1 and SRt2 overlap in terms of their selection criteria. The region SRt3 focuses on mediator masses below 100 GeV and contains events with two leptons in the final state.

4.1 Signatures with b-quarks and $E_{\mathrm{T}}^{\mathrm{miss}}$

Events assigned to SRb1 and SRb2 are required to pass the missing transverse momentum trigger and to have at least one jet ($\mathcal{N}_j$). A minimum azimuthal angle between the directions of the missing transverse momentum and any of the jets in the event ($\Delta\phi(\mathrm{j}, \vec{p}_{\mathrm{T}}^{\mathrm{miss}})$) is required, in order to reduce the contamination by multi-jet events where fake $E_{\mathrm{T}}^{\mathrm{miss}}$ arises from jet energy mismeasurements or semileptonic decays of hadrons inside jets. Events with at least one baseline muon or electron ($\mathcal{N}_\ell^{\mathrm{B}}$) are discarded to reject leptonic decays of W and Z bosons. The dominant background processes for the events passing these requirements are $t\bar{t}$ and $Z+$jets processes.

Events with at least one tight b-tagged jet ($\mathcal{N}_b^{\mathrm{T}}$) and which pass the kinematic requirements specified in Table 2 are assigned to SRb1. The high-$E_{\mathrm{T}}^{\mathrm{miss}}$ selection required is essential to discriminate the signal from the background in this SR. An upper limit on the scalar sum of the transverse momenta of the baseline jets in the events excluding the leading and subleading jets (H_{T3} [25]) is used in this SR to reduce the contributions from top-quark pair-production processes.

Events assigned to SRb2 have instead at least two tight b-tagged jets. When the b-tagged jet multiplicity is different from two, the b-tagged jets are sorted in descending order according to their b-tagging probability. For this SR, a requirement of low jet multiplicity was found to be more effective in reducing the $t\bar{t}$ background. The jet multiplicity of candidate signal events is required to not exceed three, and the transverse momentum of the third jet in the event must not exceed 60 GeV. For the same purpose, the ratio of the transverse momentum of the leading jet to H_{T}, the scalar sum of the transverse momenta of all jets in the events, ($H_{\mathrm{T}}^{\mathrm{ratio}} = p_{\mathrm{T}}(j_1)/H_{\mathrm{T}}$) is required to be larger than 75%.

Table 2 Summary of the kinematic and topology-dependent selections for signal regions SRb1 and SRb2

Observable	SRb1	SRb2
Trigger	$E_{\mathrm{T}}^{\mathrm{miss}}$	
$\mathcal{N}_j$	≥ 2	2 or 3
$\mathcal{N}_b^{\mathrm{T}}$	≥ 1	≥ 2
$\mathcal{N}_\ell^{\mathrm{B}}$	0	
$E_{\mathrm{T}}^{\mathrm{miss}}$ [GeV]	> 650	> 180
$p_{\mathrm{T}}(bj_1)$ [GeV]	> 160	> 150
$p_{\mathrm{T}}(j_1)$ [GeV]	> 160	> 150
$p_{\mathrm{T}}(j_2)$ [GeV]	> 160	> 20
$p_{\mathrm{T}}(j_3)$ [GeV]	–	< 60
H_{T3} [GeV]	< 100	–
$H_{\mathrm{T}}^{\mathrm{ratio}}$	–	> 0.75
δ^- [rad]	–	< 0
δ^+ [rad]	–	< 0.5
Multi-jet rejection specific		
$\Delta\phi(\mathrm{j}, \vec{p}_{\mathrm{T}}^{\mathrm{miss}})$ [rad]	> 0.6	> 0.4

The azimuthal separations between the b-tagged jets ($\Delta\phi_{bb}$) and the $\Delta\phi(\mathrm{j}, \vec{p}_{\mathrm{T}}^{\mathrm{miss}})$ are exploited to enhance the separation between the signal and the irreducible background in this channel ($Z(\nu\bar{\nu})+b\bar{b}$), as the latter is characterised by small $\Delta\phi_{bb}$ values when the b-jets originate from the gluon-splitting process. Linear combinations of these two variables are used to define the selection criteria in Table 2:

$$\delta^- = \Delta\phi(\mathrm{j}, \vec{p}_{\mathrm{T}}^{\mathrm{miss}}) - \Delta\phi_{bb},$$
$$\delta^+ = |\Delta\phi(\mathrm{j}, \vec{p}_{\mathrm{T}}^{\mathrm{miss}}) + \Delta\phi_{bb} - \pi|.$$

An additional handle to discriminate between the $b\bar{b} + \phi$ and $b\bar{b} + a$ signal models and the background is the spin of the particle decaying into invisible decay products. It was shown in Ref. [91] that it is possible to discriminate between such scalar, pseudoscalar and vector particles by exploiting information about the production angle of the visible particles with respect to the proton beam axis. A convenient variable to exploit this feature, proposed in Ref. [92] relies on the pseudorapidity difference between the two b-tagged jets ($\Delta\eta_{bb}$):

$$\cos\theta_{bb}^* = \left|\tanh\left(\frac{\Delta\eta_{bb}}{2}\right)\right|.$$

The variable $\cos\theta_{bb}^*$, evaluated in the laboratory frame, is the key observable used in SRb2 to discriminate the signal from the background. The distribution of $\cos\theta_{bb}^*$ is approximately flat for b-jets produced in association with scalar or vector particles with masses below 100 GeV, while it exhibits a pronounced enhancement at values near one for pseudoscalar particles in the same mass range. In order to further enhance the sensitivity to the signal, the signal region SRb2 is divided into four independent bins in $\cos\theta_{bb}^*$: SRb2-bin1 (0, 0.25), SRb2-bin2 (0.25, 0.5), SRb2-bin3 (0.5, 0.75), SRb2-bin4 (0.75, 1.0), which are statistically combined in the final result.

4.2 Signatures with top quarks and $E_{\mathrm{T}}^{\mathrm{miss}}$

Events assigned to SRt1 and SRt2 are required to contain at least four jets. At least two jets in every event must be b-tagged at the medium working-point ($\mathcal{N}_b^{\mathrm{M}}$). Events containing baseline electrons and muons are discarded. Furthermore, events with a τ-candidate are also rejected ($\mathcal{N}_\tau = 0$). The τ-candidate is defined as a jet with less than four associated tracks which has not passed the medium b-tagging requirement and which has a ϕ separation from the $\vec{p}_{\mathrm{T}}^{\mathrm{miss}}$ of no more than $\pi/5$ radians. Events are required to pass the missing transverse momentum trigger and to satisfy $E_{\mathrm{T}}^{\mathrm{miss}} > 300$ GeV. Also in this SRs, a minimum $\Delta\phi(\mathrm{j}, \vec{p}_{\mathrm{T}}^{\mathrm{miss}})$ requirement is applied in order to reject events with $E_{\mathrm{T}}^{\mathrm{miss}}$ arising from mismeasurements and semileptonic decays of hadrons inside jets. Further rejection of such events is achieved by additional requirements on the missing transverse momentum computed using only the information from the tracking system ($\vec{p}_{\mathrm{T}}^{\mathrm{miss,track}}$, with magnitude $E_{\mathrm{T}}^{\mathrm{miss,track}}$) and its angle with respect to the $\vec{p}_{\mathrm{T}}^{\mathrm{miss}}$ ($\Delta\phi(\vec{p}_{\mathrm{T}}^{\mathrm{miss}}, \vec{p}_{\mathrm{T}}^{\mathrm{miss,track}})$). The dominant backgrounds for these signal regions are top-quark pair production, Z+jets, and the production of a Z boson in association with $t\bar{t}$. Four main observables are exploited to discriminate DM signal events from the SM background processes: $m_{\mathrm{T}}^{b,\mathrm{min}}$, $m_{\mathrm{T}}^{b,\mathrm{max}}$, $E_{\mathrm{T}}^{\mathrm{miss,\,sig}}$, and ΔR_{bb}. The variables $m_{\mathrm{T}}^{b,\mathrm{min}}$ and $m_{\mathrm{T}}^{b,\mathrm{max}}$ are defined as the transverse mass[3] of the $\vec{p}_{\mathrm{T}}^{\mathrm{miss}}$ vector and b-tagged jet with the smallest and largest angular distance[4] from it, respectively. The $m_{\mathrm{T}}^{b,\mathrm{min}}$ variable is designed to be bounded from above by the top-quark mass for semileptonic $t\bar{t}$ decays, because the closest b-tagged jet to the $\vec{p}_{\mathrm{T}}^{\mathrm{miss}}$ vector usually belongs to the leg of the decay where the W boson decays into leptons. The variable $m_{\mathrm{T}}^{b,\mathrm{max}}$ recovers the discriminating power in the case of wrong pairing. The $E_{\mathrm{T}}^{\mathrm{miss,\,sig}}$ variable is defined as the ratio of the $E_{\mathrm{T}}^{\mathrm{miss}}$ to the square-root of the scalar sum of the transverse momenta of all jets in the events (H_{T}) to discriminate the high-mediator-mass signal models in SRt2 from the SM background. Finally, the angular distance between the two

[3] The transverse mass of two particles a and b is defined as $m_{\mathrm{T}}(a,b) = \sqrt{(E_{\mathrm{T},a} + E_{\mathrm{T},b})^2 - (\vec{p}_{\mathrm{T},a} + \vec{p}_{\mathrm{T},b})^2}$.

[4] The angular separation between two particles a, b used in all quantities described in this section is defined as $\Delta R_{ab} = \sqrt{(\Delta\phi_{ab})^2 + (\Delta\eta_{ab})^2}$.

Table 3 Summary of the kinematic and topology-dependent selections for signal regions SRt1, SRt2 and SRt3

Observable	SRt1	SRt2	SRt3
Trigger		$E_{\mathrm{T}}^{\mathrm{miss}}$	2ℓ
$\mathcal{N}_j$		≥ 4	≥ 1
$\mathcal{N}_b^{\mathrm{M}}$		≥ 2	≥ 1
$\mathcal{N}_\ell^{\mathrm{B}}$		0	–
$\mathcal{N}_\ell^{\mathrm{M}}$		–	2 OS
$\mathcal{N}_\tau$		0	–
$E_{\mathrm{T}}^{\mathrm{miss}}$ [GeV]		> 300	–
$p_{\mathrm{T}}(bj_1)$ [GeV]		> 20	> 30
$p_{\mathrm{T}}(j_1, j_2)$ [GeV]		$> 80, 80$	> 30
$p_{\mathrm{T}}(j_3, j_4)$ [GeV]		$> 40, 40$	–
$p_{\mathrm{T}}(\ell_1, \ell_2)$ [GeV]		–	$> 25, 20$
$m_{\ell\ell}$ [GeV]		–	> 20
$\lvert m_{\ell\ell}^{\mathrm{SF}} - m_Z \rvert$ [GeV]		–	> 20
$m_{\mathrm{R}=0.8}^{\mathrm{jet}\ 1,2}$ [GeV]	$> 80, 80$	–	–
$m_{\mathrm{R}=1.2}^{\mathrm{jet}\ 1,2}$ [GeV]	–	$> 140, 80$	–
$m_{\mathrm{T}}^{b,\mathrm{min}}$ [GeV]	> 150	> 200	–
$m_{\mathrm{T}}^{b,\mathrm{max}}$ [GeV]	> 250	–	–
ΔR_{bb}	> 1.5	> 1.5	–
$E_{\mathrm{T}}^{\mathrm{miss,\ sig}}$ [$\sqrt{\mathrm{GeV}}$]	–	> 12	–
$\Delta\phi_{\mathrm{boost}}$ [rad]		–	< 0.8
$m_{b2\ell}^{\mathrm{min}}$ [GeV]		–	< 170
ξ^+ [GeV]		–	> 170
$m_{\mathrm{T2}}^{\ell\ell}$ [GeV]		–	> 100
Multi-jet rejection specific			
$\Delta\phi(\mathrm{j}, \vec{p}_{\mathrm{T}}^{\mathrm{miss}})$ [rad]		> 0.4	–
$E_{\mathrm{T}}^{\mathrm{miss,track}}$ [GeV]		> 30	–
$\Delta\phi(\vec{p}_{\mathrm{T}}^{\mathrm{miss}}, \vec{p}_{\mathrm{T}}^{\mathrm{miss,track}})$ [rad]		$< \pi/3$	–

b-tagged jets in the event (ΔR_{bb}) is exploited to suppress $Z(\nu\nu)$+$b\bar{b}$ events where the two b-quarks arise from gluon-splitting and are characterised by a small angular separation.

The SRt1 selection is optimised for low-mass spin-0 mediators ($m(\phi/a) < 100$ GeV). Requirements on the two leading reclustered jet masses with radius 0.8 ($m_{\mathrm{R}=0.8}^{\mathrm{jet}\ 1}$, $m_{\mathrm{R}=0.8}^{\mathrm{jet}\ 2}$) exploit the presence of boosted hadronic decays of W bosons from top quarks in the event. The requirements applied in SRt1 are such that both reclustered jets are compatible with a W-boson candidate. The SRt2 signal region is optimised instead for high-mass spin-0 mediators (100 GeV $< m(\phi/a) <$ 350 GeV). Requirements on the two leading reclustered jet masses with radius 1.2 ($m_{\mathrm{R}=1.2}^{\mathrm{jet}\ 1}$, $m_{\mathrm{R}=1.2}^{\mathrm{jet}\ 2}$) are used to exploit the more boosted topology of these signal events compared to the backgrounds. The requirements applied in SRt2 are such that the leading large-radius jet is compatible with a top-quark candidate and the subleading large-radius jet is compatible with a W-boson candidate. The specific requirements for each discriminating observable in SRt1 and SRt2 are summarised in Table 3.

Finally, events assigned to SRt3 are required to have exactly two opposite-sign leptons ($\mathcal{N}_\ell^{\mathrm{M}} = 2$ OS), electrons or muons, either same- or different-flavour, with an invariant mass (regardless of the flavours of the leptons in the pair), $m_{\ell\ell}$, being larger than 20 GeV. In addition, for same-flavour lepton pairs, events with $m_{\ell\ell}$ within 20 GeV of the Z-boson mass are vetoed. Furthermore, candidate signal events are required to have at least one medium b-tagged jet. Events are required to pass the two-lepton triggers and the leading and subleading lepton transverse momenta in the event are required to be at least 25 and 20 GeV, respectively, which also guarantees that the plateau of efficiency of the triggers is reached. The main reducible backgrounds for this analysis are dileptonic $t\bar{t}$ decays, Z + jets and dibosons. The main handle for the rejection of these backgrounds is the lepton-based "stransverse mass", $m_{\mathrm{T2}}^{\ell\ell}$ [93–95], which is a kinematic

variable with an endpoint at the W-boson mass for events containing two W bosons decaying into leptons. In this selection it is used in linear combination with the $E_{\mathrm{T}}^{\mathrm{miss}}$, in order to maximise the discrimination power of the two variables [91]:

$$\xi^{+} = m_{\mathrm{T2}}^{\ell\ell} + 0.2 \cdot E_{\mathrm{T}}^{\mathrm{miss}}.$$

Further requirements are placed on $\Delta\phi_{\mathrm{boost}}$ [93], the azimuthal angular distance between $\vec{p}_{\mathrm{T}}^{\mathrm{miss}}$ and the vector sum of $\vec{p}_{\mathrm{T}}^{\mathrm{miss}}$ and the transverse momentum of the leptons, and on $m_{b2\ell}^{\mathrm{min}}$, which is the smallest invariant mass computed between the b-tagged jet and each of the two leptons in the event. Both variables are used to further reject residual contamination from reducible backgrounds for this selection. The variable $\Delta\phi_{\mathrm{boost}}$, can be interpreted as the azimuthal angular difference between the $\vec{p}_{\mathrm{T}}^{\mathrm{miss}}$ and the opposite of the vector sum of all the transverse hadronic activity in the event. The requirement on this variable reject $Z(\ell^{+}\ell^{-})$+jets events where the $E_{\mathrm{T}}^{\mathrm{miss}}$ arises from jet mismeasurements, while retaining a large fraction of the signal. In events with two top quarks decaying dileptonically such as in the signal topology, at least one of the two mass combinations must be bounded from above by $m_{b2\ell}^{\mathrm{min}} < \sqrt{m_t^2 - m_W^2}$. This variable helps to reject residual reducible backgrounds, while retaining 99% of the signal. The specific requirements for SRt3 are summarised in Table 3.

5 Background estimation

The SM backgrounds contributing to each of the five SRs are estimated with the aid of the MC simulation and using control regions (CRs) constructed to enhance a particular background and to be kinematically similar but orthogonal to the SRs. The expected background is determined separately in each SR through a profile likelihood fit based on the HistFitter package [96]. The CR yields constrain the normalisation of the dominant SM background processes. Such normalisation factors are treated as free fit parameters and are uncorrelated between fits of different SRs. The systematic uncertainties are included as nuisance parameters in the fit. In the case of a "background-only" fit set-up, only the CRs are considered and the signal contribution is neglected. The number of background events predicted by simulation in the SRs is normalised according to the results of the fit. When computing exclusion limits as described in Sect. 7, the SRs are also used to constrain the background predictions. The non-dominant SM backgrounds are determined purely from MC simulation, except fake or non-prompt lepton backgrounds (arising from jets misidentified as leptons or produced in either hadron decays or photon conversions) and the multi-jet background, both of which are estimated using a data-driven method described below. The background estimates in the SRs are validated by extrapolating the results of the likelihood fit in the CRs to dedicated validation regions (VRs), which are designed to be orthogonal to both the signal and control regions. In all CRs and VRs used in this analysis the signal contamination was found to be negligible.

An important source of background for all 0-lepton signal regions is Z bosons decaying into neutrinos when produced in conjunction with one or more jets emanating from heavy-flavour quarks. Production of top-quark pairs is a substantial background source for all selections except for SRb1, where the very high $E_{\mathrm{T}}^{\mathrm{miss}}$ requirement rejects this background. More specifically, top-quark pairs with at least one of the W bosons decaying into leptons (where the lepton is either a non-identified electron or muon, or a hadronically decaying τ lepton) enter SRb2, SRt1 and SRt2, while events with both W-bosons decaying into leptons enter SRt3. Events from $t\bar{t}+Z$ production, when the Z boson decays into neutrinos, are an irreducible background for the three SRs targeting dark matter produced in association with top quarks.

The normalisation factor for the background arising from $Z \to \nu\bar{\nu}$ events is estimated from data in CRs with two tight same-flavour opposite-sign (SFOS) leptons ($\ell = (e, \mu)$) and an invariant mass compatible with the Z-boson mass. For these CRs, labelled in the following as CRZt1, CRZt2, CRZb1 and CRZb2, the p_{T} of the leptons is added vectorially to the $\vec{p}_{\mathrm{T}}^{\mathrm{miss}}$ to mimic the expected missing transverse momentum spectrum of $Z \to \nu\bar{\nu}$ events, and is denoted in the following by $E_{\mathrm{T},\ell\ell}^{\mathrm{miss}}$. Observables that make use of $E_{\mathrm{T}}^{\mathrm{miss}}$ in their definition are recalculated for these regions by using $E_{\mathrm{T},\ell\ell}^{\mathrm{miss}}$ instead. These variables are $\delta_{\ell\ell}^{-}$, $\delta_{\ell\ell}^{+}$, $\Delta\phi(\mathrm{j}, \vec{p}_{\mathrm{T},\ell\ell}^{\mathrm{miss}})$, $m_{\mathrm{T},\ell\ell}^{b,\mathrm{min}}$, $m_{\mathrm{T},\ell\ell}^{b,\mathrm{max}}$ and $E_{\mathrm{T},\ell\ell}^{\mathrm{miss,\,sig}}$.

Single tight-lepton CRs, denoted by CRTb2, CRTt1 and CRTt2, are used to estimate the background from top-quark pairs in SRb2, SRt1 and SRt2. The transverse mass[5] (m_{T}) of the lepton and the $\vec{p}_{\mathrm{T}}^{\mathrm{miss}}$, and the angular distance between the lepton and the b-tagged jet closest to it ($\Delta R_{b\ell}^{\mathrm{min}}$) are used to enhance the purity of top-quark events. In CRTt1 and CRTt2 the lepton is treated as a jet, in order to better mimic the type of background events that contaminate the corresponding SR. The dileptonic top background, which contaminates SRt3, is instead estimated in a two-medium-leptons CR composed of events that fail the ξ^{+} requirement (CRTt3).

Finally, $t\bar{t}+V$ events, and in particular $t\bar{t}+Z$ events where the Z boson decays into neutrinos, represent the irreducible background for the three SRs targeting dark matter produced in association with top quarks. This background is estimated from data using two CRs. To estimate the normalisation factor for the $t\bar{t}+Z$ background in SRt1 and SRt2

[5] The transverse mass in this case is calculated by neglecting the lepton masses.

a control region of $t\bar{t}+\gamma$ events (CRγ) is used. Events with $p_{\mathrm{T}\gamma} > m_{\mathrm{Z}}$ are selected, for which the kinematic properties resemble those of $t\bar{t}+Z(\nu\nu)$. The CRγ contains events with exactly one energetic tight photon ($\mathcal{N}_\gamma = 1$) and at least one lepton from the decay of the $t\bar{t}$ system. This strategy substantially increases the number of events at large missing transverse momentum and allows CRγ to better mimic the hard kinematic requirements of SRt1 and SRt2. Furthermore, the p_{T} of the photon is added vectorially to the $\vec{p}_{\mathrm{T}}^{\,\mathrm{miss}}$ to mimic the expected missing transverse momentum spectrum of $Z \to \nu\bar{\nu}$ events. The variable obtained with this procedure is referred to as $E_{\mathrm{T},\gamma}^{\mathrm{miss}}$ in the following.

A second control region (CR3ℓ), is used for the background normalisation of SRt3. It makes use of $t\bar{t}+Z$ events with $Z \to \ell^+\ell^-$ and semileptonic decays of the $t\bar{t}$ system (e or μ). CR3ℓ is obtained by selecting three medium leptons out of which one SFOS pair is compatible with a Z-boson decay. This strategy allows the modelling of the lower $E_{\mathrm{T}}^{\mathrm{miss}}$ part of the SRt3 signal region. Additionally, the momenta of the leptons compatible with the Z-boson decay are added vectorially to the $\vec{p}_{\mathrm{T}}^{\,\mathrm{miss}}$ to define $\vec{p}_{\mathrm{T},\ell\ell}^{\,\mathrm{miss}}$ and $E_{\mathrm{T},\ell\ell}^{\mathrm{miss}}$ for this control region. The transverse mass of the $\vec{p}_{\mathrm{T},\ell\ell}^{\,\mathrm{miss}}$ and the lepton not associated with the Z-boson decay, $m_{\mathrm{T}}^{\ell\ell}$, is combined with the $E_{\mathrm{T},\ell\ell}^{\mathrm{miss}}$ to define a corrected ξ^+: $\xi_{\ell\ell}^{+} = m_{\mathrm{T}}^{\ell\ell} + 0.2 \cdot E_{\mathrm{T},\ell\ell}^{\mathrm{miss}}$. A requirement is placed on this variable in CR3ℓ in order to approximate the kinematic properties of the signal region. The $m_{b2\ell}^{\mathrm{min}}$ variable is redefined in this region ($m_{2b\ell}^{\mathrm{min}}$) as the smaller of the two transverse masses calculated when combining the lepton not associated with the Z-boson decay and each of the two b-tagged jets in the event.[6] All CR selections are summarised in Table 4.

The relatively small contamination of SRt3 and CR3ℓ from events with fake or non-prompt (NP) leptons is estimated from data with a method similar to that described in Refs. [97,98]. Different processes contribute to this background for the two selections. The dominant fake or non-prompt lepton contribution for SRt3 comes from semileptonic $t\bar{t}$ and W+jets processes, while for CR3ℓ it comes from dileptonic $t\bar{t}$ and Z+bb processes. The method makes use of the number of observed events containing baseline–baseline, baseline–medium, medium–baseline and medium–medium lepton pairs (see definitions in Sect. 2) in a given selection. The probability for prompt leptons satisfying the baseline selection criteria to also pass the medium selection is measured using a $Z \to \ell\ell$ sample. The equivalent probability for fake or non-prompt leptons is measured from multi-jet- and $t\bar{t}$-enriched control samples. The number of events containing a contribution from one or two fake or non-prompt leptons is calculated from these probabilities.

[6] When the b-tagged jet multiplicity is different from two, the two jets with the highest b-tagging probabilities are chosen, independently of whether they are b-tagged or not.

The background from multi-jet production for the regions with no leptons is estimated from data using a procedure described in detail in Ref. [99] and modified to account for the heavy flavour of the jets. The contribution from multi-jet production in all regions is found to be very small.

Minor background contributions to each signal region are collectively called "Others" in the following. For SRb1 and SRb2, this category contains the contributions from multi-jet, single top-quark production, diboson production, $t\bar{t}+V$ and W+jets. For SRt1 and SRt2, multi-jet, $V+\gamma$, diboson, single top-quark and $t\bar{t}$ production in association with Higgs or W boson(s) collectively define "Others". Finally, for SRt3 the "Others" category contains the contributions from $t\bar{t}+W/h/WW$, $t\bar{t}\,t\bar{t}$, $t\bar{t}t$, Wh, $(gg)h$ and Zh production.

In summary, one scaling factor is used to normalise the Z+jets background in SRb1, while two scaling factors are used to normalise the Z+jets and $t\bar{t}$ backgrounds in SRb2. For SRt1 and SRt2, three scaling factors for each region are used to independently normalise the Z+jets, $t\bar{t}$ and $t\bar{t}+Z$ backgrounds. Finally, in SRt3 the $t\bar{t}$ and $t\bar{t}+Z$ predictions are adjusted by a floating normalisation for each of the two backgrounds. The background scaling factors are treated as fully uncorrelated between the different SRs. In all selections, it is found that the normalisation of the Z+jets background is larger than unity. This may be related to the fact that in the default SHERPA v2.2.1 generator the heavy-flavour production fractions are not consistent with the measured values [100]. The normalisation factors for $t\bar{t}$ processes in the SRtX regions are found to be compatible with unity, while they are found to be considerably smaller than unity for SRb2. This is due to the angular separation requirements in this region, which select $t\bar{t}$ events in a specific corner of the phase space. Finally, the different normalisations of the $t\bar{t}+Z$ background processes found in the CRγ and CR3ℓ regions (larger and smaller than unity, respectively) are due to the different kinematic requirements on the jet momenta and the corrected $E_{\mathrm{T}}^{\mathrm{miss}}$ in the two regions, which are designed to mimic the topology of the respective signal regions.

Dedicated validation regions are used to validate the background prediction for each of the SRs and evaluate the reliability of the MC extrapolation of the SM background estimates from CRs to SRs. The background estimates in SRb2 are validated in a single VR (VRb2) which has a background composition similar to that of the SR. Selected key distributions in the control and validation regions are shown in Fig. 2. The prediction of the Z+jets background in SRb1 relies on an extrapolation over a large interval of missing transverse momentum. As CRZb1 is designed to be kinematically as close as possible to SRb1 and given the low yield in this region, it was not possible to construct a selection to validate this extrapolation. Nevertheless, the use of the same kinematic selection in control and signal region, together with the good agreement between the data and the post-fit SM

Table 4 Summary of the control region selections. Only the topological requirements modified with respect to Tables 2 and 3 are indicated. The symbol $\mathcal{N}_b$ refers to either $\mathcal{N}_b^{\mathrm{M}}$ or $\mathcal{N}_b^{\mathrm{T}}$ in order to be consistent with the SR definition for each region

Observable	CRZb1	CRZb2	CRZt1	CRZt2	CRTb2	CRTt1	CRTt2	CRTt3	CRγ	CR3ℓ
Trigger	1ℓ	1ℓ	1ℓ		1ℓ	$E_{\mathrm{T}}^{\mathrm{miss}}$		2ℓ	1γ	2ℓ
$\mathcal{N}_j$	≥ 2	$2-3$	≥ 4		$2-3$	≥ 3		≥ 1	≥ 4	≥ 3 ≥ 2 or ≥ 4 $= 1$
$\mathcal{N}_b$	≥ 1	≥ 2	≥ 2		≥ 2	≥ 2		≥ 1	≥ 2	
$\mathcal{N}_\ell^{\mathrm{T}}$	$= 2$ (SFOS)		$= 2$ (SFOS)		$= 1$	$= 1$		–	$= 1$	–
$\mathcal{N}_\ell^{\mathrm{M}}$	–	–	–		–	–		$= 2$ (OS)	–	3 (1 SFOS)
$\mathcal{N}_\tau$	–	–	0		–	0		–	–	–
$\mathcal{N}_\gamma$	–	–	–		–	–		$= 1$	–	–
$E_{\mathrm{T}}^{\mathrm{miss}}$ [GeV]	< 120	< 60	< 50		> 180	> 250		–	–	–
$E_{\mathrm{T},\ell\ell}^{\mathrm{miss}}$ [GeV]	> 300	> 120	> 160		–	–		–	–	> 80
$p_{\mathrm{T}}(\gamma)$ [GeV]	–	–	–		–	0		–	> 150	–
$p_{\mathrm{T}}(\ell_1)$, $p_{\mathrm{T}}(\ell_2)$ [GeV]	$> 30, > 25$	$> 30, > 25$	$> 28, > 28$		$> 30, -$	$> 28, -$		$> 25, 20$	> 28	$> 25, > 20$
Multi-jet rejection specific	As SR		no			As SR			No	As SR
m_{T} [GeV]	–	–	–		> 30	[30–100]		–	–	> 30
$\Delta R_{b\ell}^{\mathrm{min}}$ [rad]	–	–	–		–	< 1.0	< 1.5	–	–	–
$\lvert m_{\ell\ell} - m_Z \rvert$ [GeV]	< 20	< 30	< 5		–	–		as SR	–	< 10
$\Delta\phi(\mathrm{j}, \vec{p}_{\mathrm{T},\ell\ell}^{\mathrm{miss}})$ [rad]	> 0.6	–	–		–	–		–	–	–
$H_{\mathrm{T}}^{\mathrm{ratio}}$	–	> 0	–		as SR	–		–	–	–
$\delta_{\ell\ell}^{-}$, $\delta_{\ell\ell}^{+}$ [rad]	–	$< 1, < 0.5$	–		as SR	–		–	–	–
$m_{\mathrm{R=SR}}^{\mathrm{jet\ 0}}$ [GeV]	–	–	> 60	> 60	–	> 60	> 140	–	–	–
$m_{\mathrm{R=SR}}^{\mathrm{jet\ 1}}$ [GeV]	–	–	–		–	> 60	> 80	–	–	–
$m_{\mathrm{T}}^{b,\mathrm{min}}$ [GeV]	–	–	–		–	> 100		–	–	–
$m_{\mathrm{T}}^{b,\mathrm{max}}$ [GeV]	–	–	–		–	–		–	–	–
$m_{\mathrm{T},\ell\ell}^{b,\mathrm{min}}$ [GeV]	–	–	–	> 100	–	–		–	–	–
$m_{\mathrm{T},\ell\ell}^{b,\mathrm{max}}$ [GeV]	–	–	> 100	–	–	–		–	–	–
ΔR_{bb}	–	–	0		–	1.5		–	–	–
$E_{\mathrm{T},\ell\ell}^{\mathrm{miss,\ sig}}$ [$\sqrt{\mathrm{GeV}}$]	–	–	–	> 6	–	–		–	–	–
ξ^{+} [GeV]	–	–	–		–	–		< 150	–	–
$m_{b2\ell}^{\mathrm{min}}$ [GeV]	–	–	–		–	–		< 170	–	–
$\xi_{\ell\ell}^{+}$ [GeV]	–	–	–		–	–		–	–	> 120
$m_{2b\ell}^{\mathrm{min}}$ [GeV]	–	–	–		–	–		–	–	< 170

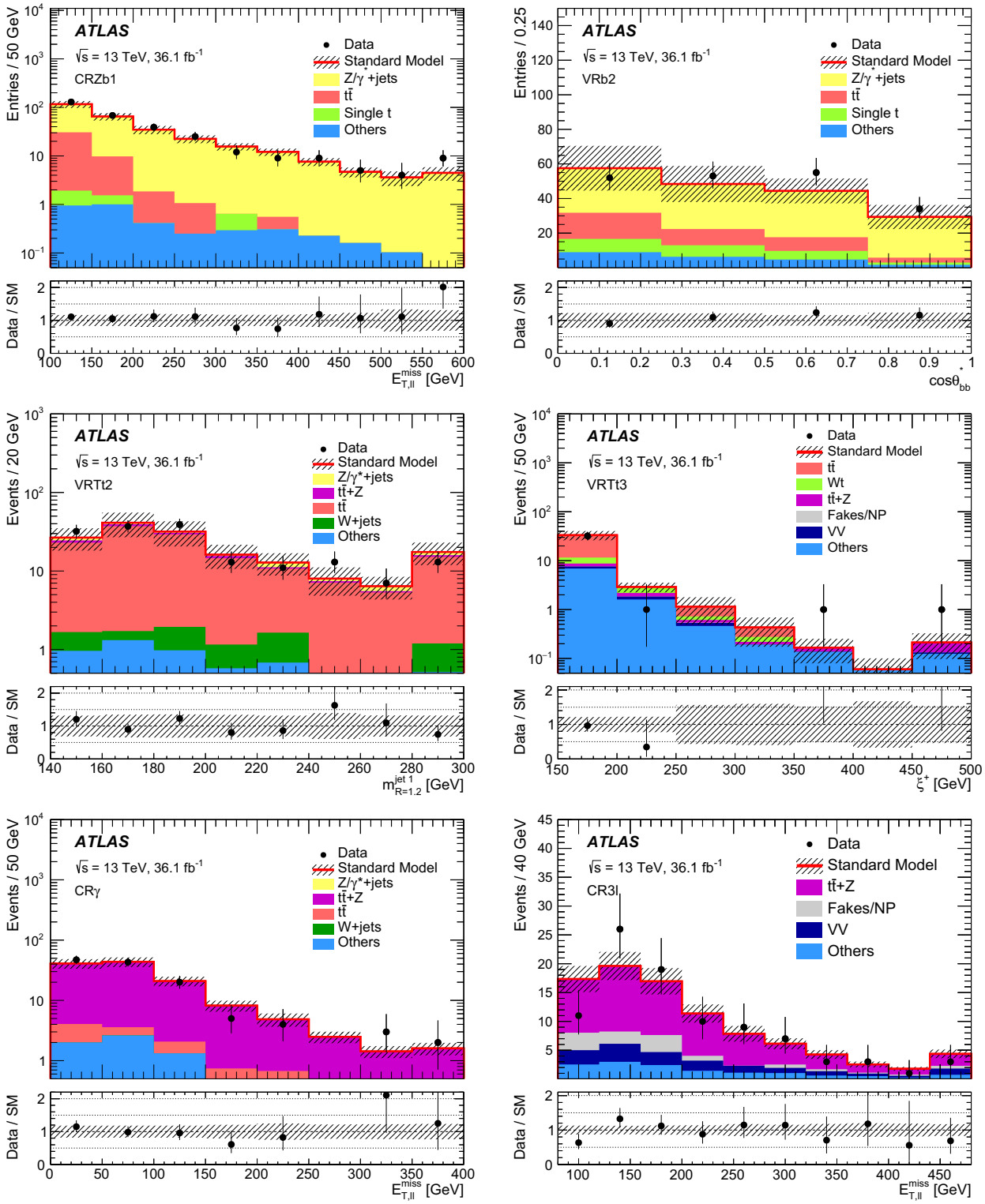

Fig. 2 Comparison of the data with the post-fit Monte Carlo prediction of some kinematic distributions in control and validation regions. The bottom panel shows the ratio of the data to the Monte Carlo prediction. The band includes all systematic uncertainties defined in Sect. 6. The last bins include overflows, where applicable. The top left panel shows the $E_{\mathrm{T},\ell\ell}^{\mathrm{miss}}$ distribution in CRZb1. The $E_{\mathrm{T},\ell\ell}^{\mathrm{miss}}$ requirement is relaxed to 100 GeV. The other panels show the $\cos\theta_{bb}^{*}$ distribution in VRb2 (top right), the $m_{\mathrm{R=1.2}}^{\mathrm{jet\ 1}}$ distribution in VRTt2 (middle left), the ξ^{+} distribution the VRTt3 (middle right), the $E_{\mathrm{T},\ell\ell}^{\mathrm{miss}}$ distribution in CRγ (bottom left) and the $E_{\mathrm{T},\ell\ell}^{\mathrm{miss}}$ distribution in CR3ℓ (bottom right)

Table 5 Summary of the validation region selections. See Tables 2 and 3 for the detailed multi-jet rejection requirements

Observable	VRb2	VRZt1	VRZt2	VRTt1	VRTt2	VRTt3
Trigger	$E_{\mathrm{T}}^{\mathrm{miss}}$	$E_{\mathrm{T}}^{\mathrm{miss}}$			$E_{\mathrm{T}}^{\mathrm{miss}}$	$2\mu\|\|2e\|\|1e1\mu$
$\mathcal{N}_j$	$2-3$	≥ 4			≥ 4	≥ 1
$\mathcal{N}_b$	≥ 2	≥ 2			≥ 2	≥ 1
$\mathcal{N}_\ell$				As SR		
τ multiplicity	–	–			0	–
$E_{\mathrm{T}}^{\mathrm{miss}}$ [GeV]	> 180	> 250			> 300	–
$p_{\mathrm{T}}(j_1, j_2)$ [GeV]	$> 150, > 20$	$> 80, > 80$			$> 80, > 80$	$> 30, -$
$p_{\mathrm{T}}(j_3, j_4)$ [GeV]	$< 60, -$	$> 40, > 40$			$> 40, > 40$	–
$p_{\mathrm{T}}(bj_1)$ [GeV]	> 150	> 20			> 20	> 30
$p_{\mathrm{T}}(\ell_1, \ell_2)$ [GeV]	–	–			–	$> 25, 20$
Multi-jet rejection				As SR		
$\lvert m_{\ell\ell}^{\mathrm{SF}} - m_Z \rvert$ [GeV]	–	–			–	> 20
δ^-, δ^+ [rad]	$< 0, > 0.5$	–			–	–
$m_{\mathrm{R=SR}}^{\mathrm{jet\ 0}}$ [GeV]	–	< 80	< 140	> 80	> 140	–
$m_{\mathrm{R=SR}}^{\mathrm{jet\ 1}}$ [GeV]	–	–		> 40	> 50	–
$m_{\mathrm{T}}^{b,\mathrm{min}}$ [GeV]	–	> 150		(80, 150)	(100, 200)	–
$m_{\mathrm{T}}^{b,\mathrm{max}}$ [GeV]	–	> 250	–	> 200	–	–
ΔR_{bb}	–	< 1.5		> 0.8	> 1.0	–
$E_{\mathrm{T}}^{\mathrm{miss,\ sig}}$ [$\sqrt{\mathrm{GeV}}$]	–	> 12	–	–	> 10	–
$\xi^+, m_{b2\ell}^{\mathrm{min}}, m_{\mathrm{T2}}^{\ell\ell}$ [GeV]	–	–			–	as SR
$\Delta\phi_{\mathrm{boost}}$ [rad]	–	–			–	> 1.5

prediction in CRZb1 in the whole $E_{\mathrm{T},\ell\ell}^{\mathrm{miss}}$ spectrum (Fig. 2) gives confidence in the accuracy of the estimate. Two validation regions, VRZt1 and VRZt2, are designed to validate the Z+jets estimate in SRt1 and SRt2. Furthermore, the top background estimate in these SRs is validated in two additional VRs: VRTt1 and VRTt2. Finally, VRTt3 is designed to validate the top background prediction in SRt3. All requirements for each validation region are summarised in Table 5. The data and the post-fit Monte Carlo background prediction yields in each CR and VR are compared in Fig. 3. The background yields in the control regions match the observed data by construction. In the validation regions, the background prediction is compatible with the observed data within two standard deviations of the total systematic uncertainty.

6 Systematic uncertainties

Experimental and theoretical sources of systematic uncertainty in the signal and background estimates are considered in this analysis. Their impact is constrained overall through the normalisation of the dominant backgrounds in the control regions defined with kinematic selections resembling those of the corresponding signal region.

The dominant sources of detector-related systematic uncertainty are the jet energy scale, the jet energy resolution, the b-tagging efficiency and mis-tagging rates, and the scale and resolution of the $E_{\mathrm{T}}^{\mathrm{miss}}$ soft term. The jet energy scale and resolution uncertainties are derived as a function of the p_{T} and η of the jet, as well as of the pile-up conditions and the jet flavour composition of the selected jet sample [37]. Uncertainties associated with the modelling of the b-tagging efficiencies for b-jets, c-jets and light-flavour jets [101,102] are derived as a function of η, p_{T} and flavour of each jet. The systematic uncertainties related to the modelling of $E_{\mathrm{T}}^{\mathrm{miss}}$ in the simulation are estimated by propagating the uncertainties in the energy and momentum scale of all identified electrons, photons, muons and jets, as well as the uncertainties in the soft-term scale and resolution [49]. Other detector-related systematic uncertainties, such as those in the lepton and photon reconstruction efficiency, energy scale and energy resolution, and in the modelling of the trigger [43], are found to have a small impact on the results.

Uncertainties in the theoretical modelling of the SM background processes from MC simulation are also taken into account. The uncertainties in the modelling of the $t\bar{t}$ process are estimated by varying the renormalisation and factorisation scales, as well as the amount of initial- and final-state radiation used to generate the samples [55]. The uncertainty connected with the parton-shower modelling is estimated as the difference between the predictions from POWHEG showered with PYTHIA or HERWIG. Additionally, the uncertainty

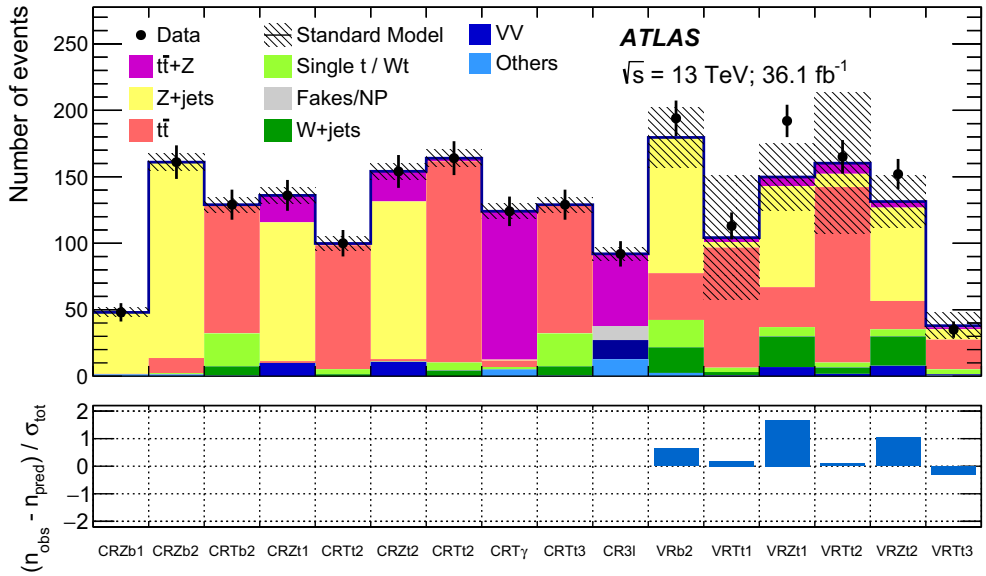

Fig. 3 Comparison of the data with the post-fit SM prediction of the background in each control and validation region. The different background components are denoted by the colour specified in the legend. All systematic uncertainties defined in Sect. 6 and statistical uncertainties are included in the shaded band. The lower panel shows the pulls in each VR. The total uncertainty σ_{tot} includes systematic and Poisson uncertainties for each given region

related to the choice of event generator is evaluated by comparing the POWHEG and MADGRAPH5_AMC@NLO predictions [55] for SRb1, SRb2 and SRt3. Due to the higher jet multiplicity required in SRt1 and SRt2 the generator uncertainty is evaluated instead by comparing the POWHEG and SHERPA predictions. The uncertainties in the modelling of the Z background are accounted for by varying the default renormalisation, factorisation, resummation and matching scales of the SHERPA samples. For SRt1 and SRt2 an additional uncertainty is included to account for effects on the ΔR_{bb} modelling not captured by the scale variations. This is estimated as the difference between the observed yield in data and the post-fit background prediction plus one times its uncertainty in each of the VRZs. The theoretical uncertainty connected with the $t\bar{t}Z$ background in SRt1 and SRt2 is estimated by varying independently the renormalisation, factorisation, resummation and matching scales in the $t\bar{t}Z$ and $t\bar{t}\gamma$ samples in signal and control regions, respectively. PDF uncertainties (estimated by varying the parametrisation of the PDF set used to generate the simulated background samples) are found to have a non-negligible impact for this background component and are treated as correlated between signal and control regions. An additional uncertainty in the extrapolation between control and signal region is derived as the difference between the ratio of the $t\bar{t}\gamma$ and $t\bar{t}Z$ cross-section predictions obtained with the nominal MC generator and with the alternative MC generator SHERPA interfaced to OPENLOOPS. For SRt3, SRb1 and SRb2 the uncertainty connected with the $t\bar{t}Z$ background estimation is assessed by varying the renormalisation, factorisation, resummation and matching scales.

Systematic uncertainties are assigned to the estimated background from fake or non-prompt leptons in SRt3 to account for potentially different compositions (heavy flavour, light flavour or conversions) between the signal regions and the control regions used for the fake-rate extraction, as well as the contamination from prompt leptons in the regions used to measure the probabilities for loose fake or non-prompt leptons to satisfy the tight signal criteria. Table 6 summarises the contributions from the different sources of systematic uncertainty in the total SM background predictions for the different signal regions after the fit to the control regions described in Sect. 5. As can be seen, the contribution from the theoretical uncertainty in the $t\bar{t}$ background and the contribution from the statistical uncertainty connected with the use of Monte Carlo simulations are higher in SRt1 than in SRt2. The reason for the higher contribution from the theoretical uncertainty in the $t\bar{t}$ background is primarily due to the larger relative importance of this source of background in SRt1. The reason for the higher contribution from the statistical uncertainty is connected with the W-boson background, which is predicted with low statistical precision in SRt1.

The impact of theoretical and detector-related uncertainties on the dark-matter signal acceptance is considered. The same procedure used to evaluate background uncertainties is applied for the detector-related uncertainties. The theoretical uncertainties in the acceptance are assessed by varying the factorisation, renormalisation, matching scales and par-

Table 6 Summary of the main systematic uncertainties and their impact on the total SM background prediction in each of the signal regions studied. A range is shown for the four bins composing SRb2. The total systematic uncertainty can be different from the sum in quadrature of individual uncertainties due to the correlations between them resulting from the fit to the data

	SRb1 (%)	SRb2 (%)	SRt1 (%)	SRt2 (%)	SRt3 (%)
Total systematic uncertainty	18	15–18	29	14	28
Z theoretical uncertainties	5.7	7.9–12	5.0	2.1	< 1
$t\bar{t} + Z$ theoretical uncertainties	< 1	< 1	3.3	5.3	8.4
$t\bar{t}$ theoretical uncertainties	< 1	2.7–9.8	17	5.7	11
MC statistical uncertainties	6.4	4.8–6.4	15	5.9	18
Z fitted normalisation	13	12–19	2.3	3.4	–
$t\bar{t} + Z$ fitted normalisation	–	–	2.2	3.5	7.1
$t\bar{t}$ fitted normalisation	–	1.9–4.2	3.9	1.4	2.0
Fake or non-prompt leptons	–	–	–	–	7.9
Pile-up	3.8	$< 1 - 1.4$	6.8	5.5	< 1
Jet energy resolution	1.5	1.3–6.9	7.0	< 1	< 1
Jet energy scale	7.7	5.0–10	5.0	2.8	8.2
$E_{\mathrm{T}}^{\mathrm{miss}}$ soft term	< 1	4.3–6.3	2.0	< 1	12
b-tagging	< 1	2.4–6.9	8.6	3.1	< 1

ton shower parameters. For SRb1 the total theoretical uncertainty in the acceptance is 6%, for SRb2 it is below 8%, and for SRt1, SRt2 and SRt3 it ranges from 10 to 12%. The theoretical uncertainties in the production cross-section of the signal are evaluated only for the colour-neutral mediator models, for which an NLO computation of the cross-section is available. It is estimated by considering the same scale variations used to assess the uncertainties in the acceptance, and by varying the parametrisation of the PDF set used to generate the simulated signal samples. An additional uncertainty due to the different scale adopted to evaluate the NLO cross-section and to generate the signal samples is also considered. The total theoretical uncertainty in the cross-section amounts to 9% for the on-shell regime in the mass range of $t\bar{t} + \phi/a$ signals to which the analysis is sensitive, and ranges from 9 to 30% for the off-shell regime. For the $b\bar{b} + \phi/a$ signals this uncertainty varies between 5 and 13%.

7 Results

The expected and observed yields in each of the five signal regions of this analysis are reported in Tables 7 and 8. The background-only fit to the control regions described in Sect. 5 is compared to the predictions based on the MC normalisation. The observed data is found to be compatible with the background prediction in each one of the SRs. The expected signal yields for selected benchmark models for colour-neutral and colour-charged mediators are also shown. In each SR the observed yield in data is above the expected background but within 1.3 standard deviations of its uncertainty.

Figure 4 shows a comparison between the SM predictions and the observed data for some relevant kinematic distributions in each signal region prior to the selection on the variable. The four bins of SRb2 are statistically combined in the final result. A model-independent fit set-up [96] where both the control and signal regions are included in the fit is used to derive 95% confidence level (CL) upper limits on the visible cross-section $\langle \epsilon \mathcal{A} \sigma \rangle_{95}$ of new physics beyond-the-SM (BSM) processes, defined as cross-section times acceptance times efficiency and obtained as the upper limit on the number of BSM events divided by the total integrated luminosity. The 95% CL exclusion limits are derived with the $\mathrm{CL_s}$ method [103] and summarised in Table 9 for each SR. These limits are calculated assuming no systematic uncertainties for the signal and neglecting any possible signal contamination in the control regions.

The results are also used to set limits on the production cross-section of colour-neutral and colour-charged mediator models decaying into dark-matter particles. An independent fit is used for each of the five signal regions. When deriving model-dependent limits, the expected signal yield in each fit region is considered.

For the signal, the experimental systematic uncertainties and theoretical systematic uncertainties in the acceptance are taken into account for this calculation. The experimental uncertainties are assumed to be fully correlated with those in the SM background. The theoretical systematic uncertainties in the signal cross-section are instead shown separately in the final exclusion result for the colour-neutral mediator models.

Figures 5 and 6 show upper limits at 95% CL on the signal cross-section scaled to the signal cross-section for coupling $g = 1$, denoted by $\sigma/\sigma(g = 1.0)$. These are the most stringent limits to date on $t\bar{t} + \phi/a$ models and the first ATLAS results for the $b\bar{b} + \phi/a$ models. To derive the results for the fully hadronic $t\bar{t}$ final state the region SRt1 or SRt2 providing the better expected sensitivity is used. The SRt1 was originally optimised for low-mass scalar mediators, while

Table 7 Fit results in SRb1 and SRb2 for an integrated luminosity of 36.1 fb^{-1}. The background normalisation parameters are obtained from the background-only fit in the CRs and are applied to the SRs. Pre-fit values are also shown. Small backgrounds are indicated as Others (see text for details). The dominant component of these smaller background sources in SRb1 is diboson processes. Benchmark signal models yields are given for each SR. The uncertainties in the yields include statistical uncertainties and all systematic uncertainties defined in Sect. 6

	SRb1	SRb2-bin1	SRb2-bin2	SRb2-bin3	SRb2-bin4
Observed	19	88	88	90	82
Total background (fit)	16.9 ± 3.3	77 ± 13	72 ± 11	76 ± 13	66.4 ± 9.1
Z/γ^*+ jets	14.2 ± 3.1	39.7 ± 6.3	44.4 ± 6.6	53.3 ± 9.9	55.6 ± 8.6
$t\bar{t}$	$0.58^{+0.60}_{-0.58}$	17.8 ± 6.5	13.8 ± 5.5	14.0 ± 4.7	7.0 ± 2.9
Single top quark	$0.25^{+0.42}_{-0.25}$	14.7 ± 5.8	10.2 ± 3.7	5.5 ± 3.1	2.6 ± 1.7
Others	2.0 ± 1.1	5.2 ± 3.4	$3.4^{+1.7}_{-1.6}$	2.7 ± 1.1	1.3 ± 1.0
Z/γ^*+ jets (pre-fit)	12.1	30.6	34.2	41.1	42.8
$t\bar{t}$ (pre-fit)	–	27.1	21.1	21.4	10.6
Signal benchmarks					
$m(\phi, \chi) = (20, 1)$ GeV, $g = 1$		0.238 ± 0.085	0.262 ± 0.079	0.320 ± 0.082	0.277 ± 0.080
$m(a, \chi) = (20, 1)$ GeV, $g = 1$		0.256 ± 0.065	0.199 ± 0.060	0.308 ± 0.085	0.267 ± 0.067
$m(\phi_b, \chi) = (1000, 35)$ GeV	18.6 ± 3.8				

Table 8 Fit results in SRt1, SRt2 and SRt3 for an integrated luminosity of 36.1 fb^{-1}. The background normalisation parameters are obtained from the background-only fit in the CRs and are applied to the SRs. Pre-fit values are also shown. Small backgrounds are indicated as Others (see text for details). Benchmark signal models yields are given for each SR. The uncertainties in the yields include statistical uncertainties and all systematic uncertainties defined in Sect. 6

	SRt1	SRt2	SRt3
Observed	23	24	18
Total background (fit)	20.5 ± 5.8	20.4 ± 2.9	15.2 ± 4.3
$t\bar{t}$	7.0 ± 3.9	3.1 ± 1.3	4.5 ± 2.5
$t\bar{t}$+Z	4.3 ± 1.1	6.9 ± 1.4	4.4 ± 1.9
W+jets	3.3 ± 2.6	1.28 ± 0.50	Incl. in fakes/NP
Wt	Incl. in others	Incl. in others	$0.33^{+0.53}_{-0.33}$
Z/γ^*+ jets	3.7 ± 1.4	6.2 ± 1.1	Incl. in others
VV	Incl. in others	Incl. in others	0.61 ± 0.25
Fakes/NP	–	–	2.7 ± 1.3
Others	2.2 ± 1.2	3.00 ± 1.6	2.69 ± 0.93
$t\bar{t}$ (pre-fit)	6.1	2.8	4.0
$t\bar{t}$+Z (pre-fit)	3.53	5.6	5.6
Z/γ^*+ jets (pre-fit)	3.2	5.72	–
Signal benchmarks			
$m(\phi, \chi) = (20, 1)$ GeV, $g = 1$	9.3 ± 1.6	12.8 ± 1.9	21.0 ± 2.3
$m(a, \chi) = (20, 1)$ GeV, $g = 1$	7.6 ± 1.5	12.1 ± 1.8	14.1 ± 1.6
$m(\phi, \chi) = (100, 1)$ GeV, $g = 1$	6.5 ± 1.3	10.1 ± 1.5	11.5 ± 1.5
$m(a, \chi) = (100, 1)$ GeV, $g = 1$	6.2 ± 1.2	11.5 ± 2.0	11.9 ± 1.5

SRt2 was optimised for high-mass scalar mediators and pseudoscalar mediators. However, SRt1 is strongly affected by systematic uncertainties in the $t\bar{t}$ modelling and therefore SRt2 sets more stringent limits for the whole parameter space. These limits are obtained both as a function of the mediator mass, assuming a specific DM mass of 1 GeV (Fig. 5), and as a function of the DM mass, assuming a specific mediator mass of 10 GeV (Fig. 6). Both the scalar and pseudoscalar mediator cases are considered. The sensitivity for $t\bar{t} + \phi/a$ on-shell decays is approximately constant for masses below 100 GeV, with SRt3 excluding the $g = 1$ assumption for scalar mediator masses up to 50 GeV. For a given mediator mass the acceptance of the analysis is independent of the value of the DM mass as long as $m(\phi/a) > 2 \cdot m(\chi)$ is fulfilled and width effects can be neglected. Under these conditions, exclusion limits for DM masses differing from the one presented can be inferred from the result shown in Fig. 5. Due to the smaller Yukawa enhancement of $b\bar{b} + \phi/a$ final states, it is possible to exclude cross-sections 300 times the nominal values for $g = 1$.

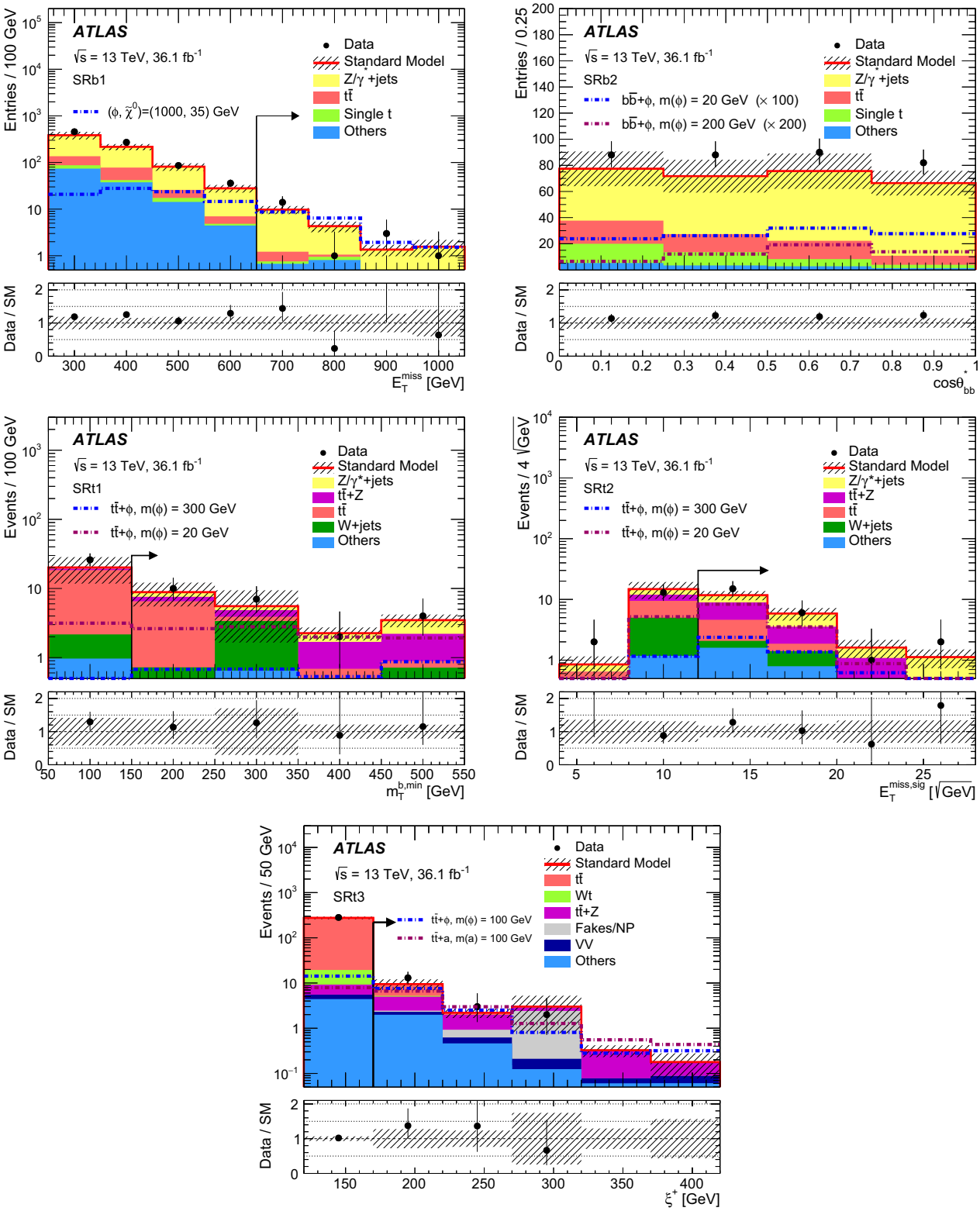

Fig. 4 Comparison of the data with the post-fit SM prediction of the $E_{\mathrm{T}}^{\mathrm{miss}}$ distribution in SRb1 (top left), $\cos\theta^{*}_{bb}$ distribution in SRb2 (top right), $m_{\mathrm{T}}^{b,\mathrm{min}}$ distribution in SRt1 (middle left), $E_{\mathrm{T}}^{\mathrm{miss,\,sig}}$ distribution in SRt2 (middle right) and ξ^{+} distribution in SRt3 (bottom). The last bins include overflows, where applicable. All signal region requirements except the one on the distribution shown are applied. The signal region requirement on the distribution shown is indicated by an arrow. The bottom panel shows the ratio of the data to the prediction. The band includes all systematic uncertainties defined in Sect. 6

Table 9 Left to right: 95% CL upper limits on the visible cross-section ($\langle\epsilon A\sigma\rangle_{95}^{\text{obs}}$) and on the number of BSM events (S_{95}^{obs}). The third column (S_{95}^{exp}) shows the 95% CL upper limit on the number of signal events, given the expected number (and $\pm 1\sigma$ excursions of the expected number) of background events. The last column indicates the discovery p-value ($p(s=0)$) and Z (the number of equivalent Gaussian standard deviations)

Signal channel	$\langle\epsilon A\sigma\rangle_{95}^{\text{obs}}$ [fb]	S_{95}^{obs}	S_{95}^{exp}	$p(s=0)$ (Z)
SRb1	0.37	13.4	12^{+5}_{-1}	0.33 (0.43)
SRb2 bin-1	1.10	39.6	33^{+12}_{-8}	0.22 (0.76)
SRb2 bin-2	1.17	42.1	31^{+10}_{-8}	0.11 (1.21)
SRb2 bin-3	1.21	43.7	33^{+11}_{-8}	0.16 (1.00)
SRb2 bin-4	1.10	39.8	26^{+11}_{-7}	0.10 (1.26)
SRt1	0.51	18.4	16^{+5}_{-4}	0.33 (0.44)
SRt2	0.44	15.7	12^{+5}_{-3}	0.24 (0.70)
SRt3	0.44	15.9	13^{+5}_{-2}	0.33 (0.45)

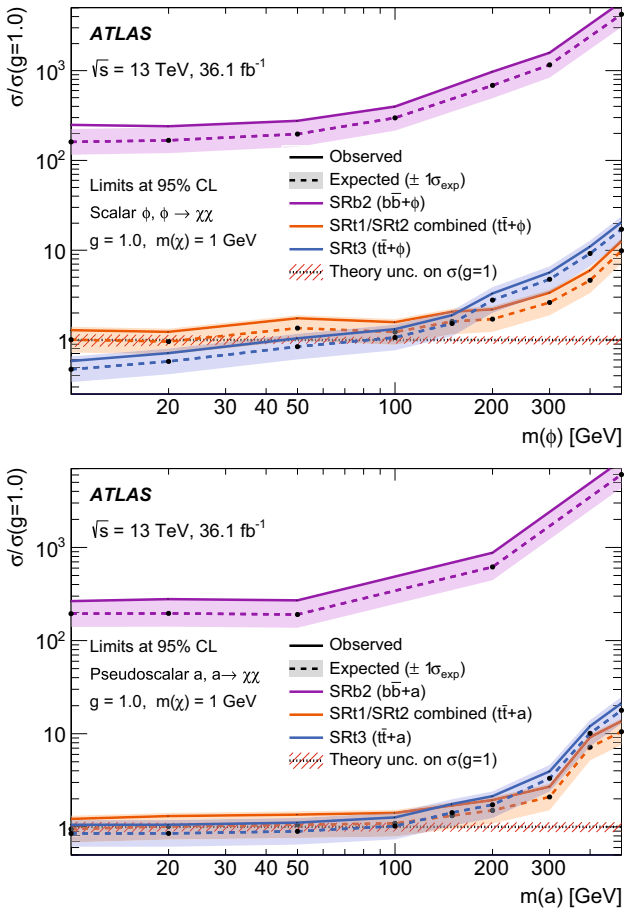

Fig. 5 Exclusion limits for colour-neutral $t\bar{t}/b\bar{b}+\phi$ scalar (top) and $t\bar{t}/b\bar{b}+a$ pseudoscalar (bottom) models as a function of the mediator mass for a DM mass of 1 GeV. The limits are calculated at 95% CL and are expressed in terms of the ratio of the excluded cross-section to the nominal cross-section for a coupling assumption of $g=g_q=g_\chi=1$. The solid (dashed) lines shows the observed (expected) exclusion limits for the different signal regions, according to the colour code specified in the legend. To derive the results for the fully hadronic $t\bar{t}$ final state the region SRt1 or SRt2 providing the better expected sensitivity is used

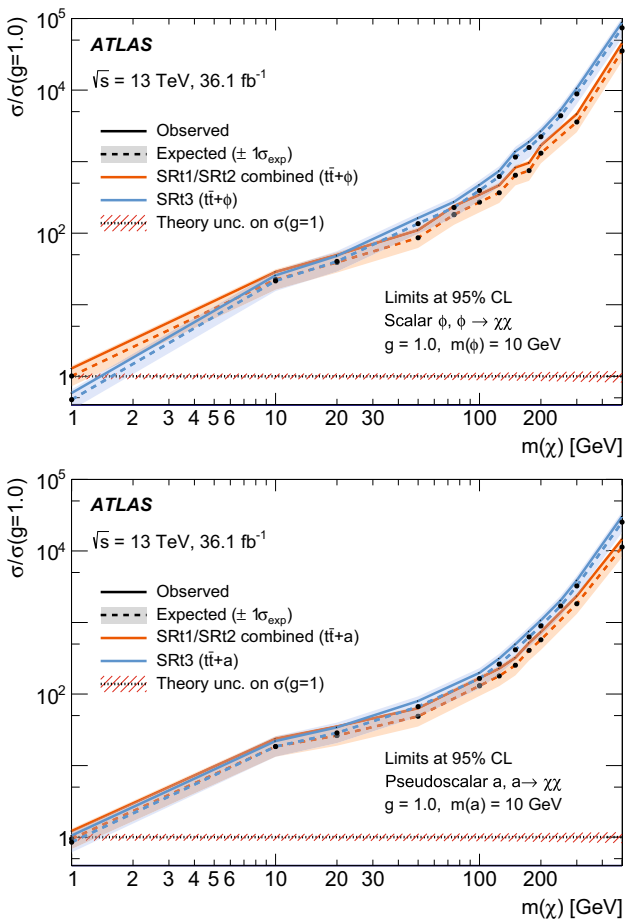

Fig. 6 Exclusion limits for colour-neutral $t\bar{t}+\phi$ scalar (top) and $t\bar{t}+a$ pseudoscalar (bottom) models as a function of the DM mass for a mediator mass of 10 GeV. The limits are calculated at 95% CL and are expressed in terms of the ratio of the excluded cross-section to the nominal cross-section for a coupling assumption of $g=g_q=g_\chi=1$. The solid (dashed) lines shows the observed (expected) exclusion limits for the different signal regions, according to the colour code specified in the legend. To derive the results for the fully hadronic $t\bar{t}$ final state the region SRt1 or SRt2 providing the better expected sensitivity is used

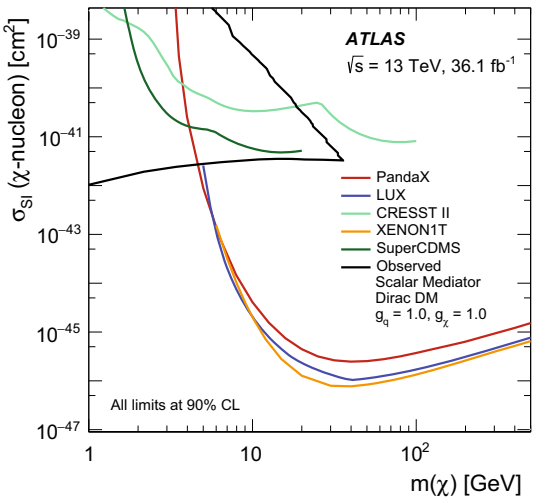

Fig. 7 Comparison of the 90% CL limits on the spin-independent DM–nucleon cross-section as a function of DM mass between these results and the direct-detection experiments, in the context of the colour-neutral simplified model with scalar mediator. The black line indicates the exclusion contour derived from the observed limits of SRt3. Values inside the contour are excluded. The exclusion limit is compared with limits from the LUX [104], PandaX-II [105], XENON [106], SuperCDMS [107] and CRESST-II [108] experiments

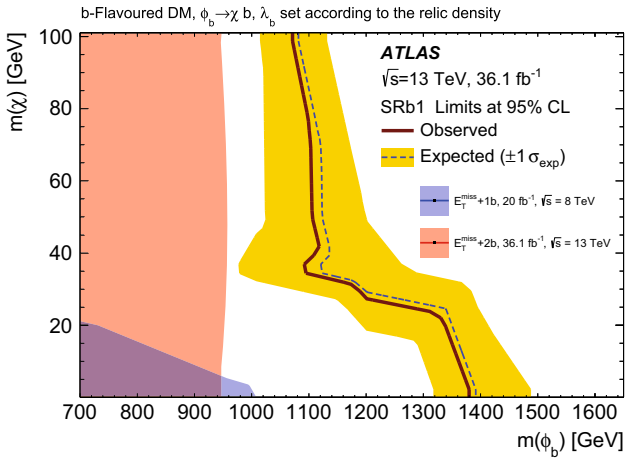

Fig. 8 Exclusion limits for colour-charged scalar mediators (b-FDM) as a function of the mediator and DM masses for 36.1 fb^{-1} of data. The limits are calculated at 95% CL. The solid (dashed) line show the observed (expected) exclusion contour for a coupling assumption λ_b yielding the measured relic density. No uncertainties on the LO cross-sections are considered for this model. The results are compared with the ATLAS search for b-FDM models [27], represented by the blue contour, and the ATLAS search for direct sbottom pair production [25], represented by the red contour

For each dark-matter and mediator mass pair, the exclusion limit on the production cross-section of colour-neutral scalar mediator particles can be converted into a limit on the spin-independent DM–nucleon scattering cross-section using the procedure described in Ref. [109]. The results can thus be compared with the results from direct-detection experiments. The most stringent limits, provided by SRt3, are used for this purpose. Figure 7 shows the constraints from this analysis expressed as exclusion limits at 90% CL in the plane defined by the dark-matter mass and the scattering cross-section. The black line indicates the exclusion contour derived from the observed limits in the top part of Fig. 5, where mediator masses between 10 GeV and 500 GeV are considered. The maximum value of the DM–nucleon scattering cross-section displayed corresponds to the result obtained for a mediator mass of 10 GeV. The results of this analysis are compared with the results from the LUX [104], PandaX-II [105], XENON [106], SuperCDMS [107] and CRESST-II [108] experiments. The comparison is model-dependent, and therefore valid only for the specific models considered in this paper. For pseudoscalar mediator models, the predicted dark-matter cross-sections in these direct-detection experiments is suppressed by velocity-dependent terms. As a result, direct-detection limits on spin-independent DM–nucleon scattering cross-section are several orders of magnitude worse than the ones obtained in this analysis, and therefore not presented.

Finally, Fig. 8 shows the exclusion contour for the b-FDM model as a function of the mediator and DM masses. In this model, the cross-section and therefore also the final sensitivity strongly depends on the coupling choice, λ_b, which is set to fulfil the relic density constraints, and determines the decrease of the sensitivity for higher DM masses. For a DM particle of approximately 35 GeV, as suggested by the interpretation of data recorded by the Fermi-LAT Collaboration, mediator masses below 1.1 TeV are excluded at 95% CL.

8 Conclusion

This article reports a search for dark-matter pair production in association with bottom or top quarks. The analysis is performed using 36.1 fb^{-1} of pp collisions collected at a centre-of-mass energy of $\sqrt{s} = 13$ TeV by the ATLAS detector at the LHC. The results are interpreted in the framework of simplified models of spin-0 mediators to the dark sector decaying into pairs of DM particles. The data are found to be consistent with the Standard Model expectations, and limits are set on the signal strength for a coupling assumption of $g = 1.0$ or on the DM and mediator masses. The results represent the most stringent limits to date for colour-neutral spin-0 mediator models for a DM mass assumption of 1 GeV in top-quark final states. It excludes at 95% CL mediator masses between 10 and 50 GeV for scalar mediators assuming couplings equal to unity and a dark-matter mass of 1 GeV. Although the analysis is expected to be sensitive to models with pseudoscalar mediators with masses between 10 and 100 GeV, no observed exclusion limit can be set for this model for the coupling assumption of $g = 1.0$

because of a small excess in the observed data. Limits of 300 times the nominal cross section for couplings equal to unity are placed for scalar and pseudoscalar mediator masses between 10 and 50 GeV for a dark-matter mass of 1 GeV in bottom-quark final states. Constraints on b-FDM models are also presented. The excluded region depends on $m(\phi_b)$ and $m(\chi)$; for $m(\chi) = 35$ GeV, mediator particles with $m(\phi) < 1.1$ TeV are excluded.

Acknowledgements We thank CERN for the very successful operation of the LHC, as well as the support staff from our institutions without whom ATLAS could not be operated efficiently. We acknowledge the support of ANPCyT, Argentina; YerPhI, Armenia; ARC, Australia; BMWFW and FWF, Austria; ANAS, Azerbaijan; SSTC, Belarus; CNPq and FAPESP, Brazil; NSERC, NRC and CFI, Canada; CERN; CONICYT, Chile; CAS, MOST and NSFC, China; COLCIENCIAS, Colombia; MSMT CR, MPO CR and VSC CR, Czech Republic; DNRF and DNSRC, Denmark; IN2P3-CNRS, CEA-DSM/IRFU, France; SRNSF, Georgia; BMBF, HGF, and MPG, Germany; GSRT, Greece; RGC, Hong Kong SAR, China; ISF, I-CORE and Benoziyo Center, Israel; INFN, Italy; MEXT and JSPS, Japan; CNRST, Morocco; NWO, Netherlands; RCN, Norway; MNiSW and NCN, Poland; FCT, Portugal; MNE/IFA, Romania; MES of Russia and NRC KI, Russian Federation; JINR; MESTD, Serbia; MSSR, Slovakia; ARRS and MIZŠ, Slovenia; DST/NRF, South Africa; MINECO, Spain; SRC and Wallenberg Foundation, Sweden; SERI, SNSF and Cantons of Bern and Geneva, Switzerland; MOST, Taiwan; TAEK, Turkey; STFC, United Kingdom; DOE and NSF, United States of America. In addition, individual groups and members have received support from BCKDF, the Canada Council, CANARIE, CRC, Compute Canada, FQRNT, and the Ontario Innovation Trust, Canada; EPLANET, ERC, ERDF, FP7, Horizon 2020 and Marie Skłodowska-Curie Actions, European Union; Investissements d'Avenir Labex and Idex, ANR, Région Auvergne and Fondation Partager le Savoir, France; DFG and AvH Foundation, Germany; Herakleitos, Thales and Aristeia programmes co-financed by EU-ESF and the Greek NSRF; BSF, GIF and Minerva, Israel; BRF, Norway; CERCA Programme Generalitat de Catalunya, Generalitat Valenciana, Spain; the Royal Society and Leverhulme Trust, United Kingdom. The crucial computing support from all WLCG partners is acknowledged gratefully, in particular from CERN, the ATLAS Tier-1 facilities at TRIUMF (Canada), NDGF (Denmark, Norway, Sweden), CC-IN2P3 (France), KIT/GridKA (Germany), INFN-CNAF (Italy), NL-T1 (Netherlands), PIC (Spain), ASGC (Taiwan), RAL (UK) and BNL (USA), the Tier-2 facilities worldwide and large non-WLCG resource providers. Major contributors of computing resources are listed in Ref. [110].

Funded by SCOAP[3].

References

1. F. Zwicky, Die Rotverschiebung von extragalaktischen Nebeln. Helv. Phys. Acta. **6**, 110–127 (1933)
2. G. Bertone, D. Hooper, J. Silk, Particle dark matter: evidence, candidates and constraints. Phys. Rep. **405**, 279 (2005). arXiv:hep-ph/0404175
3. E. Komatsu et al., Seven-year Wilkinson Microwave Anisotropy Probe (WMAP) observations: cosmological interpretation. Astrophys. J. Suppl. **192**, 18 (2011). arXiv:1001.4538 [astro-ph.CO]
4. P.A.R. Ade, Planck 2015 results. XIII. Cosmological parameters. Astron. Astrophys. A **594**, 13 (2016). arXiv:1502.01589 [astro-ph.CO]
5. G. Steigman, M.S. Turner, Cosmological constraints on the properties of weakly interacting massive particles. Nucl. Phys. B **253**, 375 (1985)
6. CMS Collaboration, Search for associated production of dark matter with a Higgs boson decaying to $b\bar{b}$ or $\gamma\gamma$ at $\sqrt{s} = 13$ TeV. (2017). arXiv:1703.05236 [hep-ex]
7. CMS Collaboration, Search for dark matter produced with an energetic jet or a hadronically decaying W or Z boson at $\sqrt{s} = 13$ TeV. JHEP **07**, 014 (2017). arXiv:1703.01651 [hep-ex]
8. CMS Collaboration, Search for new physics in the monophoton final state in proton-proton collisions at $\sqrt{s} = 13$ TeV. (2017). arXiv:1706.03794 [hep-ex]
9. ATLAS Collaboration, Search for dark matter in association with a Higgs boson decaying to two photons at $\sqrt{s}$= 13 TeV with the ATLAS detector. (2017). arXiv:1706.03948 [hep-ex]
10. ATLAS Collaboration, Search for dark matter at $\sqrt{s} = 13$ TeV in final states containing an energetic photon and large missing transverse momentum with the ATLAS detector. Eur. Phys. J. C **77**, 393 (2017). arXiv:1704.03848 [hep-ex]
11. ATLAS Collaboration, Search for new phenomena in final states with an energetic jet and large missing transverse momentum in pp collisions at $\sqrt{s} = 13$ TeV using the ATLAS detector. Phys. Rev. D **94**, 032005 (2016). arXiv:1604.07773 [hep-ex]
12. ATLAS Collaboration, Search for dark matter produced in association with a Higgs boson decaying to $b\bar{b}$ using 36 fb^{-1} of pp collisions at $\sqrt{s} = 13$ TeV with the ATLAS detector. (2017). arXiv:1707.01302 [hep-ex]
13. D. Abercrombie et al., Dark matter benchmark models for early LHC run-2 searches: report of the ATLAS/CMS Dark Matter Forum. (2015). arXiv:1507.00966 [hep-ex]
14. M.R. Buckley, D. Feld, D. Goncalves, Scalar simplified models for dark matter. Phys. Rev. D **91**, 015017 (2015). arXiv:1410.6497 [hep-ph]
15. U. Haisch, E. Re, Simplified dark matter top-quark interactions at the LHC. JHEP **06**, 078 (2015). arXiv:1503.00691 [hep-ph]
16. G. D'Ambrosio, G.F. Giudice, G. Isidori, A. Strumia, Minimal flavor violation: an effective field theory approach. Nucl. Phys. B **645**, 155 (2002). arXiv:hep-ph/0207036
17. CMS Collaboration, Search for dark matter produced in association with heavy-flavor quarks in proton–proton collisions at $\sqrt{s} = 13$ TeV. (2017). arXiv:1706.02581 [hep-ex]
18. ATLAS Collaboration, Search for a scalar partner of the top quark in the jets plus missing transverse momentum final state at $\sqrt{s} = 13$ TeV with the ATLAS detector. (2017). arXiv:1709.04183 [hep-ex]
19. ATLAS Collaboration, Search for direct top squark pair production in final states with two leptons in $\sqrt{s} = 13$ TeV pp collisions with the ATLAS detector. (2017). arXiv:1708.03247 [hep-ex]
20. ATLAS Collaboration, Search for top-squark pair production in final states with one lepton, jets, and missing transverse momentum using 36 fb^{-1} of $\sqrt{s} = 13$ TeV pp collision data with the ATLAS detector. (2017). arXiv:1711.11520 [hep-ex]
21. M. Bauer, U. Haisch, F. Kahlhoefer, Simplified dark matter models with two Higgs doublets: I. Pseudoscalar mediators. JHEP **05**, 138 (2017). arXiv:1701.07427 [hep-ph]

22. P. Agrawal, B. Batell, D. Hooper, T. Lin, Flavored dark matter and the galactic center gamma-ray excess. Phys. Rev. D **90**, 063512 (2014). arXiv:1404.1373 [hep-ph]
23. T. Daylan et al., The characterization of the gamma-ray signal from the central Milky Way: a compelling case for annihilating dark matter. Phys. Dark Univ. **12**, 1 (2016). arXiv:1402.6703 [astro-ph.HE]
24. M. Ajello et al., Characterizing the population of pulsars in the galactic bulge with the *Fermi* large area telescope. Submitted to: Astrophys. J. (2017). arXiv:1705.00009 [astro-ph.HE]
25. ATLAS Collaboration, Search for supersymmetry in events with b-tagged jets and missing transverse momentum in pp collisions at $\sqrt{s} = 13$ TeV with the ATLAS detector. (2017). arXiv:1708.09266 [hep-ex]
26. CMS Collaboration, Searches for pair production of third-generation squarks in $\sqrt{s} = 13$ TeV pp collisions. Eur. Phys. J. C **77**, 327 (2017). arXiv:1612.03877 [hep-ex]
27. ATLAS Collaboration, Search for dark matter in events with heavy quarks and missing transverse momentum in pp collisions with the ATLAS detector. Eur. Phys. J. C **75**, 92 (2015). arXiv:1410.4031 [hep-ex]
28. ATLAS Collaboration, The ATLAS experiment at the CERN large hadron collider. JINST **3**, S08003 (2008)
29. ATLAS Collaboration, ATLAS insertable B-layer technical design report, ATLAS-TDR-19. (2010). https://cds.cern.ch/record/1291633
30. ATLAS insertable B-layer technical design report addendum, ATLAS-TDR-19-ADD-1. (2012). https://cds.cern.ch/record/1451888
31. ATLAS Collaboration, Performance of the ATLAS trigger system in 2015. Eur. Phys. J. C **77**, 317 (2017). arXiv:1611.09661 [hep-ex]
32. ATLAS Collaboration, Vertex reconstruction performance of the ATLAS detector at$\sqrt{s} = 13$ TeV, ATL-PHYS-PUB-2015-026. (2015). https://cds.cern.ch/record/2037717
33. ATLAS Collaboration, Topological cell clustering in the ATLAS calorimeters and its performance in LHC Run 1. (2016). arXiv:1603.02934 [hep-ex]
34. M. Cacciari, G.P. Salam, G. Soyez, The anti-k_T jet clustering algorithm. JHEP **04**, 063 (2008). arXiv:0802.1189 [hep-ph]
35. M. Cacciari, G.P. Salam, G. Soyez, FastJet user manual. Eur. Phys. J. C **72**, 1896 (2012). arXiv:1111.6097 [hep-ph]
36. ATLAS Collaboration, Jet energy scale measurements and their systematic uncertainties in proton–proton collisions at $\sqrt{s} = 13$ TeV with the ATLAS detector. (2017). arXiv:1703.09665 [hep-ex]
37. ATLAS Collaboration, Jet calibration and systematic uncertainties for jets reconstructed in the ATLAS detector at $\sqrt{s} = 13$ TeV, ATL-PHYS-PUB-2015-015. (2015). https://cds.cern.ch/record/2037613
38. ATLAS Collaboration, Selection of jets produced in 13 TeV proton–proton collisions with the ATLAS detector, ATLAS-CONF-2015-029. (2015). https://cds.cern.ch/record/2037702
39. ATLAS Collaboration, Data-quality requirements and event cleaning for jets and missing transverse energy reconstruction with the ATLAS detector in proton–proton collisions at a center-of-mass energy of $\sqrt{s} = 7$ TeV, ATLAS-CONF-2010-038. (2010). https://cds.cern.ch/record/1277678
40. ATLAS Collaboration, Performance of pile-up mitigation techniques for jets in pp collisions at $\sqrt{s} = 8$ TeV using the ATLAS detector. Eur. Phys. J. C **76**, 581 (2016). arXiv:1510.03823 [hep-ex]
41. ATLAS Collaboration, Performance of b-jet identification in the ATLAS experiment. JINST **11**, P04008 (2016). arXiv:1512.01094 [hep-ex]
42. ATLAS Collaboration, Optimisation of the ATLAS b-tagging performance for the 2016 LHC Run, ATL-PHYS-PUB-2016-012. (2016). https://cds.cern.ch/record/2160731
43. ATLAS Collaboration, Muon reconstruction performance of the ATLAS detector in proton–proton collision data at $\sqrt{s} = 13$ TeV. Eur. Phys. J. C **76**, 292 (2016). arXiv:1603.05598 [hep-ex]
44. ATLAS Collaboration, Electron efficiency measurements with the ATLAS detector using 2012 LHC proton–proton collision data. Eur. Phys. J. C **77**, 195 (2017). arXiv:1612.01456 [hep-ex]
45. ATLAS Collaboration, Electron identification measurements in ATLAS using $\sqrt{s} = 13$ TeV data with 50 ns bunch spacing, ATL-PHYS-PUB-2015-041. (2015). https://cds.cern.ch/record/2048202
46. ATLAS Collaboration, Electron efficiency measurements with the ATLAS detector using the 2015 LHC proton–proton collision data, ATLAS-CONF-2016-024. (2016). https://cds.cern.ch/record/2157687
47. ATLAS Collaboration, Electron and photon energy calibration with the ATLAS detector using LHC Run 1 data. Eur. Phys. J. C **74**, 3071 (2014). arXiv:1407.5063 [hep-ex]
48. ATLAS Collaboration, Measurement of the photon identification efficiencies with the ATLAS detector using LHC Run-1 data. (2016). arXiv:1606.01813 [hep-ex]
49. ATLAS Collaboration, Expected performance of missing transverse momentum reconstruction for the ATLAS detector at $\sqrt{s} =$ 13 TeV, ATL-PHYS-PUB-2015-023. (2015). https://cds.cern.ch/record/2037700
50. ATLAS Collaboration, Performance of missing transverse momentum reconstruction with the ATLAS detector in the first proton–proton collisions at $\sqrt{s} = 13$ TeV, ATL-PHYS-PUB-2015-027. (2015). https://cds.cern.ch/record/2037904
51. ATLAS Collaboration, Luminosity determination in pp collisions at $\sqrt{s} = 8$ TeV using the ATLAS detector at the LHC. Eur. Phys. J. C **76**, 653 (2016). arXiv:1608.03953 [hep-ex]
52. ATLAS Collaboration, The ATLAS simulation infrastructure. Eur. Phys. J. C **70**, 823 (2010). arXiv:1005.4568 [physics.ins-det]
53. S. Agostinelli et al., GEANT4: a simulation toolkit. Nucl. Instrum. Methods A **506**, 250 (2003)
54. ATLAS Collaboration, The simulation principle and performance of the ATLAS fast calorimeter simulation FastCaloSim, ATL-PHYS-PUB-2010-013. (2010). https://cds.cern.ch/record/1300517
55. ATLAS Collaboration, Simulation of top-quark production for the ATLAS experiment at $\sqrt{s} = 13$ TeV, ATL-PHYS-PUB-2016-004. (2016). https://cds.cern.ch/record/2120417
56. ATLAS Collaboration, Monte Carlo generators for the production of a W or Z/γ^* boson in association with jets at ATLAS in Run 2, ATL-PHYS-PUB-2016-003. (2016). https://cds.cern.ch/record/2120133
57. ATLAS Collaboration, Multi-boson simulation for 13 TeV ATLAS analyses, ATL-PHYS-PUB-2016-002. (2016). https://cds.cern.ch/record/2119986
58. ATLAS Collaboration, Modelling of the $t\bar{t}H$ and $t\bar{t}V$ ($V = W, Z$) processes for $\sqrt{s} = 13$ TeV ATLAS analyses, ATL-PHYS-PUB-2016-005. (2016). https://cds.cern.ch/record/2120826
59. N. Kidonakis, Next-to-next-to-leading-order collinear and soft gluon corrections for t-channel single top quark production. Phys. Rev. D **83**, 091503 (2011). arXiv:1103.2792 [hep-ph]
60. N. Kidonakis, NNLL resummation for s-channel single top quark production. Phys. Rev. D **81**, 054028 (2010). arXiv:1001.5034 [hep-ph]
61. N. Kidonakis, Two-loop soft anomalous dimensions for single top quark associated production with a W- or H-. Phys. Rev. D **82**, 054018 (2010). arXiv:1005.4451 [hep-ph]
62. T. Gleisberg, S. Höche, Comix, a new matrix element generator. JHEP **12**, 039 (2008). arXiv:0808.3674 [hep-ph]

63. F. Cascioli, P. Maierhofer, S. Pozzorini, Scattering amplitudes with open loops. Phys. Rev. Lett. **108**, 111601 (2012). arXiv:1111.5206 [hep-ph]
64. S. Schumann, F. Krauss, A Parton shower algorithm based on Catani–Seymour dipole factorisation. JHEP **03**, 038 (2008). arXiv:0709.1027 [hep-ph]
65. S. Höche, F. Krauss, M. Schönherr, F. Siegert, QCD matrix elements + parton showers: the NLO case. JHEP **04**, 027 (2013). arXiv:1207.5030 [hep-ph]
66. R.D. Ball et al., Parton distributions with LHC data. Nucl. Phys. B **867**, 244 (2013). arXiv:1207.1303 [hep-ph]
67. J. Alwall et al., The automated computation of tree-level and next-to-leading order differential cross sections, and their matching to parton shower simulations. JHEP **07**, 079 (2014). arXiv:1405.0301 [hep-ph]
68. T. Sjöstrand, M. Mrenna, P.Z. Skands, A brief introduction to PYTHIA 8.1. Comput. Phys. Commun. **178**, 852 (2008). arXiv:0710.3820 [hep-ph]
69. O. Mattelaer, E. Vryonidou, Dark matter production through loop-induced processes at the LHC: the s-channel mediator case. Eur. Phys. J. C **75**, 436 (2015). arXiv:1508.00564 [hep-ph]
70. M. Backovic et al., Higher-order QCD predictions for dark matter production at the LHC in simplified models with s-channel mediators. Eur. Phys. J. C **75**, 482 (2015). arXiv:1508.05327 [hep-ph]
71. H.-L. Lai et al., New parton distributions for collider physics. Phys. Rev. D **82**, 074024 (2010). arXiv:1007.2241 [hep-ph]
72. ATLAS Collaboration, ATLAS Pythia8 tunes to 7 TeV data, ATL-PHYS-PUB-2014-021. (2014). https://cds.cern.ch/record/1966419
73. T. Gleisberg et al., Event generation with SHERPA 1.1. JHEP **02**, 007 (2009). arXiv:0811.4622 [hep-ph]
74. S. Catani, L. Cieri, G. Ferrera, D. de Florian, M. Grazzini, Vector boson production at hadron colliders: a fully exclusive QCD calculation at NNLO. Phys. Rev. Lett. **103**, 082001 (2009). arXiv:0903.2120 [hep-ph]
75. S. Alioli, P. Nason, C. Oleari, E. Re, A general framework for implementing NLO calculations in shower Monte Carlo programs: the POWHEG BOX. JHEP **06**, 043 (2010). arXiv:1002.2581 [hep-ph]
76. T. Sjöstrand, S. Mrenna, P.Z. Skands, PYTHIA 6.4 physics and manual. JHEP **05**, 026 (2006). arXiv:hep-ph/0603175
77. M. Czakon, P. Fiedler, A. Mitov, Total top-quark pair-production cross section at hadron colliders through $O(\alpha_S^4)$. Phys. Rev. Lett. **110**, 252004 (2013). arXiv:1303.6254 [hep-ph]
78. M. Czakon, A. Mitov, NNLO corrections to top pair production at hadron colliders: the quark–gluon reaction. JHEP **01**, 080 (2013). arXiv:1210.6832 [hep-ph]
79. M. Czakon, A. Mitov, NNLO corrections to top-pair production at hadron colliders: the all-fermionic scattering channels. JHEP **12**, 054 (2012). arXiv:1207.0236 [hep-ph]
80. P. Bärnreuther, M. Czakon, A. Mitov, Percent level precision physics at the tevatron: first genuine NNLO QCD corrections to $q\bar{q} \rightarrow t\bar{t} + X$. Phys. Rev. Lett. **109**, 132001 (2012). arXiv:1204.5201 [hep-ph]
81. M. Cacciari, M. Czakon, M. Mangano, A. Mitov, P. Nason, Top-pair production at hadron colliders with next-to-next-to-leading logarithmic soft-gluon resummation. Phys. Lett. B **710**, 612 (2012). arXiv:1111.5869 [hep-ph]
82. M. Czakon, A. Mitov, Top++: a program for the calculation of the top-pair cross-section at hadron colliders. Comput. Phys. Commun. **185**, 2930 (2014). arXiv:1112.5675 [hep-ph]
83. P.Z. Skands, Tuning Monte Carlo generators: the Perugia tunes. Phys. Rev. D **82**, 074018 (2010). arXiv:1005.3457 [hep-ph]
84. LHC Higgs Cross Section Working Group, Handbook of LHC Higgs cross sections: 2. Differential distributions, CERN-2012-002. (2012). arXiv:1201.3084 [hep-ph]
85. D.J. Lange, The EvtGen particle decay simulation package. Nucl. Instrum. Methods A **462**, 152 (2001)
86. S. Gieseke, C. Rohr, A. Siodmok, Colour reconnections in Herwig++. Eur. Phys. J. C **72**, 2225 (2012). arXiv:1206.0041 [hep-ph]
87. ATLAS Collaboration, Summary of ATLAS Pythia 8 tunes, ATL-PHYS-PUB-2012-003. (2012). https://cds.cern.ch/record/1474107
88. A.D. Martin, W.J. Stirling, R.S. Thorne, G. Watt, Parton distributions for the LHC. Eur. Phys. J. C **63**, 189 (2009). arXiv:0901.0002 [hep-ph]
89. L. Lönnblad, S. Prestel, Matching tree-level matrix elements with interleaved showers. JHEP **03**, 019 (2012). arXiv:1109.4829 [hep-ph]
90. V. Hirschi, O. Mattelaer, Automated event generation for loop-induced processes. JHEP **10**, 146 (2015). arXiv:1507.00020 [hep-ph]
91. U. Haisch, P. Pani, G. Polesello, Determining the CP nature of spin-0 mediators in associated production of dark matter and $t\bar{t}$ pairs. JHEP **02**, 131 (2017). arXiv:1611.09841 [hep-ph]
92. A.J. Barr, Measuring slepton spin at the LHC. JHEP **02**, 042 (2006). arXiv:hep-ph/0511115
93. ATLAS Collaboration, Search for direct top-squark pair production in final states with two leptons in pp collisions at $\sqrt{s} = 8$ TeV with the ATLAS detector. JHEP **06**, 124 (2014). arXiv:1403.4853 [hep-ex]
94. A. Barr, C. Lester, P. Stephens, A variable for measuring masses at hadron colliders when missing energy is expected; m(T2): the truth behind the glamour. J. Phys. G **29**, 2343 (2003). arXiv:hep-ph/0304226
95. C.G. Lester, D.J. Summers, Measuring masses of semi-invisibly decaying particles pair produced at hadron colliders. Phys. Lett. B **463**, 99 (1999). arXiv:hep-ph/9906349
96. M. Baak et al., HistFitter software framework for statistical data analysis. Eur. Phys. J. C **75**, 153 (2015). arXiv:1410.1280 [hep-ex]
97. ATLAS Collaboration, Measurement of the top quark-pair production cross section with ATLAS in pp collisions at $\sqrt{s} = 7$ TeV. Eur. Phys. J. C **71**, 1577 (2011). arXiv:1012.1792 [hep-ex]
98. ATLAS Collaboration, Measurement of the top quark pair production cross section in pp collisions at $\sqrt{s} = 7$ TeV in dilepton final states with ATLAS. Phys. Lett. B **707**, 459 (2012). arXiv:1108.3699 [hep-ex]
99. ATLAS Collaboration, Search for bottom squark pair production in proton–proton collisions at $\sqrt{s} = 13$ TeV with the ATLAS detector. Eur. Phys. J. C **76**, 547 (2016). arXiv:1606.08772 [hep-ex]
100. ATLAS Collaboration, Studies on top-quark Monte Carlo modelling with Sherpa and MG5_aMC@NLO, ATL-PHYS-PUB-2017-007. (2017). https://cds.cern.ch/record/2261938
101. ATLAS Collaboration, Calibration of b-tagging using dileptonic top pair events in a combinatorial likelihood approach with the ATLAS experiment, ATLAS-CONF-2014-004. (2014). https://cds.cern.ch/record/1664335
102. ATLAS Collaboration, Calibration of the performance of b-tagging for c and light-flavour jets in the 2012 ATLAS data, ATLAS-CONF-2014-046. (2014). https://cds.cern.ch/record/1741020
103. A.L. Read, Presentation of search results: the CL_S technique. J. Phys. G **28**, 2693 (2002)
104. LUX Collaboration, Results from a search for dark matter in the complete LUX exposure. Phys. Rev. Lett. **118**, 021303 (2017). arXiv:1608.07648 [astro-ph.CO]

105. PandaX-II Collaboration, Dark matter results from first 98.7 days of data from the PandaX-II experiment. Phys. Rev. Lett. **117**, 121303 (2016). arXiv:1607.07400 [hep-ex]
106. XENON Collaboration, First dark matter search results from the XENON1T experiment. (2017). arXiv:1705.06655 [astro-ph.CO]
107. SuperCDMS Collaboration, New results from the search for low-mass weakly interacting massive particles with the CDMS low ionization threshold experiment. Phys. Rev. Lett. **116**, 071301 (2016). arXiv:1509.02448 [astro-ph.CO]
108. CRESST Collaboration, Results on light dark matter particles with a low-threshold CRESST-II detector. Eur. Phys. J. C **76**, 25 (2016). arXiv:1509.01515 [astro-ph.CO]
109. A. Boveia et al., Recommendations on presenting LHC searches for missing transverse energy signals using simplified s-channel models of dark matter. (2016). arXiv:1603.04156 [hep-ex]
110. ATLAS Collaboration, ATLAS computing acknowledgements 2016–2017, ATL-GEN-PUB-2016-002. https://cds.cern.ch/record/2202407

ATLAS Collaboration

M. Aaboud[137d], G. Aad[88], B. Abbott[115], O. Abdinov[12,*], B. Abeloos[119], S. H. Abidi[161], O. S. AbouZeid[139], N. L. Abraham[151], H. Abramowicz[155], H. Abreu[154], R. Abreu[118], Y. Abulaiti[148a,148b], B. S. Acharya[167a,167b,a], S. Adachi[157], L. Adamczyk[41a], J. Adelman[110], M. Adersberger[102], T. Adye[133], A. A. Affolder[139], Y. Afik[154], T. Agatonovic-Jovin[14], C. Agheorghiesei[28c], J. A. Aguilar-Saavedra[128a,128f], S. P. Ahlen[24], F. Ahmadov[68,b], G. Aielli[135a,135b], S. Akatsuka[71], H. Akerstedt[148a,148b], T. P. A. Åkesson[84], E. Akilli[52], A. V. Akimov[98], G. L. Alberghi[22a,22b], J. Albert[172], P. Albicocco[50], M. J. Alconada Verzini[74], S. C. Alderweireldt[108], M. Aleksa[32], I. N. Aleksandrov[68], C. Alexa[28b], G. Alexander[155], T. Alexopoulos[10], M. Alhroob[115], B. Ali[130], M. Aliev[76a,76b], G. Alimonti[94a], J. Alison[33], S. P. Alkire[38], B. M. M. Allbrooke[151], B. W. Allen[118], P. P. Allport[19], A. Aloisio[106a,106b], A. Alonso[39], F. Alonso[74], C. Alpigiani[140], A. A. Alshehri[56], M. I. Alstaty[88], B. Alvarez Gonzalez[32], D. Álvarez Piqueras[170], M. G. Alviggi[106a,106b], B. T. Amadio[16], Y. Amaral Coutinho[26a], C. Amelung[25], D. Amidei[92], S. P. Amor Dos Santos[128a,128c], S. Amoroso[32], C. Anastopoulos[141], L. S. Ancu[52], N. Andari[19], T. Andeen[11], C. F. Anders[60b], J. K. Anders[77], K. J. Anderson[33], A. Andreazza[94a,94b], V. Andrei[60a], S. Angelidakis[37], I. Angelozzi[109], A. Angerami[38], A. V. Anisenkov[111,c], N. Anjos[13], A. Annovi[126a], C. Antel[60a], M. Antonelli[50], A. Antonov[100,*], D. J. Antrim[166], F. Anulli[134a], M. Aoki[69], L. Aperio Bella[32], G. Arabidze[93], Y. Arai[69], J. P. Araque[128a], V. Araujo Ferraz[26a], A. T. H. Arce[48], R. E. Ardell[80], F. A. Arduh[74], J.-F. Arguin[97], S. Argyropoulos[66], M. Arik[20a], A. J. Armbruster[32], L. J. Armitage[79], O. Arnaez[161], H. Arnold[51], M. Arratia[30], O. Arslan[23], A. Artamonov[99,*], G. Artoni[122], S. Artz[86], S. Asai[157], N. Asbah[45], A. Ashkenazi[155], L. Asquith[151], K. Assamagan[27], R. Astalos[146a], M. Atkinson[169], N. B. Atlay[143], K. Augsten[130], G. Avolio[32], B. Axen[16], M. K. Ayoub[35a], G. Azuelos[97,d], A. E. Baas[60a], M. J. Baca[19], H. Bachacou[138], K. Bachas[76a,76b], M. Backes[122], P. Bagnaia[134a,134b], M. Bahmani[42], H. Bahrasemani[144], J. T. Baines[133], M. Bajic[39], O. K. Baker[179], P. J. Bakker[109], E. M. Baldin[111,c], P. Balek[175], F. Balli[138], W. K. Balunas[124], E. Banas[42], A. Bandyopadhyay[23], Sw. Banerjee[176,e], A. A. E. Bannoura[178], L. Barak[155], E. L. Barberio[91], D. Barberis[53a,53b], M. Barbero[88], T. Barillari[103], M.-S. Barisits[32], J. T. Barkeloo[118], T. Barklow[145], N. Barlow[30], S. L. Barnes[36c], B. M. Barnett[133], R. M. Barnett[16], Z. Barnovska-Blenessy[36a], A. Baroncelli[136a], G. Barone[25], A. J. Barr[122], L. Barranco Navarro[170], F. Barreiro[85], J. Barreiro Guimarães da Costa[35a], R. Bartoldus[145], A. E. Barton[75], P. Bartos[146a], A. Basalaev[125], A. Bassalat[119,f], R. L. Bates[56], S. J. Batista[161], J. R. Batley[30], M. Battaglia[139], M. Bauce[134a,134b], F. Bauer[138], H. S. Bawa[145,g], J. B. Beacham[113], M. D. Beattie[75], T. Beau[83], P. H. Beauchemin[165], P. Bechtle[23], H. P. Beck[18,h], H. C. Beck[57], K. Becker[122], M. Becker[86], C. Becot[112], A. J. Beddall[20d], A. Beddall[20b], V. A. Bednyakov[68], M. Bedognetti[109], C. P. Bee[150], T. A. Beermann[32], M. Begalli[26a], M. Begel[27], J. K. Behr[45], A. S. Bell[81], G. Bella[155], L. Bellagamba[22a], A. Bellerive[31], M. Bellomo[154], K. Belotskiy[100], O. Beltramello[32], N. L. Belyaev[100], O. Benary[155,*], D. Benchekroun[137a], M. Bender[102], N. Benekos[10], Y. Benhammou[155], E. Benhar Noccioli[179], J. Benitez[66], D. P. Benjamin[48], M. Benoit[52], J. R. Bensinger[25], S. Bentvelsen[109], L. Beresford[122], M. Beretta[50], D. Berge[109], E. Bergeaas Kuutmann[168], N. Berger[5], L. J. Bergsten[25], J. Beringer[16], S. Berlendis[58], N. R. Bernard[89], G. Bernardi[83], C. Bernius[145], F. U. Bernlochner[23], T. Berry[80], P. Berta[86], C. Bertella[35a], G. Bertoli[148a,148b], I. A. Bertram[75], C. Bertsche[45], G. J. Besjes[39], O. Bessidskaia Bylund[148a,148b], M. Bessner[45], N. Besson[138], A. Bethani[87], S. Bethke[103], A. Betti[23], A. J. Bevan[79], J. Beyer[103], R. M. Bianchi[127], O. Biebel[102], D. Biedermann[17], R. Bielski[87], K. Bierwagen[86], N. V. Biesuz[126a,126b], M. Biglietti[136a], T. R. V. Billoud[97], H. Bilokon[50], M. Bindi[57], A. Bingul[20b], C. Bini[134a,134b], S. Biondi[22a,22b], T. Bisanz[57], C. Bittrich[47], D. M. Bjergaard[48], J. E. Black[145], K. M. Black[24], R. E. Blair[6], T. Blazek[146a], I. Bloch[45], C. Blocker[25], A. Blue[56], U. Blumenschein[79], S. Blunier[34a], G. J. Bobbink[109], V. S. Bobrovnikov[111,c], S. S. Bocchetta[84], A. Bocci[48], C. Bock[102], M. Boehler[51], D. Boerner[178], D. Bogavac[102], A. G. Bogdanchikov[111], C. Bohm[148a], V. Boisvert[80], P. Bokan[168,i], T. Bold[41a], A. S. Boldyrev[101], A. E. Bolz[60b], M. Bomben[83], M. Bona[79],

M. Boonekamp[138], A. Borisov[132], G. Borissov[75], J. Bortfeldt[32], D. Bortoletto[122], V. Bortolotto[62a], D. Boscherini[22a], M. Bosman[13], J. D. Bossio Sola[29], J. Boudreau[127], E. V. Bouhova-Thacker[75], D. Boumediene[37], C. Bourdarios[119], S. K. Boutle[56], A. Boveia[113], J. Boyd[32], I. R. Boyko[68], A. J. Bozson[80], J. Bracinik[19], A. Brandt[8], G. Brandt[57], O. Brandt[60a], F. Braren[45], U. Bratzler[158], B. Brau[89], J. E. Brau[118], W. D. Breaden Madden[56], K. Brendlinger[45], A. J. Brennan[91], L. Brenner[109], R. Brenner[168], S. Bressler[175], D. L. Briglin[19], T. M. Bristow[49], D. Britton[56], D. Britzger[45], F. M. Brochu[30], I. Brock[23], R. Brock[93], G. Brooijmans[38], T. Brooks[80], W. K. Brooks[34b], J. Brosamer[16], E. Brost[110], J. H Broughton[19], P. A. Bruckman de Renstrom[42], D. Bruncko[146b], A. Bruni[22a], G. Bruni[22a], L. S. Bruni[109], S. Bruno[135a,135b], B. H. Brunt[30], M. Bruschi[22a], N. Bruscino[127], P. Bryant[33], L. Bryngemark[45], T. Buanes[15], Q. Buat[144], P. Buchholz[143], A. G. Buckley[56], I. A. Budagov[68], F. Buehrer[51], M. K. Bugge[121], O. Bulekov[100], D. Bullock[8], T. J. Burch[110], S. Burdin[77], C. D. Burgard[109], A. M. Burger[5], B. Burghgrave[110], K. Burka[42], S. Burke[133], I. Burmeister[46], J. T. P. Burr[122], D. Büscher[51], V. Büscher[86], P. Bussey[56], J. M. Butler[24], C. M. Buttar[56], J. M. Butterworth[81], P. Butti[32], W. Buttinger[27], A. Buzatu[153], A. R. Buzykaev[111,c], C.-Q. Changqiao[36a], S. Cabrera Urbán[170], D. Caforio[130], H. Cai[169], V. M. Cairo[40a,40b], O. Cakir[4a], N. Calace[52], P. Calafiura[16], A. Calandri[88], G. Calderini[83], P. Calfayan[64], G. Callea[40a,40b], L. P. Caloba[26a], S. Calvente Lopez[85], D. Calvet[37], S. Calvet[37], T. P. Calvet[88], R. Camacho Toro[33], S. Camarda[32], P. Camarri[135a,135b], D. Cameron[121], R. Caminal Armadans[169], C. Camincher[58], S. Campana[32], M. Campanelli[81], A. Camplani[94a,94b], A. Campoverde[143], V. Canale[106a,106b], M. Cano Bret[36c], J. Cantero[116], T. Cao[155], M. D. M. Capeans Garrido[32], I. Caprini[28b], M. Caprini[28b], M. Capua[40a,40b], R. M. Carbone[38], R. Cardarelli[135a], F. Cardillo[51], I. Carli[131], T. Carli[32], G. Carlino[106a], B. T. Carlson[127], L. Carminati[94a,94b], R. M. D. Carney[148a,148b], S. Caron[108], E. Carquin[34b], S. Carrá[94a,94b], G. D. Carrillo-Montoya[32], D. Casadei[19], M. P. Casado[13,j], A. F. Casha[161], M. Casolino[13], D. W. Casper[166], R. Castelijn[109], V. Castillo Gimenez[170], N. F. Castro[128a,k], A. Catinaccio[32], J. R. Catmore[121], A. Cattai[32], J. Caudron[23], V. Cavaliere[169], E. Cavallaro[13], D. Cavalli[94a], M. Cavalli-Sforza[13], V. Cavasinni[126a,126b], E. Celebi[20c], F. Ceradini[136a,136b], L. Cerda Alberich[170], A. S. Cerqueira[26b], A. Cerri[151], L. Cerrito[135a,135b], F. Cerutti[16], A. Cervelli[22a,22b], S. A. Cetin[20c], A. Chafaq[137a], D. Chakraborty[110], S. K. Chan[59], W. S. Chan[109], Y. L. Chan[62a], P. Chang[169], J. D. Chapman[30], D. G. Charlton[19], C. C. Chau[131], C. A. Chavez Barajas[151], S. Che[113], S. Cheatham[167a,167c], A. Chegwidden[93], S. Chekanov[6], S. V. Chekulaev[163a], G. A. Chelkov[68,l], M. A. Chelstowska[32], C. Chen[36a], C. Chen[67], H. Chen[27], J. Chen[36a], S. Chen[35b], S. Chen[157], X. Chen[35c,m], Y. Chen[70], H. C. Cheng[92], H. J. Cheng[35a,35d], A. Cheplakov[68], E. Cheremushkina[132], R. Cherkaoui El Moursli[137e], E. Cheu[7], K. Cheung[63], L. Chevalier[138], V. Chiarella[50], G. Chiarelli[126a], G. Chiodini[76a], A. S. Chisholm[32], A. Chitan[28b], Y. H. Chiu[172], M. V. Chizhov[68], K. Choi[64], A. R. Chomont[37], S. Chouridou[156], Y. S. Chow[62a], V. Christodoulou[81], M. C. Chu[62a], J. Chudoba[129], A. J. Chuinard[90], J. J. Chwastowski[42], L. Chytka[117], A. K. Ciftci[4a], D. Cinca[46], V. Cindro[78], I. A. Cioara[23], A. Ciocio[16], F. Cirotto[106a,106b], Z. H. Citron[175], M. Citterio[94a], M. Ciubancan[28b], A. Clark[52], B. L. Clark[59], M. R. Clark[38], P. J. Clark[49], R. N. Clarke[16], C. Clement[148a,148b], Y. Coadou[88], M. Cobal[167a,167c], A. Coccaro[52], J. Cochran[67], L. Colasurdo[108], B. Cole[38], A. P. Colijn[109], J. Collot[58], T. Colombo[166], P. Conde Muiño[128a,128b], E. Coniavitis[51], S. H. Connell[147b], I. A. Connelly[87], S. Constantinescu[28b], G. Conti[32], F. Conventi[106a,n], M. Cooke[16], A. M. Cooper-Sarkar[122], F. Cormier[171], K. J. R. Cormier[161], M. Corradi[134a,134b], F. Corriveau[90,o], A. Cortes-Gonzalez[32], G. Costa[94a], M. J. Costa[170], D. Costanzo[141], G. Cottin[30], G. Cowan[80], B. E. Cox[87], K. Cranmer[112], S. J. Crawley[56], R. A. Creager[124], G. Cree[31], S. Crépé-Renaudin[58], F. Crescioli[83], W. A. Cribbs[148a,148b], M. Cristinziani[23], V. Croft[112], G. Crosetti[40a,40b], A. Cueto[85], T. Cuhadar Donszelmann[141], A. R. Cukierman[145], J. Cummings[179], M. Curatolo[50], J. Cúth[86], S. Czekierda[142], P. Czodrowski[32], G. D'amen[22a,22b], S. D'Auria[56], L. D'eramo[83], M. D'Onofrio[77], M. J. Da Cunha Sargedas De Sousa[128a,128b], C. Da Via[87], W. Dabrowski[41a], T. Dado[146a], T. Dai[92], O. Dale[15], F. Dallaire[97], C. Dallapiccola[89], M. Dam[39], J. R. Dandoy[124], M. F. Daneri[29], N. P. Dang[176], A. C. Daniells[19], N. S. Dann[87], M. Danninger[171], M. Dano Hoffmann[138], V. Dao[150], G. Darbo[53a], S. Darmora[8], J. Dassoulas[3], A. Dattagupta[118], T. Daubney[45], W. Davey[23], C. David[45], T. Davidek[131], D. R. Davis[48], P. Davison[81], E. Dawe[91], I. Dawson[141], K. De[8], R. de Asmundis[106a], A. De Benedetti[115], S. De Castro[22a,22b], S. De Cecco[83], N. De Groot[108], P. de Jong[109], H. De la Torre[93], F. De Lorenzi[67], A. De Maria[57], D. De Pedis[134a], A. De Salvo[134a], U. De Sanctis[135a,135b], A. De Santo[151], K. De Vasconcelos Corga[88], J. B. De Vivie De Regie[119], R. Debbe[27], C. Debenedetti[139], D. V. Dedovich[68], N. Dehghanian[3], I. Deigaard[109], M. Del Gaudio[40a,40b], J. Del Peso[85], D. Delgove[119], F. Deliot[138], C. M. Delitzsch[7], A. Dell'Acqua[32], L. Dell'Asta[24], M. Dell'Orso[126a,126b], M. Della Pietra[106a,106b], D. della Volpe[52], M. Delmastro[5], C. Delporte[119], P. A. Delsart[58], D. A. DeMarco[161], S. Demers[179], M. Demichev[68], A. Demilly[83], S. P. Denisov[132], D. Denysiuk[138], D. Derendarz[42], J. E. Derkaoui[137d], F. Derue[83], P. Dervan[77], K. Desch[23], C. Deterre[45], K. Dette[161], M. R. Devesa[29], P. O. Deviveiros[32], A. Dewhurst[133], S. Dhaliwal[25], F. A. Di Bello[52], A. Di Ciaccio[135a,135b], L. Di Ciaccio[5],

W. K. Di Clemente[124], C. Di Donato[106a,106b], A. Di Girolamo[32], B. Di Girolamo[32], B. Di Micco[136a,136b], R. Di Nardo[32], K. F. Di Petrillo[59], A. Di Simone[51], R. Di Sipio[161], D. Di Valentino[31], C. Diaconu[88], M. Diamond[161], F. A. Dias[39], M. A. Diaz[34a], J. Dickinson[16], E. B. Diehl[92], J. Dietrich[17], S. Díez Cornell[45], A. Dimitrievska[14], J. Dingfelder[23], P. Dita[28b], S. Dita[28b], F. Dittus[32], F. Djama[88], T. Djobava[54b], J. I. Djuvsland[60a], M. A. B. do Vale[26c], D. Dobos[32], M. Dobre[28b], D. Dodsworth[25], C. Doglioni[84], J. Dolejsi[131], Z. Dolezal[131], M. Donadelli[26d], S. Donati[126a,126b], P. Dondero[123a,123b], J. Donini[37], J. Dopke[133], A. Doria[106a], M. T. Dova[74], A. T. Doyle[56], E. Drechsler[57], M. Dris[10], Y. Du[36b], J. Duarte-Campderros[155], F. Dubinin[98], A. Dubreuil[52], E. Duchovni[175], G. Duckeck[102], A. Ducourthial[83], O. A. Ducu[97,p], D. Duda[109], A. Dudarev[32], A. Chr. Dudder[86], E. M. Duffield[16], L. Duflot[119], M. Dührssen[32], C. Dulsen[178], M. Dumancic[175], A. E. Dumitriu[28b], A. K. Duncan[56], M. Dunford[60a], A. Duperrin[88], H. Duran Yildiz[4a], M. Düren[55], A. Durglishvili[54b], D. Duschinger[47], B. Dutta[45], D. Duvnjak[1], M. Dyndal[45], B. S. Dziedzic[42], C. Eckardt[45], K. M. Ecker[103], R. C. Edgar[92], T. Eifert[32], G. Eigen[15], K. Einsweiler[16], T. Ekelof[168], M. El Kacimi[137c], R. El Kosseifi[88], V. Ellajosyula[88], M. Ellert[168], S. Elles[5], F. Ellinghaus[178], A. A. Elliot[172], N. Ellis[32], J. Elmsheuser[27], M. Elsing[32], D. Emeliyanov[133], Y. Enari[157], J. S. Ennis[173], M. B. Epland[48], J. Erdmann[46], A. Ereditato[18], M. Ernst[27], S. Errede[169], M. Escalier[119], C. Escobar[170], B. Esposito[50], O. Estrada Pastor[170], A. I. Etienvre[138], E. Etzion[155], H. Evans[64], A. Ezhilov[125], M. Ezzi[137e], F. Fabbri[22a,22b], L. Fabbri[22a,22b], V. Fabiani[108], G. Facini[81], R. M. Fakhrutdinov[132], S. Falciano[134a], R. J. Falla[81], J. Faltova[32], Y. Fang[35a], M. Fanti[94a,94b], A. Farbin[8], A. Farilla[136a], C. Farina[127], E. M. Farina[123a,123b], T. Farooque[93], S. Farrell[16], S. M. Farrington[173], P. Farthouat[32], F. Fassi[137e], P. Fassnacht[32], D. Fassouliotis[9], M. Faucci Giannelli[49], A. Favareto[53a,53b], W. J. Fawcett[122], L. Fayard[119], O. L. Fedin[125,q], W. Fedorko[171], S. Feigl[121], L. Feligioni[88], C. Feng[36b], E. J. Feng[32], M. J. Fenton[56], A. B. Fenyuk[132], L. Feremenga[8], P. Fernandez Martinez[170], J. Ferrando[45], A. Ferrari[168], P. Ferrari[109], R. Ferrari[123a], D. E. Ferreira de Lima[60b], A. Ferrer[170], D. Ferrere[52], C. Ferretti[92], F. Fiedler[86], A. Filipčič[78], M. Filipuzzi[45], F. Filthaut[108], M. Fincke-Keeler[172], K. D. Finelli[24], M. C. N. Fiolhais[128a,128c,r], L. Fiorini[170], A. Fischer[2], C. Fischer[13], J. Fischer[178], W. C. Fisher[93], N. Flaschel[45], I. Fleck[143], P. Fleischmann[92], R. R. M. Fletcher[124], T. Flick[178], B. M. Flierl[102], L. R. Flores Castillo[62a], M. J. Flowerdew[103], G. T. Forcolin[87], A. Formica[138], F. A. Förster[13], A. Forti[87], A. G. Foster[19], D. Fournier[119], H. Fox[75], S. Fracchia[141], P. Francavilla[126a,126b], M. Franchini[22a,22b], S. Franchino[60a], D. Francis[32], L. Franconi[121], M. Franklin[59], M. Frate[166], M. Fraternali[123a,123b], D. Freeborn[81], S. M. Fressard-Batraneanu[32], B. Freund[97], D. Froidevaux[32], J. A. Frost[122], C. Fukunaga[158], T. Fusayasu[104], J. Fuster[170], O. Gabizon[154], A. Gabrielli[22a,22b], A. Gabrielli[16], G. P. Gach[41a], S. Gadatsch[32], S. Gadomski[80], G. Gagliardi[53a,53b], L. G. Gagnon[97], C. Galea[108], B. Galhardo[128a,128c], E. J. Gallas[122], B. J. Gallop[133], P. Gallus[130], G. Galster[39], K. K. Gan[113], S. Ganguly[37], Y. Gao[77], Y. S. Gao[145,g], F. M. Garay Walls[34a], C. García[170], J. E. García Navarro[170], J. A. García Pascual[35a], M. Garcia-Sciveres[16], R. W. Gardner[33], N. Garelli[145], V. Garonne[121], A. Gascon Bravo[45], K. Gasnikova[45], C. Gatti[50], A. Gaudiello[53a,53b], G. Gaudio[123a], I. L. Gavrilenko[98], C. Gay[171], G. Gaycken[23], E. N. Gazis[10], C. N. P. Gee[133], J. Geisen[57], M. Geisen[86], M. P. Geisler[60a], K. Gellerstedt[148a,148b], C. Gemme[53a], M. H. Genest[58], C. Geng[92], S. Gentile[134a,134b], C. Gentsos[156], S. George[80], D. Gerbaudo[13], G. Geßner[46], S. Ghasemi[143], M. Ghneimat[23], B. Giacobbe[22a], S. Giagu[134a,134b], N. Giangiacomi[22a,22b], P. Giannetti[126a], S. M. Gibson[80], M. Gignac[171], M. Gilchriese[16], D. Gillberg[31], G. Gilles[178], D. M. Gingrich[3,d], M. P. Giordani[167a,167c], F. M. Giorgi[22a], P. F. Giraud[138], P. Giromini[59], G. Giugliarelli[167a,167c], D. Giugni[94a], F. Giuli[122], C. Giuliani[103], M. Giulini[60b], B. K. Gjelsten[121], S. Gkaitatzis[156], I. Gkialas[9,s], E. L. Gkougkousis[13], P. Gkountoumis[10], L. K. Gladilin[101], C. Glasman[85], J. Glatzer[13], P. C. F. Glaysher[45], A. Glazov[45], M. Goblirsch-Kolb[25], J. Godlewski[42], S. Goldfarb[91], T. Golling[52], D. Golubkov[132], A. Gomes[128a,128b,128d], R. Gonçalo[128a], R. Goncalves Gama[26a], J. Goncalves Pinto Firmino Da Costa[138], G. Gonella[51], L. Gonella[19], A. Gongadze[68], F. Gonnella[19], J. L. Gonski[59], S. González de la Hoz[170], S. Gonzalez-Sevilla[52], L. Goossens[32], P. A. Gorbounov[99], H. A. Gordon[27], B. Gorini[32], E. Gorini[76a,76b], A. Gorišek[78], A. T. Goshaw[48], C. Gössling[46], M. I. Gostkin[68], C. A. Gottardo[23], C. R. Goudet[119], D. Goujdami[137c], A. G. Goussiou[140], N. Govender[147b,t], E. Gozani[154], I. Grabowska-Bold[41a], P. O. J. Gradin[168], J. Gramling[166], E. Gramstad[121], S. Grancagnolo[17], V. Gratchev[125], P. M. Gravila[28f], C. Gray[56], H. M. Gray[16], Z. D. Greenwood[82,u], C. Grefe[23], K. Gregersen[81], I. M. Gregor[45], P. Grenier[145], K. Grevtsov[5], J. Griffiths[8], A. A. Grillo[139], K. Grimm[75], S. Grinstein[13,v], Ph. Gris[37], J.-F. Grivaz[119], S. Groh[86], E. Gross[175], J. Grosse-Knetter[57], G. C. Grossi[82], Z. J. Grout[81], A. Grummer[107], L. Guan[92], W. Guan[176], J. Guenther[32], F. Guescini[163a], D. Guest[166], O. Gueta[155], B. Gui[113], E. Guido[53a,53b], T. Guillemin[5], S. Guindon[32], U. Gul[56], C. Gumpert[32], J. Guo[36c], W. Guo[92], Y. Guo[36a,w], R. Gupta[43], S. Gurbuz[20a], G. Gustavino[115], B. J. Gutelman[154], P. Gutierrez[115], N. G. Gutierrez Ortiz[81], C. Gutschow[81], C. Guyot[138], M. P. Guzik[41a], C. Gwenlan[122], C. B. Gwilliam[77], A. Haas[112], C. Haber[16], H. K. Hadavand[8], N. Haddad[137e], A. Hadef[88], S. Hageböck[23], M. Hagihara[164], H. Hakobyan[180,*],

M. Haleem[45], J. Haley[116], G. Halladjian[93], G. D. Hallewell[88], K. Hamacher[178], P. Hamal[117], K. Hamano[172], A. Hamilton[147a], G. N. Hamity[141], P. G. Hamnett[45], L. Han[36a], S. Han[35a,35d], K. Hanagaki[69,x], K. Hanawa[157], M. Hance[139], D. M. Handl[102], B. Haney[124], P. Hanke[60a], J. B. Hansen[39], J. D. Hansen[39], M. C. Hansen[23], P. H. Hansen[39], K. Hara[164], A. S. Hard[176], T. Harenberg[178], F. Hariri[119], S. Harkusha[95], P. F. Harrison[173], N. M. Hartmann[102], Y. Hasegawa[142], A. Hasib[49], S. Hassani[138], S. Haug[18], R. Hauser[93], L. Hauswald[47], L. B. Havener[38], M. Havranek[130], C. M. Hawkes[19], R. J. Hawkings[32], D. Hayakawa[159], D. Hayden[93], C. P. Hays[122], J. M. Hays[79], H. S. Hayward[77], S. J. Haywood[133], S. J. Head[19], T. Heck[86], V. Hedberg[84], L. Heelan[8], S. Heer[23], K. K. Heidegger[51], S. Heim[45], T. Heim[16], B. Heinemann[45,y], J. J. Heinrich[102], L. Heinrich[112], C. Heinz[55], J. Hejbal[129], L. Helary[32], A. Held[171], S. Hellman[148a,148b], C. Helsens[32], R. C. W. Henderson[75], Y. Heng[176], S. Henkelmann[171], A. M. Henriques Correia[32], S. Henrot-Versille[119], G. H. Herbert[17], H. Herde[25], V. Herget[177], Y. Hernández Jiménez[147c], H. Herr[86], G. Herten[51], R. Hertenberger[102], L. Hervas[32], T. C. Herwig[124], G. G. Hesketh[81], N. P. Hessey[163a], J. W. Hetherly[43], S. Higashino[69], E. Higón-Rodriguez[170], K. Hildebrand[33], E. Hill[172], J. C. Hill[30], K. H. Hiller[45], S. J. Hillier[19], M. Hils[47], I. Hinchliffe[16], M. Hirose[51], D. Hirschbuehl[178], B. Hiti[78], O. Hladik[129], D. R. Hlaluku[147c], X. Hoad[49], J. Hobbs[150], N. Hod[163a], M. C. Hodgkinson[141], P. Hodgson[141], A. Hoecker[32], M. R. Hoeferkamp[107], F. Hoenig[102], D. Hohn[23], T. R. Holmes[33], M. Holzbock[102], M. Homann[46], S. Honda[164], T. Honda[69], T. M. Hong[127], B. H. Hooberman[169], W. H. Hopkins[118], Y. Horii[105], A. J. Horton[144], J.-Y. Hostachy[58], A. Hostiuc[140], S. Hou[153], A. Hoummada[137a], J. Howarth[87], J. Hoya[74], M. Hrabovsky[117], J. Hrdinka[32], I. Hristova[17], J. Hrivnac[119], T. Hryn'ova[5], A. Hrynevich[96], P. J. Hsu[63], S.-C. Hsu[140], Q. Hu[27], S. Hu[36c], Y. Huang[35a], Z. Hubacek[130], F. Hubaut[88], F. Huegging[23], T. B. Huffman[122], E. W. Hughes[38], M. Huhtinen[32], R. F. H. Hunter[31], P. Huo[150], N. Huseynov[68,b], J. Huston[93], J. Huth[59], R. Hyneman[92], G. Iacobucci[52], G. Iakovidis[27], I. Ibragimov[143], L. Iconomidou-Fayard[119], Z. Idrissi[137e], P. Iengo[32], O. Igonkina[109,z], T. Iizawa[174], Y. Ikegami[69], M. Ikeno[69], Y. Ilchenko[11,aa], D. Iliadis[156], N. Ilic[145], F. Iltzsche[47], G. Introzzi[123a,123b], P. Ioannou[9,*], M. Iodice[136a], K. Iordanidou[38], V. Ippolito[59], M. F. Isacson[168], N. Ishijima[120], M. Ishino[157], M. Ishitsuka[159], C. Issever[122], S. Istin[20a], F. Ito[164], J. M. Iturbe Ponce[62a], R. Iuppa[162a,162b], H. Iwasaki[69], J. M. Izen[44], V. Izzo[106a], S. Jabbar[3], P. Jackson[1], R. M. Jacobs[23], V. Jain[2], K. B. Jakobi[86], K. Jakobs[51], S. Jakobsen[65], T. Jakoubek[129], D. O. Jamin[116], D. K. Jana[82], R. Jansky[52], J. Janssen[23], M. Janus[57], P. A. Janus[41a], G. Jarlskog[84], N. Javadov[68,b], T. Javůrek[51], M. Javurkova[51], F. Jeanneau[138], L. Jeanty[16], J. Jejelava[54a,ab], A. Jelinskas[173], P. Jenni[51,ac], C. Jeske[173], S. Jézéquel[5], H. Ji[176], J. Jia[150], H. Jiang[67], Y. Jiang[36a], Z. Jiang[145], S. Jiggins[81], J. Jimenez Pena[170], S. Jin[35b], A. Jinaru[28b], O. Jinnouchi[159], H. Jivan[147c], P. Johansson[141], K. A. Johns[7], C. A. Johnson[64], W. J. Johnson[140], K. Jon-And[148a,148b], R. W. L. Jones[75], S. D. Jones[151], S. Jones[7], T. J. Jones[77], J. Jongmanns[60a], P. M. Jorge[128a,128b], J. Jovicevic[163a], X. Ju[176], A. Juste Rozas[13,v], M. K. Köhler[175], A. Kaczmarska[42], M. Kado[119], H. Kagan[113], M. Kagan[145], S. J. Kahn[88], T. Kaji[174], E. Kajomovitz[154], C. W. Kalderon[84], A. Kaluza[86], S. Kama[43], A. Kamenshchikov[132], N. Kanaya[157], L. Kanjir[78], V. A. Kantserov[100], J. Kanzaki[69], B. Kaplan[112], L. S. Kaplan[176], D. Kar[147c], K. Karakostas[10], N. Karastathis[10], M. J. Kareem[163b], E. Karentzos[10], S. N. Karpov[68], Z. M. Karpova[68], V. Kartvelishvili[75], A. N. Karyukhin[132], K. Kasahara[164], L. Kashif[176], R. D. Kass[113], A. Kastanas[149], Y. Kataoka[157], C. Kato[157], A. Katre[52], J. Katzy[45], K. Kawade[70], K. Kawagoe[73], T. Kawamoto[157], G. Kawamura[57], E. F. Kay[77], V. F. Kazanin[111,c], R. Keeler[172], R. Kehoe[43], J. S. Keller[31], E. Kellermann[84], J. J. Kempster[80], J Kendrick[19], H. Keoshkerian[161], O. Kepka[129], B. P. Kerševan[78], S. Kersten[178], R. A. Keyes[90], M. Khader[169], F. Khalil-zada[12], A. Khanov[116], A. G. Kharlamov[111,c], T. Kharlamova[111,c], A. Khodinov[160], T. J. Khoo[52], V. Khovanskiy[99,*], E. Khramov[68], J. Khubua[54b,ad], S. Kido[70], C. R. Kilby[80], H. Y. Kim[8], S. H. Kim[164], Y. K. Kim[33], N. Kimura[156], O. M. Kind[17], B. T. King[77], D. Kirchmeier[47], J. Kirk[133], A. E. Kiryunin[103], T. Kishimoto[157], D. Kisielewska[41a], V. Kitali[45], O. Kivernyk[5], E. Kladiva[146b], T. Klapdor-Kleingrothaus[51], M. H. Klein[92], M. Klein[77], U. Klein[77], K. Kleinknecht[86], P. Klimek[110], A. Klimentov[27], R. Klingenberg[46,*], T. Klingl[23], T. Klioutchnikova[32], F. F. Klitzner[102], E.-E. Kluge[60a], P. Kluit[109], S. Kluth[103], E. Kneringer[65], E. B. F. G. Knoops[88], A. Knue[103], A. Kobayashi[157], D. Kobayashi[73], T. Kobayashi[157], M. Kobel[47], M. Kocian[145], P. Kodys[131], T. Koffas[31], E. Koffeman[109], N. M. Köhler[103], T. Koi[145], M. Kolb[60b], I. Koletsou[5], T. Kondo[69], N. Kondrashova[36c], K. Köneke[51], A. C. König[108], T. Kono[69,ae], R. Konoplich[112,af], N. Konstantinidis[81], B. Konya[84], R. Kopeliansky[64], S. Koperny[41a], A. K. Kopp[51], K. Korcyl[42], K. Kordas[156], A. Korn[81], A. A. Korol[111,c], I. Korolkov[13], E. V. Korolkova[141], O. Kortner[103], S. Kortner[103], T. Kosek[131], V. V. Kostyukhin[23], A. Kotwal[48], A. Koulouris[10], A. Kourkoumeli-Charalampidi[123a,123b], C. Kourkoumelis[9], E. Kourlitis[141], V. Kouskoura[27], A. B. Kowalewska[42], R. Kowalewski[172], T. Z. Kowalski[41a], C. Kozakai[157], W. Kozanecki[138], A. S. Kozhin[132], V. A. Kramarenko[101], G. Kramberger[78], D. Krasnopevtsev[100], M. W. Krasny[83], A. Krasznahorkay[32], D. Krauss[103], J. A. Kremer[41a], J. Kretzschmar[77], K. Kreutzfeldt[55], P. Krieger[161], K. Krizka[16], K. Kroeninger[46], H. Kroha[103], J. Kroll[129],

J. Kroll[124], J. Kroseberg[23], J. Krstic[14], U. Kruchonak[68], H. Krüger[23], N. Krumnack[67], M. C. Kruse[48], T. Kubota[91], H. Kucuk[81], S. Kuday[4b], J. T. Kuechler[178], S. Kuehn[32], A. Kugel[60a], F. Kuger[177], T. Kuhl[45], V. Kukhtin[68], R. Kukla[88], Y. Kulchitsky[95], S. Kuleshov[34b], Y. P. Kulinich[169], M. Kuna[134a,134b], T. Kunigo[71], A. Kupco[129], T. Kupfer[46], O. Kuprash[155], H. Kurashige[70], L. L. Kurchaninov[163a], Y. A. Kurochkin[95], M. G. Kurth[35a,35d], E. S. Kuwertz[172], M. Kuze[159], J. Kvita[117], T. Kwan[172], D. Kyriazopoulos[141], A. La Rosa[103], J. L. La Rosa Navarro[26d], L. La Rotonda[40a,40b], F. La Ruffa[40a,40b], C. Lacasta[170], F. Lacava[134a,134b], J. Lacey[45], D. P. J. Lack[87], H. Lacker[17], D. Lacour[83], E. Ladygin[68], R. Lafaye[5], B. Laforge[83], T. Lagouri[179], S. Lai[57], S. Lammers[64], W. Lampl[7], E. Lançon[27], U. Landgraf[51], M. P. J. Landon[79], M. C. Lanfermann[52], V. S. Lang[45], J. C. Lange[13], R. J. Langenberg[32], A. J. Lankford[166], F. Lanni[27], K. Lantzsch[23], A. Lanza[123a], A. Lapertosa[53a,53b], S. Laplace[83], J. F. Laporte[138], T. Lari[94a], F. Lasagni Manghi[22a,22b], M. Lassnig[32], T. S. Lau[62a], P. Laurelli[50], W. Lavrijsen[16], A. T. Law[139], P. Laycock[77], T. Lazovich[59], M. Lazzaroni[94a,94b], B. Le[91], O. Le Dortz[83], E. Le Guirriec[88], E. P. Le Quilleuc[138], M. LeBlanc[172], T. LeCompte[6], F. Ledroit-Guillon[58], C. A. Lee[27], G. R. Lee[34a], S. C. Lee[153], L. Lee[59], B. Lefebvre[90], G. Lefebvre[83], M. Lefebvre[172], F. Legger[102], C. Leggett[16], G. Lehmann Miotto[32], X. Lei[7], W. A. Leight[45], M. A. L. Leite[26d], R. Leitner[131], D. Lellouch[175], B. Lemmer[57], K. J. C. Leney[81], T. Lenz[23], B. Lenzi[32], R. Leone[7], S. Leone[126a], C. Leonidopoulos[49], G. Lerner[151], C. Leroy[97], R. Les[161], A. A. J. Lesage[138], C. G. Lester[30], M. Levchenko[125], J. Levêque[5], D. Levin[92], L. J. Levinson[175], M. Levy[19], D. Lewis[79], B. Li[36a,aw], H. Li[150], L. Li[36c], Q. Li[35a,35d], Q. Li[36a], S. Li[48], X. Li[36c], Y. Li[143], Z. Liang[35a], B. Liberti[135a], A. Liblong[161], K. Lie[62c], J. Liebal[23], W. Liebig[15], A. Limosani[152], C. Y. Lin[30], K. Lin[93], S. C. Lin[182], T. H. Lin[86], R. A. Linck[64], B. E. Lindquist[150], A. E. Lionti[52], E. Lipeles[124], A. Lipniacka[15], M. Lisovyi[60b], T. M. Liss[169,ag], A. Lister[171], A. M. Litke[139], B. Liu[67], H. Liu[92], H. Liu[27], J. K. K. Liu[122], J. Liu[36b], J. B. Liu[36a], K. Liu[88], L. Liu[169], M. Liu[36a], Y. L. Liu[36a], Y. Liu[36a], M. Livan[123a,123b], A. Lleres[58], J. Llorente Merino[35a], S. L. Lloyd[79], C. Y. Lo[62b], F. Lo Sterzo[43], E. M. Lobodzinska[45], P. Loch[7], F. K. Loebinger[87], A. Loesle[51], K. M. Loew[25], T. Lohse[17], K. Lohwasser[141], M. Lokajicek[129], B. A. Long[24], J. D. Long[169], R. E. Long[75], L. Longo[76a,76b], K. A. Looper[113], J. A. Lopez[34b], I. Lopez Paz[13], A. Lopez Solis[83], J. Lorenz[102], N. Lorenzo Martinez[5], M. Losada[21], P. J. Lösel[102], X. Lou[35a], A. Lounis[119], J. Love[6], P. A. Love[75], H. Lu[62a], N. Lu[92], Y. J. Lu[63], H. J. Lubatti[140], C. Luci[134a,134b], A. Lucotte[58], C. Luedtke[51], F. Luehring[64], W. Lukas[65], L. Luminari[134a], O. Lundberg[148a,148b], B. Lund-Jensen[149], M. S. Lutz[89], P. M. Luzi[83], D. Lynn[27], R. Lysak[129], E. Lytken[84], F. Lyu[35a], V. Lyubushkin[68], H. Ma[27], L. L. Ma[36b], Y. Ma[36b], G. Maccarrone[50], A. Macchiolo[103], C. M. Macdonald[141], B. Maček[78], J. Machado Miguens[124,128b], D. Madaffari[170], R. Madar[37], W. F. Mader[47], A. Madsen[45], N. Madysa[47], J. Maeda[70], S. Maeland[15], T. Maeno[27], A. S. Maevskiy[101], V. Magerl[51], C. Maiani[119], C. Maidantchik[26a], T. Maier[102], A. Maio[128a,128b,128d], O. Majersky[146a], S. Majewski[118], Y. Makida[69], N. Makovec[119], B. Malaescu[83], Pa. Malecki[42], V. P. Maleev[125], F. Malek[58], U. Mallik[66], D. Malon[6], C. Malone[30], S. Maltezos[10], S. Malyukov[32], J. Mamuzic[170], G. Mancini[50], I. Mandić[78], J. Maneira[128a,128b], L. Manhaes de Andrade Filho[26b], J. Manjarres Ramos[47], K. H. Mankinen[84], A. Mann[102], A. Manousos[32], B. Mansoulie[138], J. D. Mansour[35a], R. Mantifel[90], M. Mantoani[57], S. Manzoni[94a,94b], L. Mapelli[32], G. Marceca[29], L. March[52], L. Marchese[122], G. Marchiori[83], M. Marcisovsky[129], C. A. Marin Tobon[32], M. Marjanov ic[37], D. E. Marley[92], F. Marroquim[26a], S. P. Marsden[87], Z. Marshall[16], M. U. F. Martensson[168], S. Marti-Garcia[170], C. B. Martin[113], T. A. Martin[173], V. J. Martin[49], B. Martin dit Latour[15], M. Martinez[13,v], V. I. Martinez Outschoorn[169], S. Martin-Haugh[133], V. S. Martoiu[28b], A. C. Martyniuk[81], A. Marzin[32], L. Masetti[86], T. Mashimo[157], R. Mashinistov[98], J. Masik[87], A. L. Maslennikov[111,c], L. H. Mason[91], L. Massa[135a,135b], P. Mastrandrea[5], A. Mastroberardino[40a,40b], T. Masubuchi[157], P. Mättig[178], J. Maurer[28b], S. J. Maxfield[77], D. A. Maximov[111,c], R. Mazini[153], I. Maznas[156], S. M. Mazza[94a,94b], N. C. Mc Fadden[107], G. Mc Goldrick[161], S. P. Mc Kee[92], A. McCarn[92], R. L. McCarthy[150], T. G. McCarthy[103], L. I. McClymont[81], E. F. McDonald[91], J. A. Mcfayden[32], G. Mchedlidze[57], S. J. McMahon[133], P. C. McNamara[91], C. J. McNicol[173], R. A. McPherson[172,o], S. Meehan[140], T. J. Megy[51], S. Mehlhase[102], A. Mehta[77], T. Meideck[58], K. Meier[60a], B. Meirose[44], D. Melini[170,ah], B. R. Mellado Garcia[147c], J. D. Mellenthin[57], M. Melo[146a], F. Meloni[18], A. Melzer[23], S. B. Menary[87], L. Meng[77], X. T. Meng[92], A. Mengarelli[22a,22b], S. Menke[103], E. Meoni[40a,40b], S. Mergelmeyer[17], C. Merlassino[18], P. Mermod[52], L. Merola[106a,106b], C. Meroni[94a], F. S. Merritt[33], A. Messina[134a,134b], J. Metcalfe[6], A. S. Mete[166], C. Meyer[124], J.-P. Meyer[138], J. Meyer[109], H. Meyer Zu Theenhausen[60a], F. Miano[151], R. P. Middleton[133], S. Miglioranzi[53a,53b], L. Mijović[49], G. Mikenberg[175], M. Mikestikova[129], M. Mikuž[78], M. Milesi[91], A. Milic[161], D. A. Millar[79], D. W. Miller[33], C. Mills[49], A. Milov[175], D. A. Milstead[148a,148b], A. A. Minaenko[132], Y. Minami[157], I. A. Minashvili[54b], A. I. Mincer[112], B. Mindur[41a], M. Mineev[68], Y. Minegishi[157], Y. Ming[176], L. M. Mir[13],

A. Mirto[76a,76b], K. P. Mistry[124], T. Mitani[174], J. Mitrevski[102], V. A. Mitsou[170], A. Miucci[18], P. S. Miyagawa[141], A. Mizukami[69], J. U. Mjörnmark[84], T. Mkrtchyan[180], M. Mlynarikova[131], T. Moa[148a,148b], K. Mochizuki[97], P. Mogg[51], S. Mohapatra[38], S. Molander[148a,148b], R. Moles-Valls[23], M. C. Mondragon[93], K. Mönig[45], J. Monk[39], E. Monnier[88], A. Montalbano[150], J. Montejo Berlingen[32], F. Monticelli[74], S. Monzani[94a], R. W. Moore[3], N. Morange[119], D. Moreno[21], M. Moreno Llácer[32], P. Morettini[53a], S. Morgenstern[32], D. Mori[144], T. Mori[157], M. Morii[59], M. Morinaga[174], V. Morisbak[121], A. K. Morley[32], G. Mornacchi[32], J. D. Morris[79], L. Morvaj[150], P. Moschovakos[10], M. Mosidze[54b], H. J. Moss[141], J. Moss[145,ai], K. Motohashi[159], R. Mount[145], E. Mountricha[27], E. J. W. Moyse[89], S. Muanza[88], F. Mueller[103], J. Mueller[127], R. S. P. Mueller[102], D. Muenstermann[75], P. Mullen[56], G. A. Mullier[18], F. J. Munoz Sanchez[87], W. J. Murray[173,133], H. Musheghyan[32], M. Muškinja[78], A. G. Myagkov[132,aj], M. Myska[130], B. P. Nachman[16], O. Nackenhorst[52], K. Nagai[122], R. Nagai[69,ae], K. Nagano[69], Y. Nagasaka[61], K. Nagata[164], M. Nagel[51], E. Nagy[88], A. M. Nairz[32], Y. Nakahama[105], K. Nakamura[69], T. Nakamura[157], I. Nakano[114], R. F. Naranjo Garcia[45], R. Narayan[11], D. I. Narrias Villar[60a], I. Naryshkin[125], T. Naumann[45], G. Navarro[21], R. Nayyar[7], H. A. Neal[92], P. Yu. Nechaeva[98], T. J. Neep[138], A. Negri[123a,123b], M. Negrini[22a], S. Nektarijevic[108], C. Nellist[57], A. Nelson[166], M. E. Nelson[122], S. Nemecek[129], P. Nemethy[112], M. Nessi[32,ak], M. S. Neubauer[169], M. Neumann[178], P. R. Newman[19], T. Y. Ng[62c], Y. S. Ng[17], T. Nguyen Manh[97], R. B. Nickerson[122], R. Nicolaidou[138], J. Nielsen[139], N. Nikiforou[11], V. Nikolaenko[132,aj], I. Nikolic-Audit[83], K. Nikolopoulos[19], P. Nilsson[27], Y. Ninomiya[69], A. Nisati[134a], N. Nishu[36c], R. Nisius[103], I. Nitsche[46], T. Nitta[174], T. Nobe[157], Y. Noguchi[71], M. Nomachi[120], I. Nomidis[31], M. A. Nomura[27], T. Nooney[79], M. Nordberg[32], N. Norjoharuddeen[122], O. Novgorodova[47], M. Nozaki[69], L. Nozka[117], K. Ntekas[166], E. Nurse[81], F. Nuti[91], K. O'connor[25], D. C. O'Neil[144], A. A. O'Rourke[45], V. O'Shea[56], F. G. Oakham[31,d], H. Oberlack[103], T. Obermann[23], J. Ocariz[83], A. Ochi[70], I. Ochoa[38], J. P. Ochoa-Ricoux[34a], S. Oda[73], S. Odaka[69], A. Oh[87], S. H. Oh[48], C. C. Ohm[149], H. Ohman[168], H. Oide[53a,53b], H. Okawa[164], Y. Okumura[157], T. Okuyama[69], A. Olariu[28b], L. F. Oleiro Seabra[128a], S. A. Olivares Pino[34a], D. Oliveira Damazio[27], J. Olszowska[42], A. Onofre[128a,128e], K. Onogi[105], P. U. E. Onyisi[11,aa], H. Oppen[121], M. J. Oreglia[33], Y. Oren[155], D. Orestano[136a,136b], N. Orlando[62b], R. S. Orr[161], B. Osculati[53a,53b,*], R. Ospanov[36a], G. Otero y Garzon[29], H. Otono[73], M. Ouchrif[137d], F. Ould-Saada[121], A. Ouraou[138], K. P. Oussoren[109], Q. Ouyang[35a], M. Owen[56], R. E. Owen[19], V. E. Ozcan[20a], N. Ozturk[8], K. Pachal[144], A. Pacheco Pages[13], L. Pacheco Rodriguez[138], C. Padilla Aranda[13], S. Pagan Griso[16], M. Paganini[179], F. Paige[27], G. Palacino[64], S. Palazzo[40a,40b], S. Palestini[32], M. Palka[41b], D. Pallin[37], E. St. Panagiotopoulou[10], I. Panagoulias[10], C. E. Pandini[52], J. G. Panduro Vazquez[80], P. Pani[32], S. Panitkin[27], D. Pantea[28b], L. Paolozzi[52], Th. D. Papadopoulou[10], K. Papageorgiou[9,s], A. Paramonov[6], D. Paredes Hernandez[179], A. J. Parker[75], M. A. Parker[30], K. A. Parker[45], F. Parodi[53a,53b], J. A. Parsons[38], U. Parzefall[51], V. R. Pascuzzi[161], J. M. Pasner[139], E. Pasqualucci[134a], S. Passaggio[53a], Fr. Pastore[80], S. Pataraia[86], J. R. Pater[87], T. Pauly[32], B. Pearson[103], S. Pedraza Lopez[170], R. Pedro[128a,128b], S. V. Peleganchuk[111,c], O. Penc[129], C. Peng[35a,35d], H. Peng[36a], J. Penwell[64], B. S. Peralva[26b], M. M. Perego[138], D. V. Perepelitsa[27], F. Peri[17], L. Perini[94a,94b], H. Pernegger[32], S. Perrella[106a,106b], R. Peschke[45], V. D. Peshekhonov[68,*], K. Peters[45], R. F. Y. Peters[87], B. A. Petersen[32], T. C. Petersen[39], E. Petit[58], A. Petridis[1], C. Petridou[156], P. Petroff[119], E. Petrolo[134a], M. Petrov[122], F. Petrucci[136a,136b], N. E. Pettersson[89], A. Peyaud[138], R. Pezoa[34b], F. H. Phillips[93], P. W. Phillips[133], G. Piacquadio[150], E. Pianori[173], A. Picazio[89], M. A. Pickering[122], R. Piegaia[29], J. E. Pilcher[33], A. D. Pilkington[87], M. Pinamonti[135a,135b], J. L. Pinfold[3], H. Pirumov[45], M. Pitt[175], L. Plazak[146a], M.-A. Pleier[27], V. Pleskot[86], E. Plotnikova[68], D. Pluth[67], P. Podberezko[111], R. Poettgen[84], R. Poggi[123a,123b], L. Poggioli[119], I. Pogrebnyak[93], D. Pohl[23], I. Pokharel[57], G. Polesello[123a], A. Poley[45], A. Policicchio[40a,40b], R. Polifka[32], A. Polini[22a], C. S. Pollard[56], V. Polychronakos[27], K. Pommès[32], D. Ponomarenko[100], L. Pontecorvo[134a], G. A. Popeneciu[28d], D. M. Portillo Quintero[83], S. Pospisil[130], K. Potamianos[45], I. N. Potrap[68], C. J. Potter[30], H. Potti[11], T. Poulsen[84], J. Poveda[32], M. E. Pozo Astigarraga[32], P. Pralavorio[88], A. Pranko[16], S. Prell[67], D. Price[87], M. Primavera[76a], S. Prince[90], N. Proklova[100], K. Prokofiev[62c], F. Prokoshin[34b], S. Protopopescu[27], J. Proudfoot[6], M. Przybycien[41a], A. Puri[169], P. Puzo[119], J. Qian[92], G. Qin[56], Y. Qin[87], A. Quadt[57], M. Queitsch-Maitland[45], D. Quilty[56], S. Raddum[121], V. Radeka[27], V. Radescu[122], S. K. Radhakrishnan[150], P. Radloff[118], P. Rados[91], F. Ragusa[94a,94b], G. Rahal[181], J. A. Raine[87], S. Rajagopalan[27], C. Rangel-Smith[168], T. Rashid[119], S. Raspopov[5], M. G. Ratti[94a,94b], D. M. Rauch[45], F. Rauscher[102], S. Rave[86], I. Ravinovich[175], J. H. Rawling[87], M. Raymond[32], A. L. Read[121], N. P. Readioff[58], M. Reale[76a,76b], D. M. Rebuzzi[123a,123b], A. Redelbach[177], G. Redlinger[27], R. Reece[139], R. G. Reed[147c], K. Reeves[44], L. Rehnisch[17], J. Reichert[124], A. Reiss[86], C. Rembser[32], H. Ren[35a,35d], M. Rescigno[134a], S. Resconi[94a], E. D. Resseguie[124], S. Rettie[171], E. Reynolds[19], O. L. Rezanova[111,c], P. Reznicek[131], R. Rezvani[97], R. Richter[103], S. Richter[81], E. Richter-Was[41b], O. Ricken[23], M. Ridel[83], P. Rieck[103], C. J. Riegel[178], J. Rieger[57], O. Rifki[115], M. Rijssenbeek[150], A. Rimoldi[123a,123b],

M. Rimoldi[18], L. Rinaldi[22a], G. Ripellino[149], B. Ristić[32], E. Ritsch[32], I. Riu[13], F. Rizatdinova[116], E. Rizvi[79], C. Rizzi[13], R. T. Roberts[87], S. H. Robertson[90,o], A. Robichaud-Veronneau[90], D. Robinson[30], J. E. M. Robinson[45], A. Robson[56], E. Rocco[86], C. Roda[126a,126b], Y. Rodina[88,al], S. Rodriguez Bosca[170], A. Rodriguez Perez[13], D. Rodriguez Rodriguez[170], S. Roe[32], C. S. Rogan[59], O. Røhne[121], J. Roloff[59], A. Romaniouk[100], M. Romano[22a,22b], S. M. Romano Saez[37], E. Romero Adam[170], N. Rompotis[77], M. Ronzani[51], L. Roos[83], S. Rosati[134a], K. Rosbach[51], P. Rose[139], N.-A. Rosien[57], E. Rossi[106a,106b], L. P. Rossi[53a], J. H. N. Rosten[30], R. Rosten[140], M. Rotaru[28b], J. Rothberg[140], D. Rousseau[119], D. Roy[147c], A. Rozanov[88], Y. Rozen[154], X. Ruan[147c], F. Rubbo[145], F. Rühr[51], A. Ruiz-Martinez[31], Z. Rurikova[51], N. A. Rusakovich[68], H. L. Russell[90], J. P. Rutherfoord[7], N. Ruthmann[32], E. M. Rüttinger[45], Y. F. Ryabov[125], M. Rybar[169], G. Rybkin[119], S. Ryu[6], A. Ryzhov[132], G. F. Rzehorz[57], A. F. Saavedra[152], G. Sabato[109], S. Sacerdoti[29], H. F.-W. Sadrozinski[139], R. Sadykov[68], F. Safai Tehrani[134a], P. Saha[110], M. Sahinsoy[60a], M. Saimpert[45], M. Saito[157], T. Saito[157], H. Sakamoto[157], Y. Sakurai[174], G. Salamanna[136a,136b], J. E. Salazar Loyola[34b], D. Salek[109], P. H. Sales De Bruin[168], D. Salihagic[103], A. Salnikov[145], J. Salt[170], D. Salvatore[40a,40b], F. Salvatore[151], A. Salvucci[62a,62b,62c], A. Salzburger[32], D. Sammel[51], D. Sampsonidis[156], D. Sampsonidou[156], J. Sánchez[170], V. Sanchez Martinez[170], A. Sanchez Pineda[167a,167c], H. Sandaker[121], R. L. Sandbach[79], C. O. Sander[45], M. Sandhoff[178], C. Sandoval[21], D. P. C. Sankey[133], M. Sannino[53a,53b], Y. Sano[105], A. Sansoni[50], C. Santoni[37], H. Santos[128a], I. Santoyo Castillo[151], A. Sapronov[68], J. G. Saraiva[128a,128d], B. Sarrazin[23], O. Sasaki[69], K. Sato[164], E. Sauvan[5], G. Savage[80], P. Savard[161,d], N. Savic[103], C. Sawyer[133], L. Sawyer[82,u], J. Saxon[33], C. Sbarra[22a], A. Sbrizzi[22a,22b], T. Scanlon[81], D. A. Scannicchio[166], J. Schaarschmidt[140], P. Schacht[103], B. M. Schachtner[102], D. Schaefer[33], L. Schaefer[124], R. Schaefer[45], J. Schaeffer[86], S. Schaepe[32], S. Schaetzel[60b], U. Schäfer[86], A. C. Schaffer[119], D. Schaile[102], R. D. Schamberger[150], V. A. Schegelsky[125], D. Scheirich[131], F. Schenck[17], M. Schernau[166], C. Schiavi[53a,53b], S. Schier[139], L. K. Schildgen[23], C. Schillo[51], M. Schioppa[40a,40b], S. Schlenker[32], K. R. Schmidt-Sommerfeld[103], K. Schmieden[32], C. Schmitt[86], S. Schmitt[45], S. Schmitz[86], U. Schnoor[51], L. Schoeffel[138], A. Schoening[60b], B. D. Schoenrock[93], E. Schopf[23], M. Schott[86], J. F. P. Schouwenberg[108], J. Schovancova[32], S. Schramm[52], N. Schuh[86], A. Schulte[86], M. J. Schultens[23], H.-C. Schultz-Coulon[60a], H. Schulz[17], M. Schumacher[51], B. A. Schumm[139], Ph. Schune[138], A. Schwartzman[145], T. A. Schwarz[92], H. Schweiger[87], Ph. Schwemling[138], R. Schwienhorst[93], J. Schwindling[138], A. Sciandra[23], G. Sciolla[25], M. Scornajenghi[40a,40b], F. Scuri[126a], F. Scutti[91], J. Searcy[92], P. Seema[23], S. C. Seidel[107], A. Seiden[139], J. M. Seixas[26a], G. Sekhniaidze[106a], K. Sekhon[92], S. J. Sekula[43], N. Semprini-Cesari[22a,22b], S. Senkin[37], C. Serfon[121], L. Serin[119], L. Serkin[167a,167b], M. Sessa[136a,136b], R. Seuster[172], H. Severini[115], T. Šfiligoj[78], F. Sforza[165], A. Sfyrla[52], E. Shabalina[57], N. W. Shaikh[148a,148b], L. Y. Shan[35a], R. Shang[169], J. T. Shank[24], M. Shapiro[16], P. B. Shatalov[99], K. Shaw[167a,167b], S. M. Shaw[87], A. Shcherbakova[148a,148b], C. Y. Shehu[151], Y. Shen[115], N. Sherafati[31], A. D. Sherman[24], P. Sherwood[81], L. Shi[153,am], S. Shimizu[70], C. O. Shimmin[179], M. Shimojima[104], I. P. J. Shipsey[122], S. Shirabe[73], M. Shiyakova[68,an], J. Shlomi[175], A. Shmeleva[98], D. Shoaleh Saadi[97], M. J. Shochet[33], S. Shojaii[94a,94b], D. R. Shope[115], S. Shrestha[113], E. Shulga[100], M. A. Shupe[7], P. Sicho[129], A. M. Sickles[169], P. E. Sidebo[149], E. Sideras Haddad[147c], O. Sidiropoulou[177], A. Sidoti[22a,22b], F. Siegert[47], Dj. Sijacki[14], J. Silva[128a,128d], S. B. Silverstein[148a], V. Simak[130], L. Simic[68], S. Simion[119], E. Simioni[86], B. Simmons[81], M. Simon[86], P. Sinervo[161], N. B. Sinev[118], M. Sioli[22a,22b], G. Siragusa[177], I. Siral[92], S. Yu. Sivoklokov[101], J. Sjölin[148a,148b], M. B. Skinner[75], P. Skubic[115], M. Slater[19], T. Slavicek[130], M. Slawinska[42], K. Sliwa[165], R. Slovak[131], V. Smakhtin[175], B. H. Smart[5], J. Smiesko[146a], N. Smirnov[100], S. Yu. Smirnov[100], Y. Smirnov[100], L. N. Smirnova[101,ao], O. Smirnova[84], J. W. Smith[57], M. N. K. Smith[38], R. W. Smith[38], M. Smizanska[75], K. Smolek[130], A. A. Snesarev[98], I. M. Snyder[118], S. Snyder[27], R. Sobie[172,o], F. Socher[47], A. Soffer[155], A. Søgaard[49], D. A. Soh[153], G. Sokhrannyi[78], C. A. Solans Sanchez[32], M. Solar[130], E. Yu. Soldatov[100], U. Soldevila[170], A. A. Solodkov[132], A. Soloshenko[68], O. V. Solovyanov[132], V. Solovyev[125], P. Sommer[141], H. Son[165], A. Sopczak[130], D. Sosa[60b], C. L. Sotiropoulou[126a,126b], S. Sottocornola[123a,123b], R. Soualah[167a,167c], A. M. Soukharev[111,c], D. South[45], B. C. Sowden[80], S. Spagnolo[76a,76b], M. Spalla[126a,126b], M. Spangenberg[173], F. Spanò[80], D. Sperlich[17], F. Spettel[103], T. M. Spieker[60a], R. Spighi[22a], G. Spigo[32], L. A. Spiller[91], M. Spousta[131], R. D. St. Denis[56,*], A. Stabile[94a,94b], R. Stamen[60a], S. Stamm[17], E. Stanecka[42], R. W. Stanek[6], C. Stanescu[136a], M. M. Stanitzki[45], B. S. Stapf[109], S. Stapnes[121], E. A. Starchenko[132], G. H. Stark[33], J. Stark[58], S. H Stark[39], P. Staroba[129], P. Starovoitov[60a], S. Stärz[32], R. Staszewski[42], M. Stegler[45], P. Steinberg[27], B. Stelzer[144], H. J. Stelzer[32], O. Stelzer-Chilton[163a], H. Stenzel[55], T. J. Stevenson[79], G. A. Stewart[56], M. C. Stockton[118], M. Stoebe[90], G. Stoicea[28b], P. Stolte[57], S. Stonjek[103], A. R. Stradling[8], A. Straessner[47], M. E. Stramaglia[18], J. Strandberg[149], S. Strandberg[148a,148b], M. Strauss[115], P. Strizenec[146b], R. Ströhmer[177], D. M. Strom[118], R. Stroynowski[43], A. Strubig[49], S. A. Stucci[27], B. Stugu[15], N. A. Styles[45], D. Su[145], J. Su[127], S. Suchek[60a], Y. Sugaya[120], M. Suk[130], V. V. Sulin[98], D. M. S. Sultan[162a,162b], S. Sultansoy[4c], T. Sumida[71], S. Sun[59],

X. Sun[3], K. Suruliz[151], C. J. E. Suster[152], M. R. Sutton[151], S. Suzuki[69], M. Svatos[129], M. Swiatlowski[33], S. P. Swift[2], I. Sykora[146a], T. Sykora[131], D. Ta[51], K. Tackmann[45], J. Taenzer[155], A. Taffard[166], R. Tafirout[163a], E. Tahirovic[79], N. Taiblum[155], H. Takai[27], R. Takashima[72], E. H. Takasugi[103], K. Takeda[70], T. Takeshita[142], Y. Takubo[69], M. Talby[88], A. A. Talyshev[111,c], J. Tanaka[157], M. Tanaka[159], R. Tanaka[119], S. Tanaka[69], R. Tanioka[70], B. B. Tannenwald[113], S. Tapia Araya[34b], S. Tapprogge[86], S. Tarem[154], G. F. Tartarelli[94a], P. Tas[131], M. Tasevsky[129], T. Tashiro[71], E. Tassi[40a,40b], A. Tavares Delgado[128a,128b], Y. Tayalati[137e], A. C. Taylor[107], A. J. Taylor[49], G. N. Taylor[91], P. T. E. Taylor[91], W. Taylor[163b], P. Teixeira-Dias[80], D. Temple[144], H. Ten Kate[32], P. K. Teng[153], J. J. Teoh[120], F. Tepel[178], S. Terada[69], K. Terashi[157], J. Terron[85], S. Terzo[13], M. Testa[50], R. J. Teuscher[161,o], S. J. Thais[179], T. Theveneaux-Pelzer[88], F. Thiele[39], J. P. Thomas[19], J. Thomas-Wilsker[80], P. D. Thompson[19], A. S. Thompson[56], L. A. Thomsen[179], E. Thomson[124], Y. Tian[38], M. J. Tibbetts[16], R. E. Ticse Torres[57], V. O. Tikhomirov[98,ap], Yu. A. Tikhonov[111,c], S. Timoshenko[100], P. Tipton[179], S. Tisserant[88], K. Todome[159], S. Todorova-Nova[5], S. Todt[47], J. Tojo[73], S. Tokár[146a], K. Tokushuku[69], E. Tolley[113], L. Tomlinson[87], M. Tomoto[105], L. Tompkins[145,aq], K. Toms[107], B. Tong[59], P. Tornambe[51], E. Torrence[118], H. Torres[47], E. Torró Pastor[140], J. Toth[88,ar], F. Touchard[88], D. R. Tovey[141], C. J. Treado[112], T. Trefzger[177], F. Tresoldi[151], A. Tricoli[27], I. M. Trigger[163a], S. Trincaz-Duvoid[83], M. F. Tripiana[13], W. Trischuk[161], B. Trocmé[58], A. Trofymov[45], C. Troncon[94a], M. Trottier-McDonald[16], M. Trovatelli[172], L. Truong[147b], M. Trzebinski[42], A. Trzupek[42], K. W. Tsang[62a], J. C.-L. Tseng[122], P. V. Tsiareshka[95], N. Tsirintanis[9], S. Tsiskaridze[13], V. Tsiskaridze[51], E. G. Tskhadadze[54a], I. I. Tsukerman[99], V. Tsulaia[16], S. Tsuno[69], D. Tsybychev[150], Y. Tu[62b], A. Tudorache[28b], V. Tudorache[28b], T. T. Tulbure[28a], A. N. Tuna[59], S. Turchikhin[68], D. Turgeman[175], I. Turk Cakir[4b,as], R. Turra[94a], P. M. Tuts[38], G. Ucchielli[22a,22b], I. Ueda[69], M. Ughetto[148a,148b], F. Ukegawa[164], G. Unal[32], A. Undrus[27], G. Unel[166], F. C. Ungaro[91], Y. Unno[69], K. Uno[157], C. Unverdorben[102], J. Urban[146b], P. Urquijo[91], P. Urrejola[86], G. Usai[8], J. Usui[69], L. Vacavant[88], V. Vacek[130], B. Vachon[90], K. O. H. Vadla[121], A. Vaidya[81], C. Valderanis[102], E. Valdes Santurio[148a,148b], M. Valente[52], S. Valentinetti[22a,22b], A. Valero[170], L. Valéry[13], S. Valkar[131], A. Vallier[5], J. A. Valls Ferrer[170], W. Van Den Wollenberg[109], H. van der Graaf[109], P. van Gemmeren[6], J. Van Nieuwkoop[144], I. van Vulpen[109], M. C. van Woerden[109], M. Vanadia[135a,135b], W. Vandelli[32], A. Vaniachine[160], P. Vankov[109], G. Vardanyan[180], R. Vari[134a], E. W. Varnes[7], C. Varni[53a,53b], T. Varol[43], D. Varouchas[119], A. Vartapetian[8], K. E. Varvell[152], J. G. Vasquez[179], G. A. Vasquez[34b], F. Vazeille[37], D. Vazquez Furelos[13], T. Vazquez Schroeder[90], J. Veatch[57], V. Veeraraghavan[7], L. M. Veloce[161], F. Veloso[128a,128c], S. Veneziano[134a], A. Ventura[76a,76b], M. Venturi[172], N. Venturi[32], A. Venturini[25], V. Vercesi[123a], M. Verducci[136a,136b], W. Verkerke[109], A. T. Vermeulen[109], J. C. Vermeulen[109], M. C. Vetterli[144,d], N. Viaux Maira[34b], O. Viazlo[84], I. Vichou[169,*], T. Vickey[141], O. E. Vickey Boeriu[141], G. H. A. Viehhauser[122], S. Viel[16], L. Vigani[122], M. Villa[22a,22b], M. Villaplana Perez[94a,94b], E. Vilucchi[50], M. G. Vincter[31], V. B. Vinogradov[68], A. Vishwakarma[45], C. Vittori[22a,22b], I. Vivarelli[151], S. Vlachos[10], M. Vogel[178], P. Vokac[130], G. Volpi[13], H. von der Schmitt[103], E. von Toerne[23], V. Vorobel[131], K. Vorobev[100], M. Vos[170], R. Voss[32], J. H. Vossebeld[77], N. Vranjes[14], M. Vranjes Milosavljevic[14], V. Vrba[130], M. Vreeswijk[109], R. Vuillermet[32], I. Vukotic[33], P. Wagner[23], W. Wagner[178], J. Wagner-Kuhr[102], H. Wahlberg[74], S. Wahrmund[47], K. Wakamiya[70], J. Walder[75], R. Walker[102], W. Walkowiak[143], V. Wallangen[148a,148b], C. Wang[35b], C. Wang[36b,at], F. Wang[176], H. Wang[16], H. Wang[3], J. Wang[45], J. Wang[152], Q. Wang[115], R.-J. Wang[83], R. Wang[6], S. M. Wang[153], T. Wang[38], W. Wang[153,au], W. Wang[36a,av], Z. Wang[36c], C. Wanotayaroj[45], A. Warburton[90], C. P. Ward[30], D. R. Wardrope[81], A. Washbrook[49], P. M. Watkins[19], A. T. Watson[19], M. F. Watson[19], G. Watts[140], S. Watts[87], B. M. Waugh[81], A. F. Webb[11], S. Webb[86], M. S. Weber[18], S. M. Weber[60a], S. W. Weber[177], S. A. Weber[31], J. S. Webster[6], A. R. Weidberg[122], B. Weinert[64], J. Weingarten[57], M. Weirich[86], C. Weiser[51], H. Weits[109], P. S. Wells[32], T. Wenaus[27], T. Wengler[32], S. Wenig[32], N. Wermes[23], M. D. Werner[67], P. Werner[32], M. Wessels[60a], T. D. Weston[18], K. Whalen[118], N. L. Whallon[140], A. M. Wharton[75], A. S. White[92], A. White[8], M. J. White[1], R. White[34b], D. Whiteson[166], B. W. Whitmore[75], F. J. Wickens[133], W. Wiedenmann[176], M. Wielers[133], C. Wiglesworth[39], L. A. M. Wiik-Fuchs[51], A. Wildauer[103], F. Wilk[87], H. G. Wilkens[32], H. H. Williams[124], S. Williams[109], C. Willis[93], S. Willocq[89], J. A. Wilson[19], I. Wingerter-Seez[5], E. Winkels[151], F. Winklmeier[118], O. J. Winston[151], B. T. Winter[23], M. Wittgen[145], M. Wobisch[82,u], A. Wolf[86], T. M. H. Wolf[109], R. Wolff[88], M. W. Wolter[42], H. Wolters[128a,128c], V. W. S. Wong[171], N. L. Woods[139], S. D. Worm[19], B. K. Wosiek[42], J. Wotschack[32], K. W. Wozniak[42], M. Wu[33], S. L. Wu[176], X. Wu[52], Y. Wu[92], T. R. Wyatt[87], B. M. Wynne[49], S. Xella[39], Z. Xi[92], L. Xia[35c], D. Xu[35a], L. Xu[27], T. Xu[138], W. Xu[92], B. Yabsley[152], S. Yacoob[147a], D. Yamaguchi[159], Y. Yamaguchi[159], A. Yamamoto[69], S. Yamamoto[157], T. Yamanaka[157], F. Yamane[70], M. Yamatani[157], T. Yamazaki[157], Y. Yamazaki[70], Z. Yan[24], H. Yang[36c], H. Yang[16], Y. Yang[153], Z. Yang[15], W.-M. Yao[16], Y. C. Yap[45], Y. Yasu[69], E. Yatsenko[5], K. H. Yau Wong[23], J. Ye[43], S. Ye[27], I. Yeletskikh[68], E. Yigitbasi[24], E. Yildirim[86], K. Yorita[174], K. Yoshihara[124], C. Young[145], C. J. S. Young[32], J. Yu[8],

J. Yu[67], S. P. Y. Yuen[23], I. Yusuff[30,aw], B. Zabinski[42], G. Zacharis[10], R. Zaidan[13], A. M. Zaitsev[132,aj], N. Zakharchuk[45], J. Zalieckas[15], A. Zaman[150], S. Zambito[59], D. Zanzi[91], C. Zeitnitz[178], G. Zemaityte[122], A. Zemla[41a], J. C. Zeng[169], Q. Zeng[145], O. Zenin[132], T. Ženiš[146a], D. Zerwas[119], D. Zhang[36b], D. Zhang[92], F. Zhang[176], G. Zhang[36a,av], H. Zhang[119], J. Zhang[6], L. Zhang[51], L. Zhang[36a], M. Zhang[169], P. Zhang[35b], R. Zhang[23], R. Zhang[36a,at], X. Zhang[36b], Y. Zhang[35a,35d], Z. Zhang[119], X. Zhao[43], Y. Zhao[36b,ax], Z. Zhao[36a], A. Zhemchugov[68], B. Zhou[92], C. Zhou[176], L. Zhou[43], M. Zhou[35a,35d], M. Zhou[150], N. Zhou[36c], Y. Zhou[7], C. G. Zhu[36b], H. Zhu[35a], J. Zhu[92], Y. Zhu[36a], X. Zhuang[35a], K. Zhukov[98], A. Zibell[177], D. Zieminska[64], N. I. Zimine[68], C. Zimmermann[86], S. Zimmermann[51], Z. Zinonos[103], M. Zinser[86], M. Ziolkowski[143], L. Živković[14], G. Zobernig[176], A. Zoccoli[22a,22b], R. Zou[33], M. zur Nedden[17], L. Zwalinski[32]

[1] Department of Physics, University of Adelaide, Adelaide, Australia
[2] Physics Department, SUNY Albany, Albany, NY, USA
[3] Department of Physics, University of Alberta, Edmonton, AB, Canada
[4] [(a)]Department of Physics, Ankara University, Ankara, Turkey; [(b)]Istanbul Aydin University, Istanbul, Turkey; [(c)]Division of Physics, TOBB University of Economics and Technology, Ankara, Turkey
[5] LAPP, CNRS/IN2P3 and Université Savoie Mont Blanc, Annecy-le-Vieux, France
[6] High Energy Physics Division, Argonne National Laboratory, Argonne, IL, USA
[7] Department of Physics, University of Arizona, Tucson, AZ, USA
[8] Department of Physics, The University of Texas at Arlington, Arlington, TX, USA
[9] Physics Department, National and Kapodistrian University of Athens, Athens, Greece
[10] Physics Department, National Technical University of Athens, Zografou, Greece
[11] Department of Physics, The University of Texas at Austin, Austin, TX, USA
[12] Institute of Physics, Azerbaijan Academy of Sciences, Baku, Azerbaijan
[13] Institut de Física d'Altes Energies (IFAE), The Barcelona Institute of Science and Technology, Barcelona, Spain
[14] Institute of Physics, University of Belgrade, Belgrade, Serbia
[15] Department for Physics and Technology, University of Bergen, Bergen, Norway
[16] Physics Division, Lawrence Berkeley National Laboratory, University of California, Berkeley, CA, USA
[17] Department of Physics, Humboldt University, Berlin, Germany
[18] Albert Einstein Center for Fundamental Physics, Laboratory for High Energy Physics, University of Bern, Bern, Switzerland
[19] School of Physics and Astronomy, University of Birmingham, Birmingham, UK
[20] [(a)]Department of Physics, Bogazici University, Istanbul, Turkey; [(b)]Department of Physics Engineering, Gaziantep University, Gaziantep, Turkey; [(c)]Faculty of Engineering and Natural Sciences, Istanbul Bilgi University, Istanbul, Turkey; [(d)]Faculty of Engineering and Natural Sciences, Bahcesehir University, Istanbul, Turkey
[21] Centro de Investigaciones, Universidad Antonio Narino, Bogota, Colombia
[22] [(a)]INFN Sezione di Bologna, Bologna, Italy; [(b)]Dipartimento di Fisica e Astronomia, Università di Bologna, Bologna, Italy
[23] Physikalisches Institut, University of Bonn, Bonn, Germany
[24] Department of Physics, Boston University, Boston, MA, USA
[25] Department of Physics, Brandeis University, Waltham, MA, USA
[26] [(a)]Universidade Federal do Rio De Janeiro COPPE/EE/IF, Rio de Janeiro, Brazil; [(b)]Electrical Circuits Department, Federal University of Juiz de Fora (UFJF), Juiz de Fora, Brazil; [(c)]Federal University of Sao Joao del Rei (UFSJ), Sao Joao del Rei, Brazil; [(d)]Instituto de Fisica, Universidade de Sao Paulo, Sao Paulo, Brazil
[27] Physics Department, Brookhaven National Laboratory, Upton, NY, USA
[28] [(a)]Transilvania University of Brasov, Brasov, Romania; [(b)]Horia Hulubei National Institute of Physics and Nuclear Engineering, Bucharest, Romania; [(c)]Department of Physics, Alexandru Ioan Cuza University of Iasi, Iasi, Romania ; [(d)]Physics Department, National Institute for Research and Development of Isotopic and Molecular Technologies, Cluj-Napoca, Romania; [(e)]University Politehnica Bucharest, Bucharest, Romania; [(f)]West University in Timisoara, Timisoara, Romania
[29] Departamento de Física, Universidad de Buenos Aires, Buenos Aires, Argentina
[30] Cavendish Laboratory, University of Cambridge, Cambridge, UK
[31] Department of Physics, Carleton University, Ottawa, ON, Canada

[32] CERN, Geneva, Switzerland
[33] Enrico Fermi Institute, University of Chicago, Chicago, IL, USA
[34] [(a)]Departamento de Física, Pontificia Universidad Católica de Chile, Santiago, Chile; [(b)]Departamento de Física, Universidad Técnica Federico Santa María, Valparaíso, Chile
[35] [(a)]Institute of High Energy Physics, Chinese Academy of Sciences, Beijing, China; [(b)]Department of Physics, Nanjing University, Nanjing, Jiangsu, China; [(c)]Physics Department, Tsinghua University, Beijing 100084, China; [(d)]University of Chinese Academy of Science (UCAS), Beijing, China
[36] [(a)]Department of Modern Physics and State Key Laboratory of Particle Detection and Electronics, University of Science and Technology of China, Hefei, Anhui, China; [(b)]School of Physics, Shandong University, Jinan, Shandong, China; [(c)]Department of Physics and Astronomy, Key Laboratory for Particle Physics, Astrophysics and Cosmology, Ministry of Education, Shanghai Key Laboratory for Particle Physics and Cosmology, Shanghai Jiao Tong University, Tsung-Dao Lee Institute , Shanghai, China
[37] Université Clermont Auvergne, CNRS/IN2P3, LPC, Clermont-Ferrand, France
[38] Nevis Laboratory, Columbia University, Irvington, NY, USA
[39] Niels Bohr Institute, University of Copenhagen, Copenhagen, Denmark
[40] [(a)]INFN Gruppo Collegato di Cosenza, Laboratori Nazionali di Frascati, Frascati, Italy; [(b)]Dipartimento di Fisica, Università della Calabria, Rende, Italy
[41] [(a)]Faculty of Physics and Applied Computer Science, AGH University of Science and Technology, Kraków, Poland; [(b)]Marian Smoluchowski Institute of Physics, Jagiellonian University, Kraków, Poland
[42] Institute of Nuclear Physics, Polish Academy of Sciences, Kraków, Poland
[43] Physics Department, Southern Methodist University, Dallas, TX, USA
[44] Physics Department, University of Texas at Dallas, Richardson, TX, USA
[45] DESY, Hamburg and Zeuthen, Germany
[46] Lehrstuhl für Experimentelle Physik IV, Technische Universität Dortmund, Dortmund, Germany
[47] Institut für Kern- und Teilchenphysik, Technische Universität Dresden, Dresden, Germany
[48] Department of Physics, Duke University, Durham, NC, USA
[49] SUPA-School of Physics and Astronomy, University of Edinburgh, Edinburgh, UK
[50] INFN e Laboratori Nazionali di Frascati, Frascati, Italy
[51] Fakultät für Mathematik und Physik, Albert-Ludwigs-Universität, Freiburg, Germany
[52] Departement de Physique Nucleaire et Corpusculaire, Université de Genève, Geneva, Switzerland
[53] [(a)]INFN Sezione di Genova, Genoa, Italy; [(b)]Dipartimento di Fisica, Università di Genova, Genoa, Italy
[54] [(a)]E. Andronikashvili Institute of Physics, Iv. Javakhishvili Tbilisi State University, Tbilisi, Georgia; [(b)]High Energy Physics Institute, Tbilisi State University, Tbilisi, Georgia
[55] II Physikalisches Institut, Justus-Liebig-Universität Giessen, Giessen, Germany
[56] SUPA-School of Physics and Astronomy, University of Glasgow, Glasgow, UK
[57] II Physikalisches Institut, Georg-August-Universität, Göttingen, Germany
[58] Laboratoire de Physique Subatomique et de Cosmologie, Université Grenoble-Alpes, CNRS/IN2P3, Grenoble, France
[59] Laboratory for Particle Physics and Cosmology, Harvard University, Cambridge, MA, USA
[60] [(a)]Kirchhoff-Institut für Physik, Ruprecht-Karls-Universität Heidelberg, Heidelberg, Germany; [(b)]Physikalisches Institut, Ruprecht-Karls-Universität Heidelberg, Heidelberg, Germany
[61] Faculty of Applied Information Science, Hiroshima Institute of Technology, Hiroshima, Japan
[62] [(a)]Department of Physics, The Chinese University of Hong Kong, Shatin, NT, Hong Kong; [(b)]Department of Physics, The University of Hong Kong, Hong Kong, China; [(c)]Department of Physics, Institute for Advanced Study, The Hong Kong University of Science and Technology, Clear Water Bay, Kowloon, Hong Kong, China
[63] Department of Physics, National Tsing Hua University, Hsinchu, Taiwan
[64] Department of Physics, Indiana University, Bloomington, IN, USA
[65] Institut für Astro- und Teilchenphysik, Leopold-Franzens-Universität, Innsbruck, Austria
[66] University of Iowa, Iowa City, IA, USA
[67] Department of Physics and Astronomy, Iowa State University, Ames, IA, USA
[68] Joint Institute for Nuclear Research, JINR Dubna, Dubna, Russia
[69] KEK, High Energy Accelerator Research Organization, Tsukuba, Japan

[70] Graduate School of Science, Kobe University, Kobe, Japan
[71] Faculty of Science, Kyoto University, Kyoto, Japan
[72] Kyoto University of Education, Kyoto, Japan
[73] Research Center for Advanced Particle Physics and Department of Physics, Kyushu University, Fukuoka, Japan
[74] Instituto de Física La Plata, Universidad Nacional de La Plata and CONICET, La Plata, Argentina
[75] Physics Department, Lancaster University, Lancaster, UK
[76] [(a)]INFN Sezione di Lecce, Lecce, Italy; [(b)]Dipartimento di Matematica e Fisica, Università del Salento, Lecce, Italy
[77] Oliver Lodge Laboratory, University of Liverpool, Liverpool, UK
[78] Department of Experimental Particle Physics, Jožef Stefan Institute and Department of Physics, University of Ljubljana, Ljubljana, Slovenia
[79] School of Physics and Astronomy, Queen Mary University of London, London, UK
[80] Department of Physics, Royal Holloway University of London, Surrey, UK
[81] Department of Physics and Astronomy, University College London, London, UK
[82] Louisiana Tech University, Ruston, LA, USA
[83] Laboratoire de Physique Nucléaire et de Hautes Energies, UPMC and Université Paris-Diderot and CNRS/IN2P3, Paris, France
[84] Fysiska institutionen, Lunds universitet, Lund, Sweden
[85] Departamento de Fisica Teorica C-15, Universidad Autonoma de Madrid, Madrid, Spain
[86] Institut für Physik, Universität Mainz, Mainz, Germany
[87] School of Physics and Astronomy, University of Manchester, Manchester, UK
[88] CPPM, Aix-Marseille Université and CNRS/IN2P3, Marseille, France
[89] Department of Physics, University of Massachusetts, Amherst, MA, USA
[90] Department of Physics, McGill University, Montreal, QC, Canada
[91] School of Physics, University of Melbourne, Victoria, Australia
[92] Department of Physics, The University of Michigan, Ann Arbor, MI, USA
[93] Department of Physics and Astronomy, Michigan State University, East Lansing, MI, USA
[94] [(a)]INFN Sezione di Milano, Milan, Italy; [(b)]Dipartimento di Fisica, Università di Milano, Milan, Italy
[95] B.I. Stepanov Institute of Physics, National Academy of Sciences of Belarus, Minsk, Republic of Belarus
[96] Research Institute for Nuclear Problems of Byelorussian State University, Minsk, Republic of Belarus
[97] Group of Particle Physics, University of Montreal, Montreal, QC, Canada
[98] P.N. Lebedev Physical Institute of the Russian Academy of Sciences, Moscow, Russia
[99] Institute for Theoretical and Experimental Physics (ITEP), Moscow, Russia
[100] National Research Nuclear University MEPhI, Moscow, Russia
[101] D.V. Skobeltsyn Institute of Nuclear Physics, M.V. Lomonosov Moscow State University, Moscow, Russia
[102] Fakultät für Physik, Ludwig-Maximilians-Universität München, Munich, Germany
[103] Max-Planck-Institut für Physik (Werner-Heisenberg-Institut), Munich, Germany
[104] Nagasaki Institute of Applied Science, Nagasaki, Japan
[105] Graduate School of Science and Kobayashi-Maskawa Institute, Nagoya University, Nagoya, Japan
[106] [(a)]INFN Sezione di Napoli, Naples, Italy; [(b)]Dipartimento di Fisica, Università di Napoli, Naples, Italy
[107] Department of Physics and Astronomy, University of New Mexico, Albuquerque, NM, USA
[108] Institute for Mathematics, Astrophysics and Particle Physics, Radboud University Nijmegen/Nikhef, Nijmegen, The Netherlands
[109] Nikhef National Institute for Subatomic Physics, University of Amsterdam, Amsterdam, The Netherlands
[110] Department of Physics, Northern Illinois University, DeKalb, IL, USA
[111] Budker Institute of Nuclear Physics, SB RAS, Novosibirsk, Russia
[112] Department of Physics, New York University, New York, NY, USA
[113] Ohio State University, Columbus, OH, USA
[114] Faculty of Science, Okayama University, Okayama, Japan
[115] Homer L. Dodge Department of Physics and Astronomy, University of Oklahoma, Norman, OK, USA
[116] Department of Physics, Oklahoma State University, Stillwater, OK, USA
[117] Palacký University, RCPTM, Olomouc, Czech Republic
[118] Center for High Energy Physics, University of Oregon, Eugene, OR, USA

[119] LAL, Univ. Paris-Sud, CNRS/IN2P3, Université Paris-Saclay, Orsay, France
[120] Graduate School of Science, Osaka University, Osaka, Japan
[121] Department of Physics, University of Oslo, Oslo, Norway
[122] Department of Physics, Oxford University, Oxford, UK
[123] [(a)]INFN Sezione di Pavia, Pavia, Italy; [(b)]Dipartimento di Fisica, Università di Pavia, Pavia, Italy
[124] Department of Physics, University of Pennsylvania, Philadelphia, PA, USA
[125] National Research Centre "Kurchatov Institute" B.P. Konstantinov Petersburg Nuclear Physics Institute, St. Petersburg, Russia
[126] [(a)]INFN Sezione di Pisa, Pisa, Italy; [(b)]Dipartimento di Fisica E. Fermi, Università di Pisa, Pisa, Italy
[127] Department of Physics and Astronomy, University of Pittsburgh, Pittsburgh, PA, USA
[128] [(a)]Laboratório de Instrumentação e Física Experimental de Partículas-LIP, Lisbon, Portugal; [(b)]Faculdade de Ciências, Universidade de Lisboa, Lisbon, Portugal; [(c)]Department of Physics, University of Coimbra, Coimbra, Portugal; [(d)]Centro de Física Nuclear da Universidade de Lisboa, Lisbon, Portugal; [(e)]Departamento de Fisica, Universidade do Minho, Braga, Portugal; [(f)]Departamento de Fisica Teorica y del Cosmos, Universidad de Granada, Granada, Spain; [(g)]Dep Fisica and CEFITEC of Faculdade de Ciencias e Tecnologia, Universidade Nova de Lisboa, Caparica, Portugal
[129] Institute of Physics, Academy of Sciences of the Czech Republic, Prague, Czech Republic
[130] Czech Technical University in Prague, Prague, Czech Republic
[131] Faculty of Mathematics and Physics, Charles University, Prague, Czech Republic
[132] State Research Center Institute for High Energy Physics (Protvino), NRC KI, Protvino, Russia
[133] Particle Physics Department, Rutherford Appleton Laboratory, Didcot, UK
[134] [(a)]INFN Sezione di Roma, Rome, Italy; [(b)]Dipartimento di Fisica, Sapienza Università di Roma, Rome, Italy
[135] [(a)]INFN Sezione di Roma Tor Vergata, Rome, Italy; [(b)]Dipartimento di Fisica, Università di Roma Tor Vergata, Rome, Italy
[136] [(a)]INFN Sezione di Roma Tre, Rome, Italy; [(b)]Dipartimento di Matematica e Fisica, Università Roma Tre, Rome, Italy
[137] [(a)]Faculté des Sciences Ain Chock, Réseau Universitaire de Physique des Hautes Energies-Université Hassan II, Casablanca, Morocco; [(b)]Centre National de l'Energie des Sciences Techniques Nucleaires, Rabat, Morocco; [(c)]Faculté des Sciences Semlalia, Université Cadi Ayyad, LPHEA-Marrakech, Marrakech, Morocco; [(d)]Faculté des Sciences, Université Mohamed Premier and LPTPM, Oujda, Morocco; [(e)]Faculté des Sciences, Université Mohammed V, Rabat, Morocco
[138] DSM/IRFU (Institut de Recherches sur les Lois Fondamentales de l'Univers), CEA Saclay (Commissariat à l'Energie Atomique et aux Energies Alternatives), Gif-sur-Yvette, France
[139] Santa Cruz Institute for Particle Physics, University of California Santa Cruz, Santa Cruz, CA, USA
[140] Department of Physics, University of Washington, Seattle, WA, USA
[141] Department of Physics and Astronomy, University of Sheffield, Sheffield, UK
[142] Department of Physics, Shinshu University, Nagano, Japan
[143] Department Physik, Universität Siegen, Siegen, Germany
[144] Department of Physics, Simon Fraser University, Burnaby, BC, Canada
[145] SLAC National Accelerator Laboratory, Stanford, CA, USA
[146] [(a)]Faculty of Mathematics, Physics and Informatics, Comenius University, Bratislava, Slovak Republic; [(b)]Department of Subnuclear Physics, Institute of Experimental Physics of the Slovak Academy of Sciences, Kosice, Slovak Republic
[147] [(a)]Department of Physics, University of Cape Town, Cape Town, South Africa; [(b)]Department of Physics, University of Johannesburg, Johannesburg, South Africa; [(c)]School of Physics, University of the Witwatersrand, Johannesburg, South Africa
[148] [(a)]Department of Physics, Stockholm University, Stockholm, Sweden; [(b)]The Oskar Klein Centre, Stockholm, Sweden
[149] Physics Department, Royal Institute of Technology, Stockholm, Sweden
[150] Departments of Physics and Astronomy and Chemistry, Stony Brook University, Stony Brook, NY, USA
[151] Department of Physics and Astronomy, University of Sussex, Brighton, UK
[152] School of Physics, University of Sydney, Sydney, Australia
[153] Institute of Physics, Academia Sinica, Taipei, Taiwan
[154] Department of Physics, Technion: Israel Institute of Technology, Haifa, Israel

[155] Raymond and Beverly Sackler School of Physics and Astronomy, Tel Aviv University, Tel Aviv, Israel
[156] Department of Physics, Aristotle University of Thessaloniki, Thessaloniki, Greece
[157] International Center for Elementary Particle Physics and Department of Physics, The University of Tokyo, Tokyo, Japan
[158] Graduate School of Science and Technology, Tokyo Metropolitan University, Tokyo, Japan
[159] Department of Physics, Tokyo Institute of Technology, Tokyo, Japan
[160] Tomsk State University, Tomsk, Russia
[161] Department of Physics, University of Toronto, Toronto, ON, Canada
[162] [(a)]INFN-TIFPA, Trento, Italy; [(b)]University of Trento, Trento, Italy
[163] [(a)]TRIUMF, Vancouver, BC, Canada; [(b)]Department of Physics and Astronomy, York University, Toronto, ON, Canada
[164] Faculty of Pure and Applied Sciences, and Center for Integrated Research in Fundamental Science and Engineering, University of Tsukuba, Tsukuba, Japan
[165] Department of Physics and Astronomy, Tufts University, Medford, MA, USA
[166] Department of Physics and Astronomy, University of California Irvine, Irvine, CA, USA
[167] [(a)]INFN Gruppo Collegato di Udine, Sezione di Trieste, Udine, Italy; [(b)]ICTP, Trieste, Italy; [(c)]Dipartimento di Chimica, Fisica e Ambiente, Università di Udine, Udine, Italy
[168] Department of Physics and Astronomy, University of Uppsala, Uppsala, Sweden
[169] Department of Physics, University of Illinois, Urbana, IL, USA
[170] Instituto de Fisica Corpuscular (IFIC), Centro Mixto Universidad de Valencia-CSIC, Valencia, Spain
[171] Department of Physics, University of British Columbia, Vancouver, BC, Canada
[172] Department of Physics and Astronomy, University of Victoria, Victoria, BC, Canada
[173] Department of Physics, University of Warwick, Coventry, UK
[174] Waseda University, Tokyo, Japan
[175] Department of Particle Physics, The Weizmann Institute of Science, Rehovot, Israel
[176] Department of Physics, University of Wisconsin, Madison, WI, USA
[177] Fakultät für Physik und Astronomie, Julius-Maximilians-Universität, Würzburg, Germany
[178] Fakultät für Mathematik und Naturwissenschaften, Fachgruppe Physik, Bergische Universität Wuppertal, Wuppertal, Germany
[179] Department of Physics, Yale University, New Haven, CT, USA
[180] Yerevan Physics Institute, Yerevan, Armenia
[181] Centre de Calcul de l'Institut National de Physique Nucléaire et de Physique des Particules (IN2P3), Villeurbanne, France
[182] Academia Sinica Grid Computing, Institute of Physics, Academia Sinica, Taipei, Taiwan

[a] Also at Department of Physics, King's College London, London, UK
[b] Also at Institute of Physics, Azerbaijan Academy of Sciences, Baku, Azerbaijan
[c] Also at Novosibirsk State University, Novosibirsk, Russia
[d] Also at TRIUMF, Vancouver, BC, Canada
[e] Also at Department of Physics and Astronomy, University of Louisville, Louisville, KY, USA
[f] Also at Physics Department, An-Najah National University, Nablus, Palestine
[g] Also at Department of Physics, California State University, Fresno, CA, USA
[h] Also at Department of Physics, University of Fribourg, Fribourg, Switzerland
[i] Also at II Physikalisches Institut, Georg-August-Universität, Göttingen, Germany
[j] Also at Departament de Fisica de la Universitat Autonoma de Barcelona, Barcelona, Spain
[k] Also at Departamento de Fisica e Astronomia, Faculdade de Ciencias, Universidade do Porto, Porto, Portugal
[l] Also at Tomsk State University, Tomsk, and Moscow Institute of Physics and Technology State University, Dolgoprudny, Russia
[m] Also at The Collaborative Innovation Center of Quantum Matter (CICQM), Beijing, China
[n] Also at Universita di Napoli Parthenope, Naples, Italy
[o] Also at Institute of Particle Physics (IPP), Victoria, Canada
[p] Also at Horia Hulubei National Institute of Physics and Nuclear Engineering, Bucharest, Romania
[q] Also at Department of Physics, St. Petersburg State Polytechnical University, St. Petersburg, Russia
[r] Also at Borough of Manhattan Community College, City University of New York, New York, USA

[s] Also at Department of Financial and Management Engineering, University of the Aegean, Chios, Greece
[t] Also at Centre for High Performance Computing, CSIR Campus, Rosebank, Cape Town, South Africa
[u] Also at Louisiana Tech University, Ruston, LA, USA
[v] Also at Institucio Catalana de Recerca i Estudis Avancats, ICREA, Barcelona, Spain
[w] Also at Department of Physics, The University of Michigan, Ann Arbor, MI, USA
[x] Also at Graduate School of Science, Osaka University, Osaka, Japan
[y] Also at Fakultät für Mathematik und Physik, Albert-Ludwigs-Universität, Freiburg, Germany
[z] Also at Institute for Mathematics, Astrophysics and Particle Physics, Radboud University Nijmegen/Nikhef, Nijmegen, The Netherlands
[aa] Also at Department of Physics, The University of Texas at Austin, Austin, TX, USA
[ab] Also at Institute of Theoretical Physics, Ilia State University, Tbilisi, Georgia
[ac] Also at CERN, Geneva, Switzerland
[ad] Also at Georgian Technical University (GTU), Tbilisi, Georgia
[ae] Also at Ochadai Academic Production, Ochanomizu University, Tokyo, Japan
[af] Also at Manhattan College, New York, NY, USA
[ag] Also at The City College of New York, New York, NY, USA
[ah] Also at Departamento de Fisica Teorica y del Cosmos, Universidad de Granada, Granada, Portugal
[ai] Also at Department of Physics, California State University, Sacramento, CA, USA
[aj] Also at Moscow Institute of Physics and Technology State University, Dolgoprudny, Russia
[ak] Also at Departement de Physique Nucleaire et Corpusculaire, Université de Genève, Geneva, Switzerland
[al] Also at Institut de Física d'Altes Energies (IFAE), The Barcelona Institute of Science and Technology, Barcelona, Spain
[am] Also at School of Physics, Sun Yat-sen University, Guangzhou, China
[an] Also at Institute for Nuclear Research and Nuclear Energy (INRNE) of the Bulgarian Academy of Sciences, Sofia, Bulgaria
[ao] Also at Faculty of Physics, M.V. Lomonosov Moscow State University, Moscow, Russia
[ap] Also at National Research Nuclear University MEPhI, Moscow, Russia
[aq] Also at Department of Physics, Stanford University, Stanford, CA, USA
[ar] Also at Institute for Particle and Nuclear Physics, Wigner Research Centre for Physics, Budapest, Hungary
[as] Also at Faculty of Engineering, Giresun University, Giresun, Turkey
[at] Also at CPPM, Aix-Marseille Université and CNRS/IN2P3, Marseille, France
[au] Also at Department of Physics, Nanjing University, Jiangsu, China
[av] Also at Institute of Physics, Academia Sinica, Taipei, Taiwan
[aw] Also at University of Malaya, Department of Physics, Kuala Lumpur, Malaysia
[ax] Also at LAL, Univ. Paris-Sud, CNRS/IN2P3, Université Paris-Saclay, Orsay, France
[*]Deceased